Effect of Part Thickness Variation on the Mold Filling in Vacuum Infusion Process

by

Mehmet Akif Yalçınkaya

A Thesis Submitted to the

Graduate School of Engineering

in Partial Fulfillment of the Requirements for the Degree of

Master of Science

in

Mechanical Engineering

Koç University

August 2012

Koç University

Graduate School of Sciences and Engineering

This is to certify that I have examined this copy of a master's thesis by

Mehmet Akif Yalçınkaya

and have found that it is complete and satisfactory in all respects,

and that any and all revisions required by the final

examining committee have been made.

Committee Members:

_____

Murat Sözer, Ph.D. (Advisor)

_____

Demircan Canadinç, Ph.D.

_____

Rıza Kızılel, Ph.D.

Date: _____

AUTHOR'S DECLARATION

I hereby declare that I am the sole author of this thesis. This is a true copy of the thesis, including any required final revisions, as accepted by my examiners.

I understand that my thesis may be made electronically available to the public.

Mehmet Akif Yalçınkaya

ABSTRACT

Vacuum infusion (VI) is a common composite molding process to manufacture large parts using vacuum pressure which compacts the fibers and drives the resin flow. A straightforward model has not been developed for the process and hence, current models for the mold filling require a coupled analysis of compaction and flow, and it is not so obvious if this tedious work is worth for the result which could have been calculated with less accuracy however with very simple approach. Due to the plastic vacuum bag in VI, compaction pressure varies within the mold which causes thickness variation in the part. Implementing the thickness variation to the modeling of the process is difficult and it is not clear whether the variation makes a significant difference in the mold filling results. In this study, the effect of the thickness variation was studied further; and a simple and useful model was proposed. Experiments and a model were compared to show if the thickness variation has a significant effect on the mold filling in VI. It was concluded that experimental mold filling time in VI is 13-17% shorter than in RTM (in which thickness is constant). Similar trend was also seen in the simplified coupled models of flow and compaction.

ÖZET

Vakum İnfüzyonu (VI), büyük boyutlu kompozit parçaların imalatında yaygın olarak kullanılan bir üretim tekniğidir. Bu teknikte kullanılan vakum basıncı, elyafları sıkıştırır ve aynı zamanda da reçinenin akışını sağlar. Söz konusu imal usulü için basit bir model henüz geliştirilmemiştir. Mevcut modeller reçine akışını ve elyaf sıkışmasını birbiriyle etkileşimli olarak kullanmaktadır ve bu nedenle bazı zorlukları vardır. Bu karmaşık modellerin, daha basit bir modele göre ne kadar fark yarattığı açık değildir. Vakum İnfüzyonu'nda, üst kalıp plastik vakum torbası olduğundan, sıkıştırma basıncı kalıp içerisinde farklılık göstermektedir ve bu durum elyaf içerisinde kalınlık farklarına neden olmaktadır. Kalınlık değişiminin modele entegrasyonu zor bir işlemdir ve kalıp dolum süresi üzerindeki etkisi açık değildir. Bu tez çalışmasında, kalınlık değişiminin kalıp dolum süresi üzerindeki etkisi incelenerek, literatürdeki modellere alternatif olarak basitleştirilmiş bir model önerilmiştir. Yapılan deneyler sonucunda, VI kalıp dolum süresi RTM kalıp (kalınlığı sabit) dolum süresinden %13-17 kısa olarak gözlemlenmiştir. Önerilen model de aynı davranışı göstermektedir.

ACKNOWLEDGEMENTS

I would like to thank my advisor Murat Sözer for all his help and guidance in my studies for these two years at Koç University. His positive attitude and encouragement played a very major role in my academic achievements and in the completion of this graduate study. I would also like to thank Demircan Canadinç and Rıza Kızılel for their participation in the thesis committee; my colleagues, Bekir Yenilmez, Barış Çağlar, Talha Akyol, Mustafa Haboğlu, and Ayşen Sarıoğlu in Composite Materials Manufacturing Laboratory for all kinds of support they gave in the laboratory studies and in writing this thesis report.

Finally, I thank my parents, Meral and Nadir Yalçınkaya, and my brother, Uğur Alp Yalçınkaya for their endless love and support.

Table of Contents

List of Tables

List of Figures

1. Introduction

Vacuum infusion (VI) is one of the composite manufacturing processes in which one side of the mold is a plastic foil called vacuum bag while the other part is made of a solid material (usually steel, aluminum or fiber reinforced plastic). After the fiber preform is placed, the mold is closed by using a sealant tape between the vacuum bag and the mold. The resin is driven from an inlet reservoir due to the pressure gradient created by vacuum pressure at the exit which also compacts the fiber preform in the mold.

In Resin Transfer Molding (RTM), both sides of the mold are made of solid material. Thus, the reinforcement material is mechanically compacted between the mold parts using clamps or a press, compared to the compaction pressure which can have a maximum value of one atmospheric pressure in VI. The resin is injected under positive pressure by using an injection machine into the mold in RTM compared to the limited vacuum pressure differential in VI.

These two processes have both advantages and disadvantages. For instance, VI requires lower investment costs than RTM since VI has only one side of the mold to be manufactured. Moreover, mold costs increase as the size of the part increases which means that VI is more suitable for the production of large parts. However, VI requires much longer labor than RTM because of tedious and skill-intense vacuum bagging. On the other hand, tighter dimensional tolerances can be achieved in RTM while it is not possible in VI due to non-uniform compaction pressure which causes thickness variation in the part. Additionally, the fiber content in the final part (typically 40-65%) is higher in RTM since higher compaction pressure can be applied under a press or using clamps than in VI (typically less than 50%). In RTM, both surfaces of the part may have low surface roughness by using a gel coat on the mold surfaces; however in VI, the vacuum bag side of the part has high surface roughness due to the texture of the fiber preform and/or the distribution medium used.

To overcome the process issues, increase the part quality or shorten the cycle time, one needs process modeling. In VI, modeling is more complex than in RTM since the compaction pressure and part thickness change as the resin flows, and these changes consequently affect the permeability of the fiber preform. Thus, fiber compaction and resin flow are coupled. In previous works by Correia et al. [1] and Sozer et al. [2], a coupled model for VI was used to calculate the final thickness distribution of the part and the time required to fill the mold. However, among the coupled models of flow and compaction available in the literature, it is not obvious if the coupled model makes a significant difference in the results compared to analytical mold filling time corresponding to RTM in which h and K are constants. A coupled model is expected to give a more accurate result, however it requires tedious material characterization experiments which relates compaction pressure to fiber volume fraction besides the permeability to fiber volume fraction. In addition, care must be taken while designing the compaction characterization experiments such that they should ideally mimic the actual fiber compaction in VI (see references [3–6] for dry/wet, loading/unloading cycles with settling and relaxation stages included). In this study, a) experimental VI results were compared with b) experimental RTM results in which the initial mold thickness was set to the initial average thickness in VI, c) a simplified coupled flow and compaction model, and d) analytical solution of 1D Darcy law for constant thickness to observe whether the difference between experiments and models is significant or not. This study aims to give a straightforward method to calculate the mold filling time in VI and the error involves in it.

2. Previous Work

Modeling of fiber compaction and resin flow in the VI process, and material characterization such as permeability measurement have been studied in many previous works. Although a lot of work has been done on modeling and simulation of RTM process [7–9], they did not have to address the thickness changes in preform during the impregnation which occurs in VI. Some other researchers focused on developing thorough models for VI to investigate the thickness change as well as resin flow. However, nonlinear resin pressure distribution that was either measured or modeled was not so significantly different than the linear distribution corresponding to 1D flow in RTM [1], [4], [10]. Thus, in this study, we will investigate a straightforward model and its error.

Correia et al. [1] analyzed VI analytically and presented a numerical solution scheme for 1D flow. The thickness of the preform is calculated by using a compaction model which is given in Eq. 2.1.

$$h = \frac{\rho_{\sup}}{\rho_f v_f} \tag{2.1}$$

where $h(P_{comp})$ is the thickness of the preform, P_{comp} is the compaction pressure, ρ_f is the density of the fiber, $\rho_{\sup}$ is the superficial density of the fabric, and $v_f(P_{comp})$ is the fiber volume fraction. For permeability calculations, they used Kozeny-Carman Equation (Eq. 2.2).

$$K = k\frac{(1-v_f)^3}{{v_f}^2} \tag{2.2}$$

where K is the permeability and k is the Kozeny constant. By combining these equations with Darcy law, they proposed a model to estimate the mold filling time (Eq. 2.3) and pressure distribution (Eq. 2.4).

$$t_{fill} = -\frac{L^2 \mu}{2\Delta P} \frac{1}{C_\alpha (K)_{\alpha=1}} \tag{2.3}$$

$$\frac{\partial^2 P}{\partial \alpha^2} = \left(\left(\frac{h^* \alpha - 1}{h} \right) \frac{\partial h}{\partial P} - \frac{1}{K} \frac{\partial K}{\partial P} \right) \left(\frac{\partial P}{\partial \alpha} \right)^2 \tag{2.4}$$

where α is dimensionless flow coordinate (x/L), P is the pressure, h^* is the thickness value normalized with the thickness at the flow front ($h/h(1)$), t_{fill} is the mold filling time, L is the mold length, and C_α is flow front fluid pressure gradient ratio (P_{VI} / P_{RTM}).

Hammami et al. [11] analyzed VI by conducting experiments and modeling the 1D flow in which compaction and permeability of the fabric are implemented. In their work, compaction experiments are conducted and compaction behavior of the fabric is modeled by using dual kriging method which fits the experimental data to a polynomial expression. They implied that, stacking sequence does not have an important effect on the compaction behavior of dry fabrics, whereas for wet case it is opposite. They calculated permeability using Kozeny-Carman equation. Using Darcy law (Eq. 2.5) and continuity equation (Eq. 2.6) they estimated the filling time for VI by calculating the flow front location, x_f (Eq. 2.7). In addition, they compared the effect of various flow enhancement layers.

$$u = -\frac{K}{\mu} \frac{\partial P}{\partial x} \tag{2.5}$$

$$\frac{\partial}{\partial x} uh = -\frac{\partial h}{\partial t} \tag{2.6}$$

$$x_f = \int_0^t \frac{u}{(1 - v_f)} dt \tag{2.7}$$

where u is the velocity of the resin, t is the time, and x_f is the flow front position.

Yenilmez et al. [2] investigated the variation of part thickness and compaction pressure in VI. They conducted dry and wet compaction characterization experiments to model the compaction behavior of the fabric. Permeability measurement experiments were also done at various fiber volume fractions. They conducted two material characterizations: 1) a relationship between compaction pressure and preform thickness, and 2) a relationship between fiber volume fraction and permeability of the preform. By using Correia et al.'s model [1], they simulated the mold filling in VI. However, instead of using Kozeny-Carman equation, they experimentally measured permeability values.

Correia et al. [10] used the software package LIMS, which is typically used for RTM simulations, illustrating that LIMS can be appropriately used for VI as well by revising the thickness, fiber volume fraction and permeability of each element in the FEM mesh as the resin propagates in the mold. Thus, they could investigate the effect of variations in thickness and permeability on the pressure distribution. In addition, they developed a formulation for the mold filling time in VI. Andersson et al. [12] modeled the flow in VI by using a 3D flow approach and including the change in the porous medium's permeability. They used a computational fluid dynamics software, CFX-4, to implement their model in which conservation of momentum equation is solved for flow through a porous medium with an anisotropic and time dependent permeability.

Yenilmez et al. [3] investigated and constructed a database for the compaction and decompaction behavior of three different types of e-glass fabrics to mimic the VI process. Then, they used this database in another work [4] in which a coupled model for compaction and flow was used, and experimental results were compared with simulations.

Mathur et al. [13] studied the flow front propagation in VI both experimentally and analytically. Since they used a distribution medium on the fabric preform, they included the transverse flow in their solution. Chen et al. [14] developed a model which is named as "equivalent permeability method". They included a high permeable distribution

medium and its effects in the simulations of flow in VI. Their model reduced the computational time for the mold filling simulations because they proposed an equivalent permeability for the high permeable distribution medium and preform. Hsiao et al. [15] developed a model for the optimization of distribution medium placement which is a significant issue in manufacturing of complex shaped parts in VI. They assumed that the thickness does not change along the preform hence the permeability is constant. Sun et al. [16] simulated the VI process with a FEM solution which includes the effect of high permeable medium. They assumed that the flow through the mold is driven by the high permeable medium and the flow through the preform occurs by the resin leakage from the high permeable medium.

Kang et al. [17] analyzed the mold filling in VI by including the effect of thickness change in the preform. Acheson et al. [18] included the effect of fiber tow saturation by modeling the tow impregnation at micro scale and coupling it with the global resin flow in the preform at macro scale by using the Kozeny-Carman equation for the permeability value calculation. Another study which couples 1D resin flow and compaction of the preform was presented by Lopatnikov et al. [19]. In this study, the preform was assumed to be linearly elastic and the permeability was calculated by using the Kozeny-Carman equation.

3. Experimental Setup and Procedure

One dimensional VI and RTM experiments were conducted to measure the total mold filling times for the comparison purpose such that the constant thickness in RTM was set to the initial average thickness in VI for the sake of fairness. In addition, transient (unsaturated) 1D flow permeability measurement experiments were conducted under constant flow rate at various thicknesses to relate permeability to the fiber volume fraction. In each of these characterization experiments, an RTM mold was used with a fixed and uniform thickness. This data was used in the uncoupled and coupled models of flow and compaction in the next sections.

3.1. Materials Used

Diluted corn syrup was used as the test fluid rather than using an actual resin. Diluted corn syrup seen in Figure 3.1 is appropriate to use in the characterization and compaction experiments since it is easier to clean after the experiment and there is no curing stage of the material which shortens the duration of the experiment. In addition, it does not cause any threat to human health. The viscosity of the corn syrup can be adjusted by adding water so that its viscosity (0.2-0.3 Pa.s) is the same as the viscosity of the actual polyester resin used in our lab to manufacture composite parts. Furthermore, corn syrup can be colored by adding ink which provides better visualization of the flow front propagation during the experiments.

Figure 3.1 *Vaniköy corn syrup (Supplier: Cargill, Bayrampaşa/Istanbul)*

Figure 3.2 *Fibroteks E-glass random fabric*

The fabric preform is made by stacking 8 layers of Fibroteks e-glass random fabric (see Figure 3.2) with a superficial density of 450 g/m^2 per layer.

3.2. 1D Permeability Measurement Experiments

Permeability measurement is an essential part of process modeling in composite materials manufacturing. Models and software packages for the resin flow, which may be coupled with fiber compaction in VI due to the presence of vacuum bag that functions as the upper elastic mold part, require the permeability of the preform as an input material parameter. Since the flow through a fibrous medium is commonly modeled with a porous flow and Darcy law is used. Darcy law for two-dimensional flow (Eqs. 3.1 and) relates the resin velocity components u and v to pressure gradient:

$$u = -\frac{K_{xx}}{\mu}\frac{\partial P}{\partial x} - \frac{K_{xy}}{\mu}\frac{\partial P}{\partial y} \qquad 3.1$$

$$v = -\frac{K_{yx}}{\mu}\frac{\partial P}{\partial x} - \frac{K_{yy}}{\mu}\frac{\partial P}{\partial y} \qquad 3.2$$

where $K_{xy} = K_{yx} = 0$, if x and y are the principal permeability axes of the fiber preform, μ is the resin viscosity and permeability tensor components (K_{xx} and K_{yy}) need to be determined either using material characterization experiments (a.k.a. permeability measurement experiments) or permeability predictor models which are

usually based on flow through a unit cell with periodic boundary conditions. Isotropic fiber preforms such as made of random fabric mats have $K_{xx} = K_{yy} \equiv K$. The accuracy of resin velocity is dominated with the accuracy of the permeability; and unfortunately the permeability values from experimental databases usually have a very significant scatter due to inherent variability during the specimen preparation and experimental errors [20], [21]. Conventional permeability measurement experiments require tedious work due to long mold preparation time and need to use separate specimens at each particular fiber volume fraction which means that the mold must be opened and cleaned before a new specimen is placed in the mold cavity to be tested at a new fiber volume fraction. A typical mold used for this purpose has a fixed gap dimension; and the preform is prepared by stacking n, n+1, … layers of mats or plies which results in a fiber volume domain to be considered in the simulations. This approach may cause an inconsistent (and misleading) material characterization due to wall effects. For example, if the number of plies/mats is uniform everywhere in the actual mold cavity with varying gap thickness, then the conventional permeability measurement in the material characterization mold setup is not the appropriate approach. The ideal approach should be to keep the number of layers fixed and vary the thickness as done in the continuous experiments [22]. No matter what experimental procedure used (conventional versus continuous; 1D versus radial; steady versus unsteady; constant-pressure versus constant-flow rate boundary condition), very significant scatter in the permeability values is typically observed in the literature [20], [21] due to inconsistent labor, nonuniform fiber structure caused by fiber nesting and racetracking channels, and experimental inconsistencies caused by mold deflection, sealing, deviation from the required 1D flow, and so on.

In this study, a novel mold for one dimensional continuous permeability measurement experiments with adjustable mold cavity thickness is used. A set of experiments and results are presented to illustrate its straightforward use and reliable results.

3.2.1. Previous Work on Permeability Measurement of Fabric Preforms

3.2.1.1. 1D Permeability Measurement Experiments

There are various types of 1D permeability measurement experiments which are conventional (unsteady and steady), and continuous experiments. Alms et al. [23] who used a mold with constant cavity thickness, explained how 1D conventional permeability measurement experiments are conducted and showed a set of experimental results. Antonucci et al. [24] conducted VI experiments to measure permeability by using fiber optic sensors to monitor the flow-front under unsteady flow. They assumed that the thickness variation in the part is negligible so that the permeability of the preform is constant within the part. Gauvin et al. [25] presented results for both 1D and radial permeability measurement experiments and drew attention to the importance of the resin inlet hole diameter which should not be too small not to overestimate the permeability, location of the pressure transducer and the flow-front monitoring system which is essential in constant pressure experiments. In addition, to get more consistent results the preform should be weighted before each experiment. If there is a huge difference between the specimens then the results will be too different for the same number of layers.

Stadtfeld et al. [22] conducted continuous permeability measurement experiments at different fiber volume fractions only for woven fabrics with their RTM mold. The mold they used was compressed to a desired thickness by using a hydraulic press and in-plane permeability values are calculated for saturated and unsaturated flows. The sealing of the mold was maintained by using rubber foam. Sozer et al. [26] coupled their mold with an Instron Machine which can change the thickness of the cavity during continuous experiments according to the desired fiber volume fraction.

3.2.1.2. Radial Permeability Experiments

Liu et al. [27] and Hoes et al. [28] designed a setup for conventional, radial permeability measurement of woven glass fabrics under unsteady flow. The cavity

thickness of their mold cannot be adjusted in Liu et al. [27]'s work whereas, Hoes et al. [28]'s mold has three constant thickness values at which conventional permeability experiments can be conducted. To detect the resin flow and track the flow front in both studies, electrical sensors are used by measuring the resistance change as the resin reaches to sensor. Different than these studies, Weitzenböck et al. [29] used thermistors and frame grabber to track the flow-front.

On the other hand, another alternative approach for continuous radial permeability measurement is used by Comas-Cardona et al. [30] and Buntain and Bickerton [31]. They compressed the impregnated preform and observed the stress response of the material as the test fluid flows through the preform. Buntain and Bickerton [31] expressed that they had problems with the mold deflection and clamping at high volume fractions.

3.2.1.3. Other Studies

Some authors [32], [33] used gas flow method to measure the permeability. Moon-Kwang Um et al. [31] proposed a gas flow method by using the mass flow rate of the air which is injected through the fabric preform. This method is good for preventing the edge effects such as racetracking and deflections in the mold because the experiments are conducted at low gas pressures. Kim et al. [32] designed a mold with pressure sensors to measure the pressure of the gas which is injected through the fabric preform. Then, permeability was computed by using control volume finite element method using the pressure data.

Some studies compared different methods to measure the permeability and pointed important issues. Arbter et al. [20] presented an overview of 16 different experimental procedures for permeability measurement and showed that each of these methods give different results which were obtained by various institutes. This study included both steady and unsteady flow methods. Results showed that there can be an order of magnitude variation in the permeability values measured by different institutes.

Lundström et al. [34] compared three methods to measure the in-plane permeability which were parallel wetting, parallel saturated wetting and radial wetting technique. In parallel wetting technique, fabric preforms which were cut in different directions were tested simultaneously. They concluded that all of these methods have a good stability with low standard deviation. Sharma and Siginer [35] reviewed various methods for permeability measurement and widely discussed the inconsistencies of the present methods and models in their work. They noted that channel flow (1D flow) methods give more consistent results than the radial flow methods.

3.2.2. Mold Design

As mentioned earlier, previous designs in the literature had some drawbacks. In this study, a novel RTM mold was designed and constructed by Recep Mert and Deniz Yıldız as their senior design project in Mechanical Engineering curriculum at Koç University. The most important design criteria are considered as the ease of use, perfect sealing in continuous experiments, simplicity of the mold, and repeatability of the experiments in which variations are minimized. The features of the mold will be discussed in the following sections and a general view of the mold and its parts are shown in Figure 3.3.

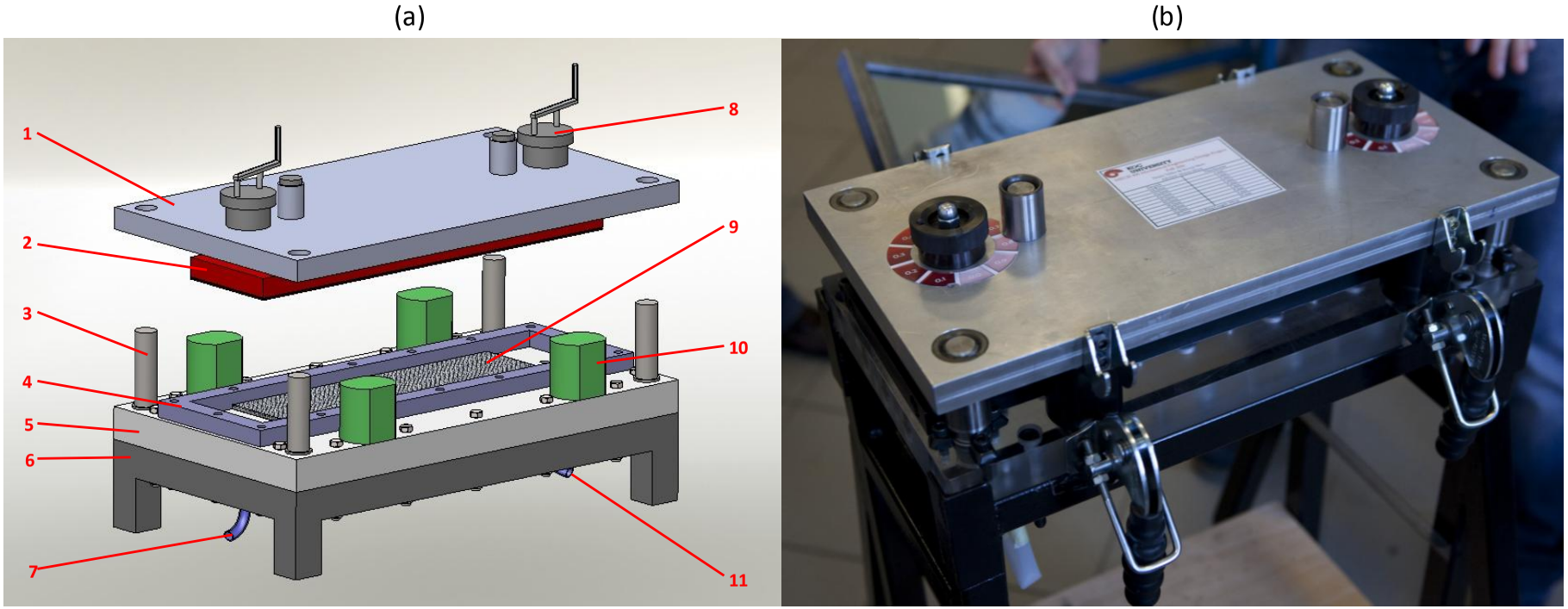

Figure 3.3 *Mold for continuous permeability measurement experiments: (a) Open, (b) Closed. The parts of the mold are: 1-aluminum block, 2-steel mold, , 3-guides, 4-steel mold frame 5-acrylic lower mold, 6-lower mold frame, 7-resin inlet, 8-handles, 9-preform, 10-spacers, 11-resin exit*

3.2.2.1. Mold Closure and Opening

The closure and the opening of the mold are guided by four steel guides. The upper aluminum block moves along these guides so that it moves without any tilting. To position the upper aluminum block with a fixed distance from the lower acrylic plate, four hardened steel spacers are used. The clamps are placed just on these spacers to obtain optimum contact pressure between the upper and lower mold so that the distance between the aluminum block and the acrylic lower mold remains constant. The upper and lower molds are shown in Figure 3.3.

3.2.2.2. Clamping Mechanism and Thickness Adjustment

The required clamping force during the mold closure and the desired gap thickness is maintained easily by the experimenter. Instead of using hydraulic presses or electric motors, clamping of the mold can be obtained by simple mechanical clamps which are placed on the upper aluminum block and lower acrylic plate. By clamping these two parts a constant gap between them is maintained with the help of 50 mm spacers as seen in Figure 3.4.

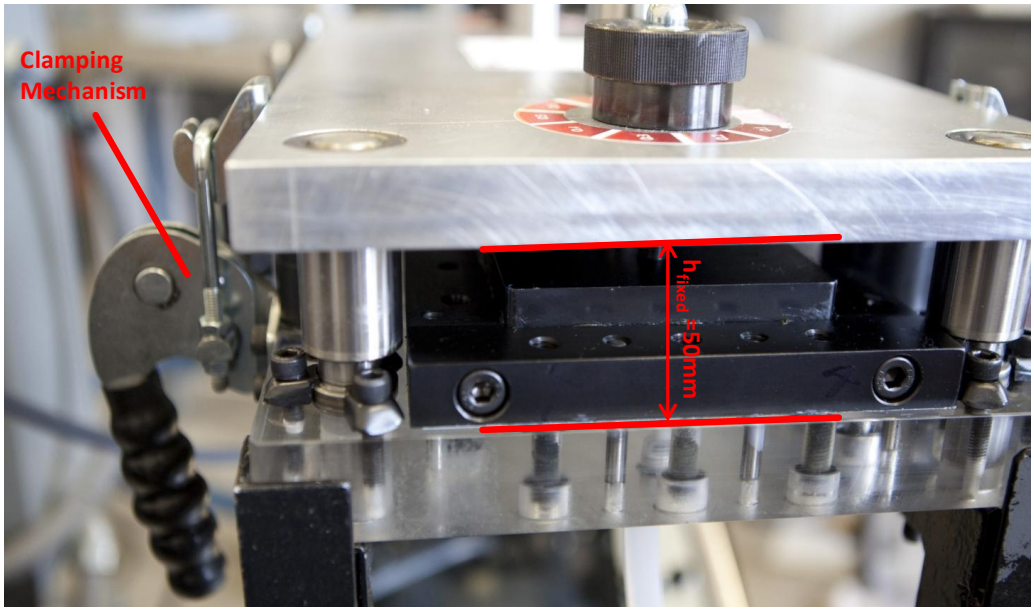

Figure 3.4 *Clamping mechanism*

The mold cavity thickness can be changed between 10 mm to 2 mm by using the handle operators. The mechanism basically consists of two screws which move the upper steel mold away from the upper aluminum block in the steel mold frame (see Figure 3.5) as the handles are rotated.

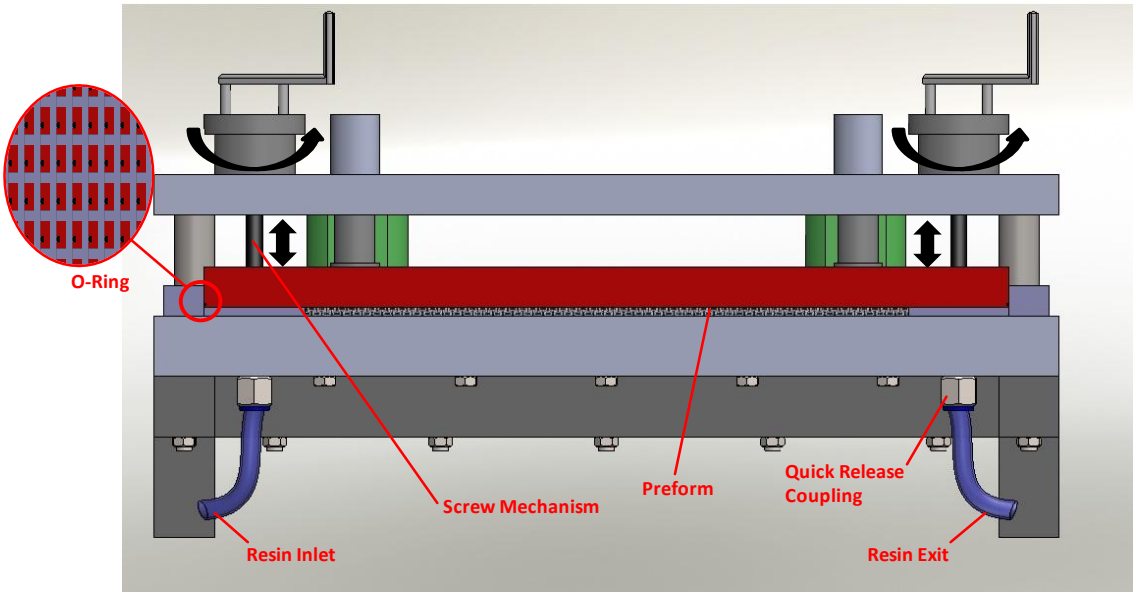

Figure 3.5 *Section view of the closed mold*

The handles are connected to screws and the pitch of the screws is determined accurately so that the full rotation of the handle changes the cavity thickness 1 mm. One full rotation of the handle is divided into 10 intervals which provide an accuracy of 0.1 mm while adjusting the cavity thickness. In addition, the thickness value can be measured and verified by using the holes on the aluminum block by using a vernier caliper. A detailed view of the cavity thickness adjustment is given in Figure 3.6. The mechanism has been working without any problem for more than 200 permeability measurement experiments. The cavity thickness of the mold is calculated in Eq.3.3.

$$h = h_{fixed} - h_{adjustable} \tag{3.3}$$

where h is the mold cavity thickness, h_{fixed} is the fixed distance between lower acrylic mold and upper aluminum block which is checked by dial-gages during the experiment not to have irrelevant results due to deflections, and $h_{adjustable}$ is the distance which varies when the handles are rotated.

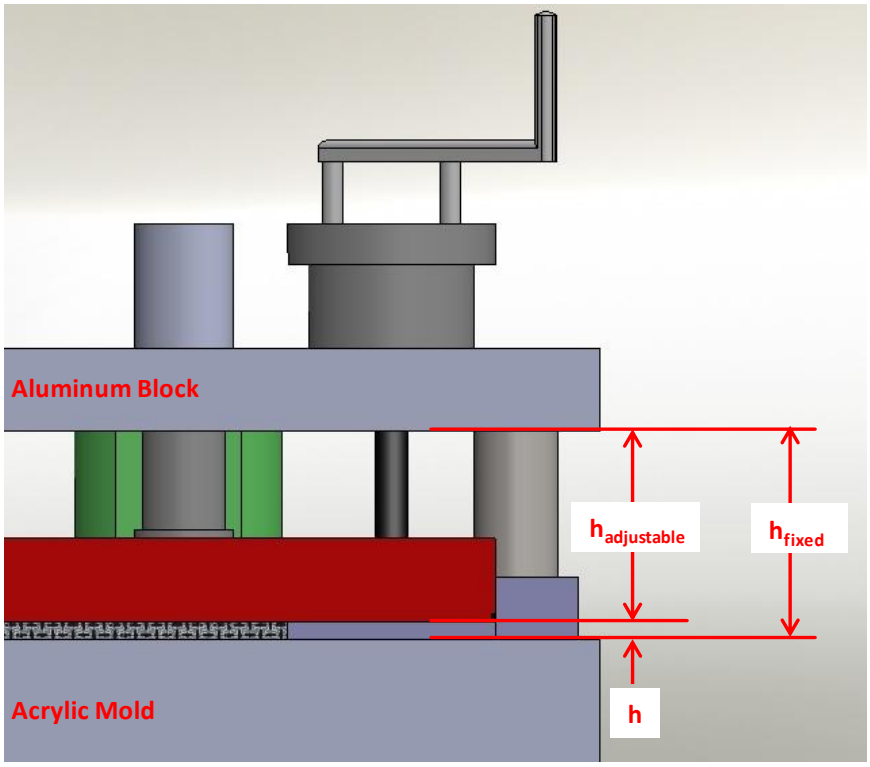

Figure 3.6 *Mold cavity thickness*

3.2.2.3. Sealing

The sealing of the mold is obtained by inserting a rubber O-Ring with a diameter of 1 mm into the channel shown in Figure 3.5. The sealing prevents the leakage of liquid resin up to an injection pressure of 6 bars. The edges of the O-Ring are cut with an angle of 45 degrees and the tips are joined by using an adhesive. The joined section of the O-Ring is placed to the exit side of the mold to reduce the risk of leakage since the fluid pressure will be lower at that location. As a result, no leakage is observed during the experiments. The lower mold which consists of the acrylic plate and hardened steel

frame is also critical for the sealing. The steel frame which houses the upper steel mold is bolted to the acrylic plate after liquid sealant is applied carefully between them.

3.2.2.4. Lower Mold

The lower mold is made of an acrylic plate to visualize the propagation of flow-front. It can be easily verified whether the flow is 1D or not, so that the experiment is valid or not. In addition, the flow-front propagation during the unsteady flow experiments under constant injection pressure is recorded by a camera (see Figure 3.7) and used in the calculation of permeability.

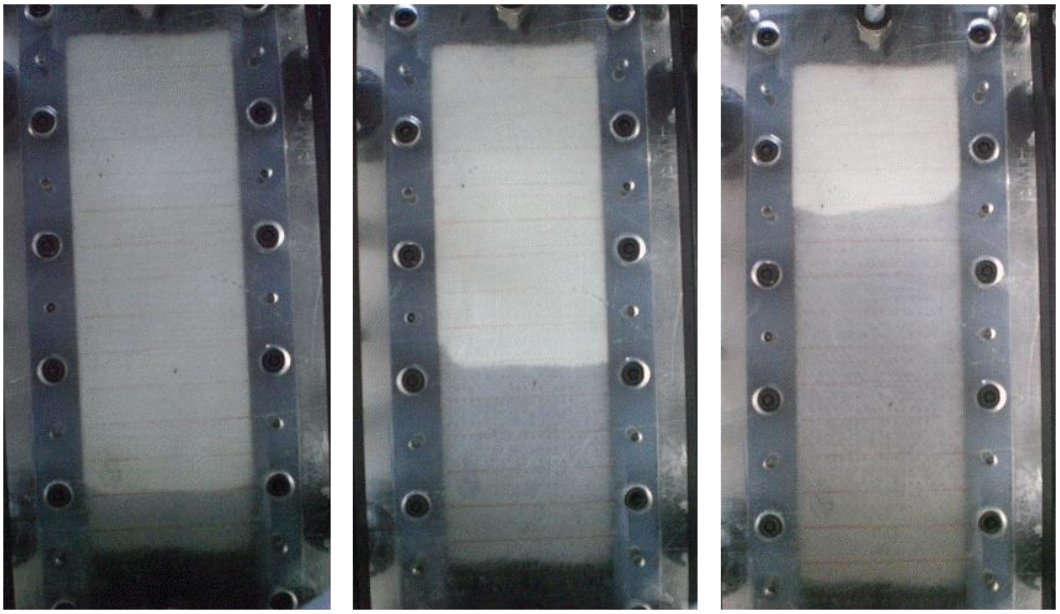

Figure 3.7 *Flow front visualization*

The transparency of the acrylic plate is a significant advantage; however, there are some difficulties to overcome when a material with low stiffness such as acrylic is used. The deflection of the mold due to fluid pressure should be minimum so that the experimental data is reliable for a certain fiber volume fraction. The upper steel mold is made of hardened steel and the deflection is not expected. Even though the acrylic plate has a thickness of 30 mm, it can still deflect as the fluid pressure and the required

clamping force increases. To overcome this issue the acrylic plate is supported by an outer steel frame, using screw-bolt connections. In addition, the steel frame in which the upper steel mold moves also increases the stiffness of the acrylic plate.

3.2.3. Permeability Measurement Experiments

3.2.3.1. Procedure

The procedure of doing experiments is very simple and does not require any intensive labor. Firstly, the preform is prepared by cutting certain number of layers of glass fabric which is Fibroteks Random Fiber Mat or Fibroteks Woven Fiber Mat in our experiments. The in-plane dimensions of the preform are 100 mm in width and 300 mm in length. In the second step, the upper portion of the mold is detached and the preform is placed onto the lower acrylic mold. Then, the upper mold is closed and clamped to the lower mold. At this stage, the thickness of the mold cavity is 10 mm which does not apply any compaction pressure to the preform. The desired cavity thickness is adjusted by rotating the handles on the upper mold. The next step is to fill the injection machine (Radius Engineering RTM 2100) with the test fluid and connect it to the inlet of the mold. The connection of the injection pipe is very easy since quick release couplings are used as shown in Figure 3.5. The injection machine is able to maintain a constant flow rate and on the other hand, the injection pressure is measured by a pressure transducer and recorded during the experiment so that the pressure data can be used in the permeability calculations (Table 3.1).

Once the injection with a constant flow rate starts, the unsteady part of the experiment is conducted until the test fluid impregnates the preform totally. After the mold is completely filled, the steady flow experiments are conducted by adjusting the mold cavity thickness to the desired value. As the thickness decreases, the pressure increases as well which is shown in Figure 3.98 and Figure 3.9 [36]. When the injection pressure settles and a smooth plateau is observed, the thickness can be changed and permeability for another thickness value can be determined.

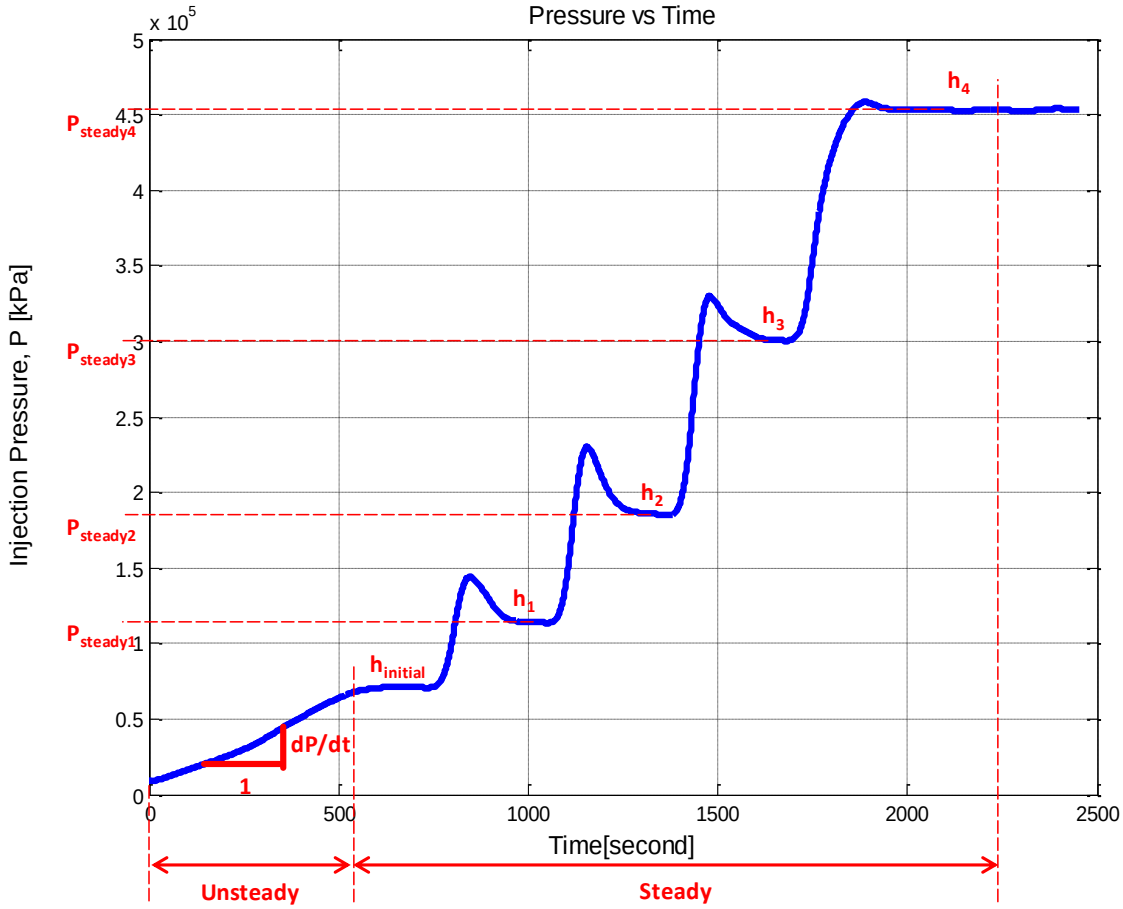

Figure 3.8 *Injection pressure versus time graph for 8 layers of random fabric (h_{init}= 5, h_1= 4.5, h_2=4, h_3=3.5, and h_4=3 mm)* [36]

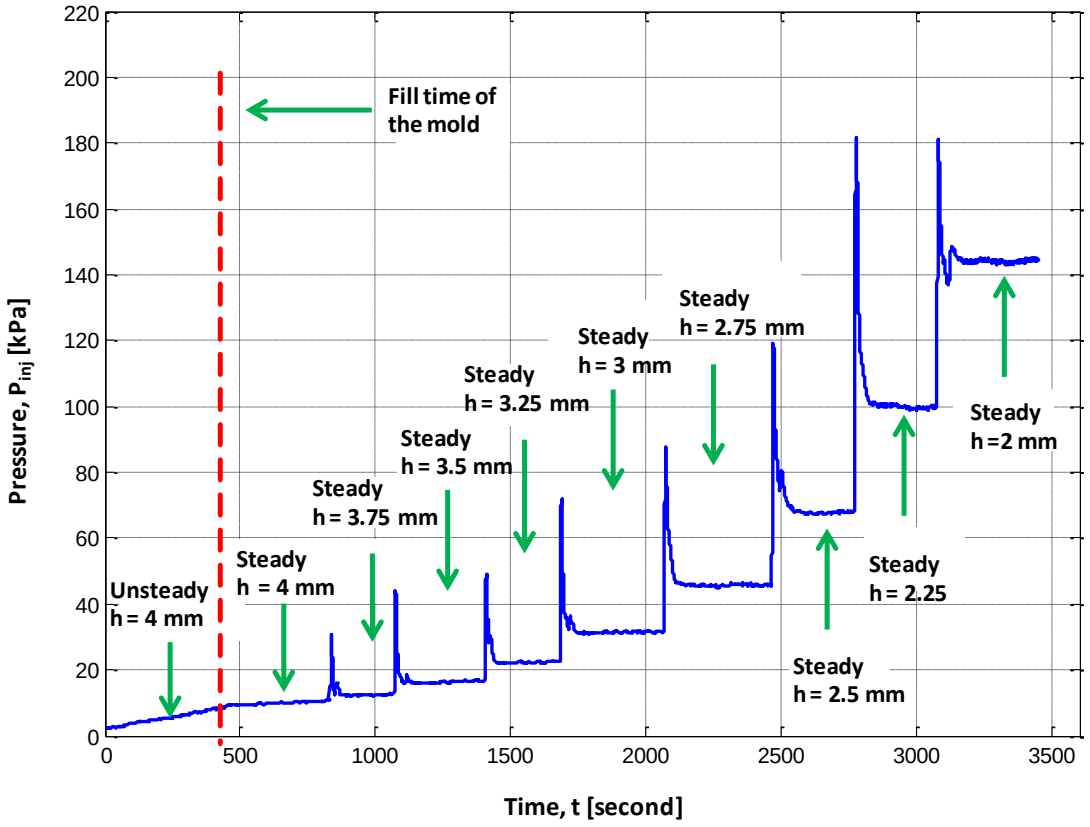

Figure 3.9 *Injection pressure vs. time graph for 8 layers of woven fabric* [36]

Permeability measurement experiments may also be conducted under constant injection pressure (P_{in}=100kPa). In experiments with constant injection pressure, the flow front is tracked by using a camera. An experimental result is shown in Figure 3.10 and the permeability calculation for injection with constant pressure is presented in Table 3.1.

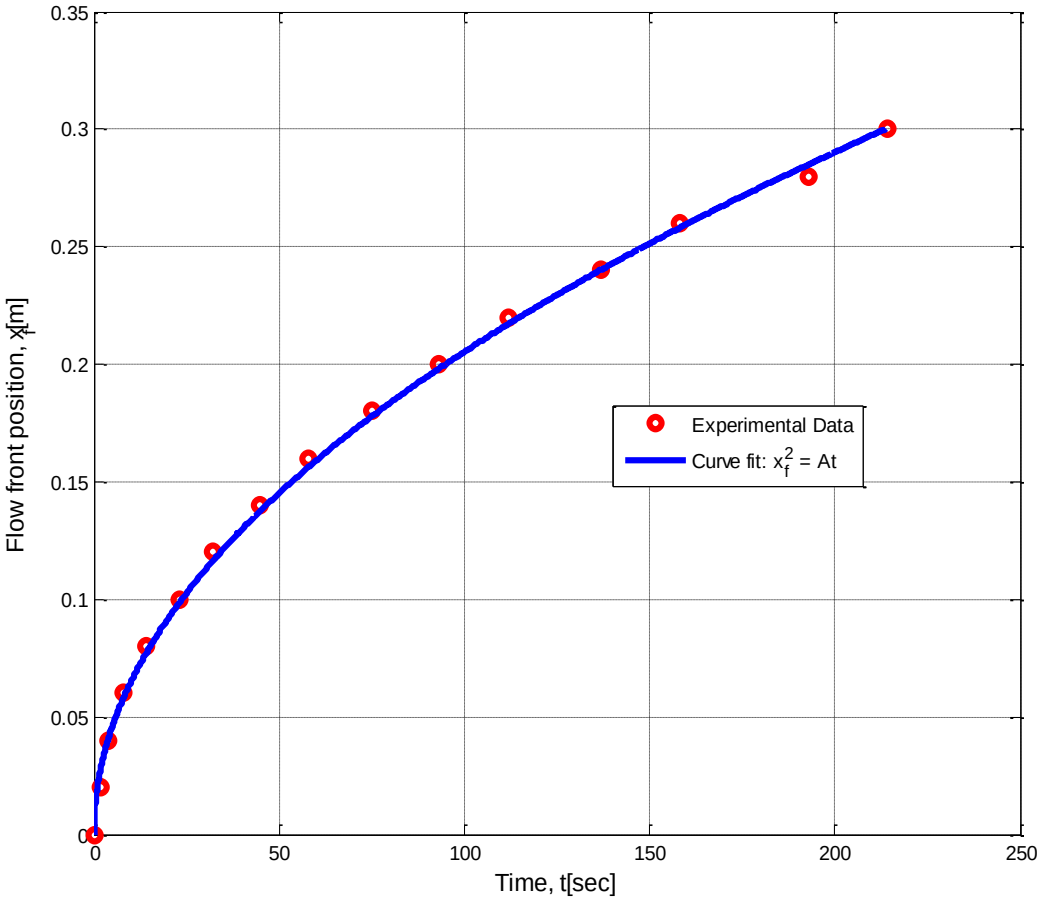

Figure 3.10 *Flow front location vs. time graph for an experiment with constant pressure*[36]

3.2.3.2. Permeability Calculations

Experimental characterization of permeability for fabric preforms is explained in detail in [37]. Table 3.1 shows how permeability values for 1D unsteady (transient) and 1D steady flow are calculated by conducting continuous experiments at constant flow rate (Q = constant) and constant injection pressure (P_{in} = constant).

Table 3.1 Permeability calculation [37]

Boundary Condition	Flow	Recorded Data	Formula to calculate K
Constant Q	Unsteady	$P_{inj}(t)$ @ $h_{initial}$	$K_{unsteady} = (\frac{Q}{wh_{initial}})^2 \frac{\mu}{\phi} \frac{1}{\frac{dP_{inj}}{dt}}$
Constant Q	Steady at $h_{initial}$	$P_{inj}(t)$ @ $h_{initial}$	$K_{steady} = \frac{Q\mu}{wh_{initial}} \frac{L}{P_{in} - P_{out}}$
Constant Q	Steady at h_n	$P_{inj}(t)$ @ h_n	$K_{steady} = \frac{Q\mu}{wh_n} \frac{L}{P_{in} - P_{out}}$
Constant P_{inj}	Unsteady	$x_f(t)$ @ $h_{initial}$	$x_f = \sqrt{\frac{2K(P_{in} - P_{out})t}{\mu\phi}}$ $K = \frac{J\mu\phi}{2(P_{in} - P_{out})}$ where J is determined by using the following curve fit for the experimental data: $x_f = \sqrt{Jt}$

3.2.4. Experimental Results for Permeability Calculation

Continuous permeability measurement experiments were conducted by Sarıoğlu [36] for the following methods:

Table 3.2 Permeability measurement experiment methods used by Sarioglu [36]

Boundary Condition	Steady	Unsteady
Q_{in} = Constant	✓	✓
P_{in} = Constant	✓	✓

The unsteady results for constant pressure boundary condition were taken from [36] (seen Table 3.3) and they will be used in the model of this study later in Chapter 4.

Table 3.3 Permeability values for 8 layers of Fibroteks random e-glass mat [36]

h [mm]	Vf	K [m^2]
6	0.224	3.888E-10
6	0.238	3.647E-10
6	0.227	4.675E-10
5.5	0.247	3.092E-10
5.5	0.247	3.014E-10
5.5	0.246	3.043E-10
5	0.287	1.425E-10
5	0.277	1.819E-10
5	0.261	1.477E-10
4.5	0.312	1.344E-10
4.5	0.324	1.017E-10
4.5	0.315	1.014E-10
4	0.329	8.895E-11
4	0.348	8.417E-11
4	0.356	9.886E-11
3.5	0.407	5.097E-11
3.5	0.405	5.460E-11
3.5	0.417	4.987E-11
3	0.466	3.926E-11
3	0.503	2.307E-11
3	0.503	2.271E-11

3.3. VI and RTM Experiments

A special setup was designed and constructed for the VI experiments as seen in Figure 3.11(a) and 3.12. On the left hand side of the setup seen in Figure 3.11, regular VI experiments are conducted. On the right hand side, the preform's thickness is set to a constant value by adjusting the gap between the acrylic lid and the lower mold plate which eliminates the thickness variation in the VI process. Thus, the setup behaves as an RTM mold with constant thickness (i.e., $h_{RTM} = \text{constant} \neq f(x,t)$).

The experimental setup shown schematically in Figure 3.11 and 3.12 consists of a lower flat mold made of stainless steel, an acrylic lid with adjustable position relative to the lower plate, a rail-car mechanism which drives a laser displacement sensor along the preform, a set of dial gages, a vacuum pump connected to the exit, and a vacuum pressure regulator. The test fluid and the preform properties are the same as in the permeability measurement experiments. Detailed figures are given in Appendix A.

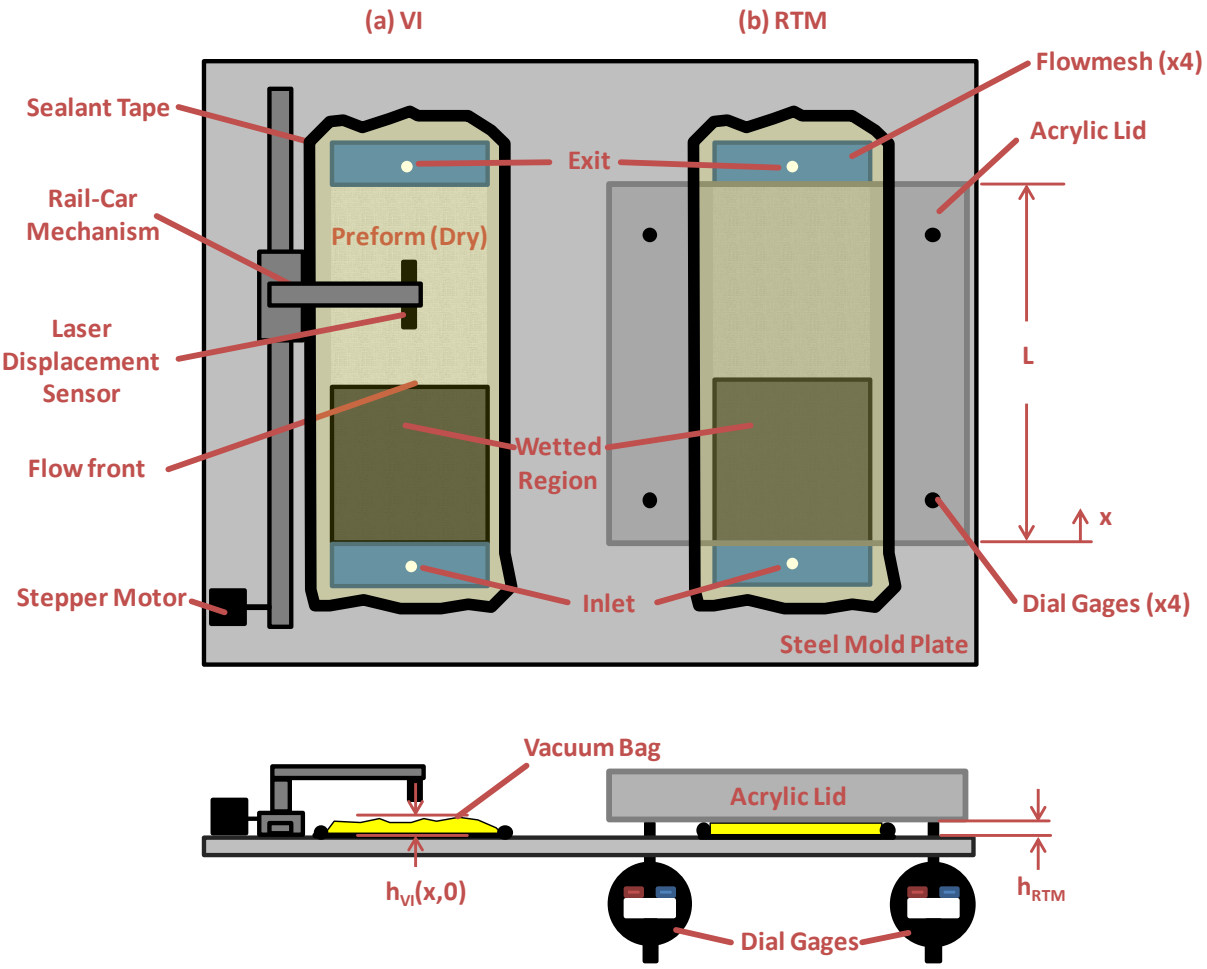

Figure 3.11 *(a) VI mold in which thickness varies with time; (b) RTM mold which is actually a solid acrylic lid placed on top of the vacuum bag. (h_{RTM} is controlled by using the clamps shown)*

3.3.1. Preparation of the Two Setups

Two similar preforms are cut, weighed and laid on both setups and covered with a peel-ply. To have consistent results, the difference in the preform weight should be minimal which is not more than 3% in the experiments presented here. 50 mm of flow mesh is placed at both edges of each preform to ensure a 1D flow of the test fluid by creating highly permeable pools before effectively wetting the fibers. The flow mesh at the vent helps the vacuum to be effectively distributed in the mold. Then, both molds

are covered with a vacuum bag and sealant tape is used along the four edges of each mold for sealing the molds. Before starting the infusion, the gap between the acrylic lid and the mold, seen in Figure 3.11(b), is set to the value which is equal to the average thickness of the compacted VI preform under 80 kPa compaction pressure.

The average thickness value, $h_{VI,average}$ of the preform under this initial compaction pressure, Pc =80 kPa, is calculated in Eq. 3.4.

$$h_{VI,average} \equiv \frac{1}{L}\int_0^L h_{VI}(x,0)dx \qquad 3.4$$

where h_{RTM} is the thickness between the acrylic lid and the steel mold plate, $h_{VI}(x,0)$ is the initial thickness of the fiber preform along its length $h_{VI,average}$.

The laser sensor system seen in Figure 3.11 and 3.12 scans the preform thickness such that it measures $h(x,t)$ at 800 equally-spaced locations between $x=0$ and $x=L=300\,\text{mm}$ by adjusting the sampling frequency and the speed of the scanner. Finally, the thickness of the RTM mold, h_{RTM}, is set to $h_{VI,average}$ and kept constant during the experiment.

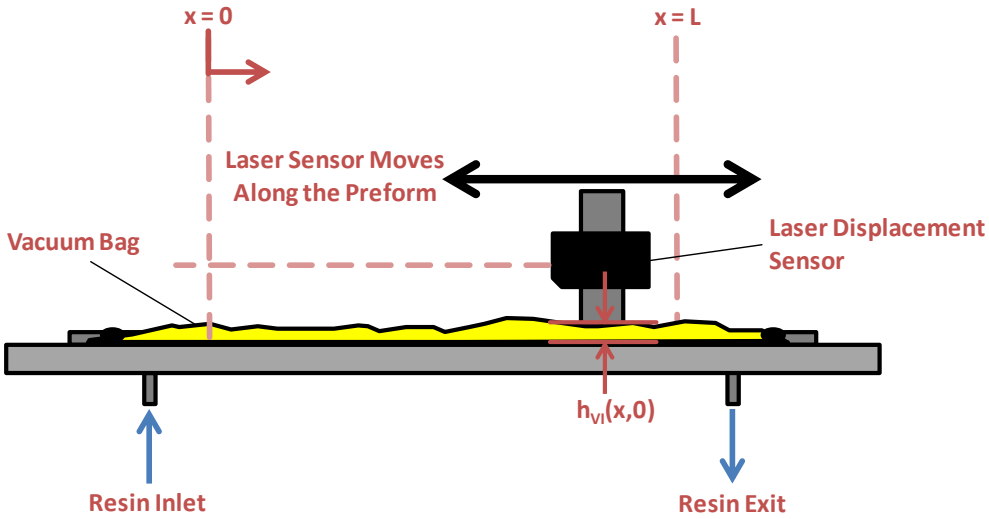

Figure 3.12 *Side view of the VI mold: illustration of thickness measurement of the part*

The laser sensor is driven by a stepper motor along the preform on a rail-car mechanism. The thickness data is measured by a laser displacement sensor and collected by using an Arduino Nano microcontroller which also controls the motor. The controller scheme of the setup is shown in Figure 3.13. The details (code and the data sheet) about the controller are given in Appendix A. In addition, Matlab is used to monitor and save the data. The user interface of the Matlab code is shown in

Figure **3.14**. The Matlab code, data sheets for the laser sensor and the stepper motor are given in Appendix A.

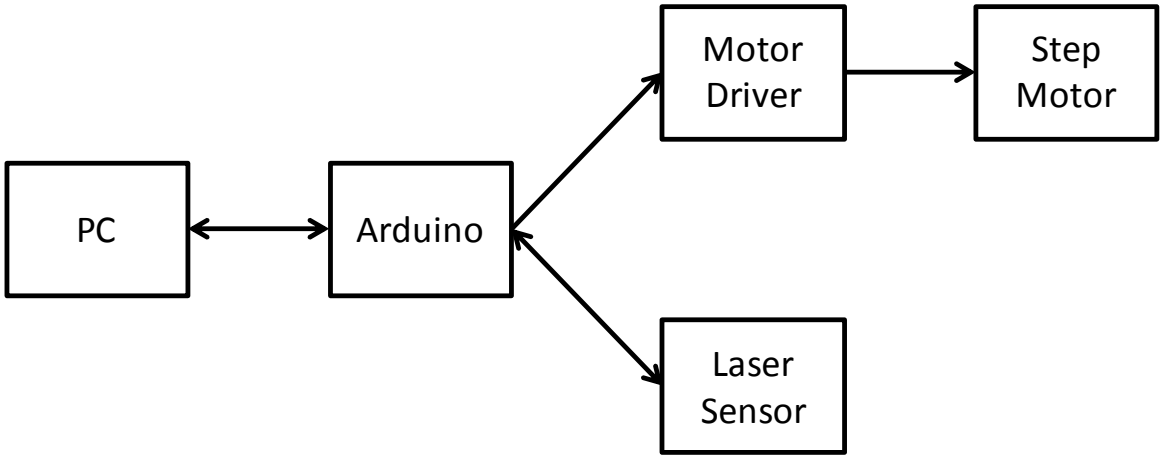

Figure 3.13 *Controller scheme of the experimental setup*

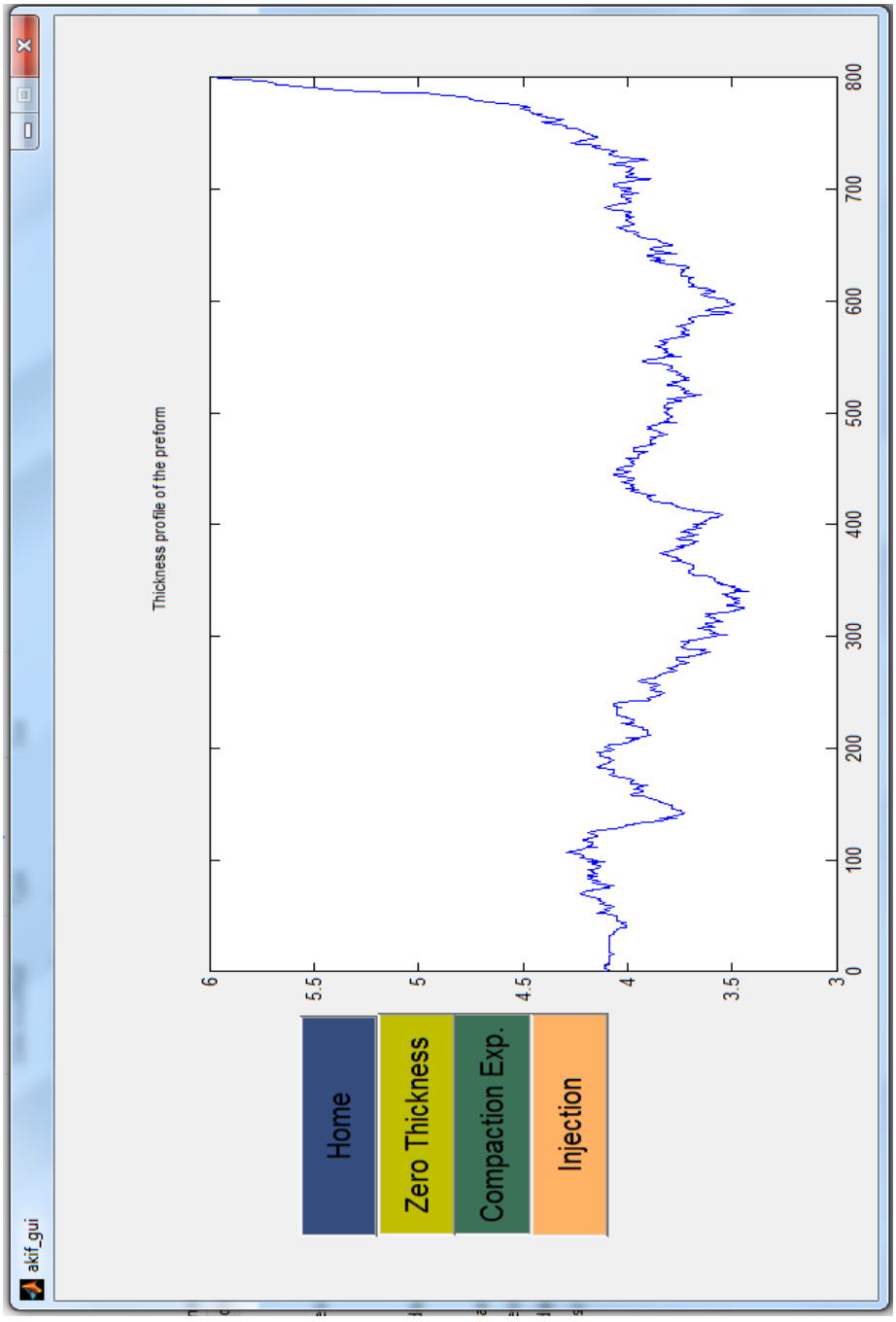

Figure 3.14 *Matlab user interface for thickness measurement. The graph illustrates the raw data; the x-axis is the discrete nodal points along x-axis; the y-axis is the thickness of the specimen which will be adjusted by subtracting the initial calibration*

An example of thickness measurement just before the injection is shown in Figure 3.15. The whole set of measurements are given in Appendix B.

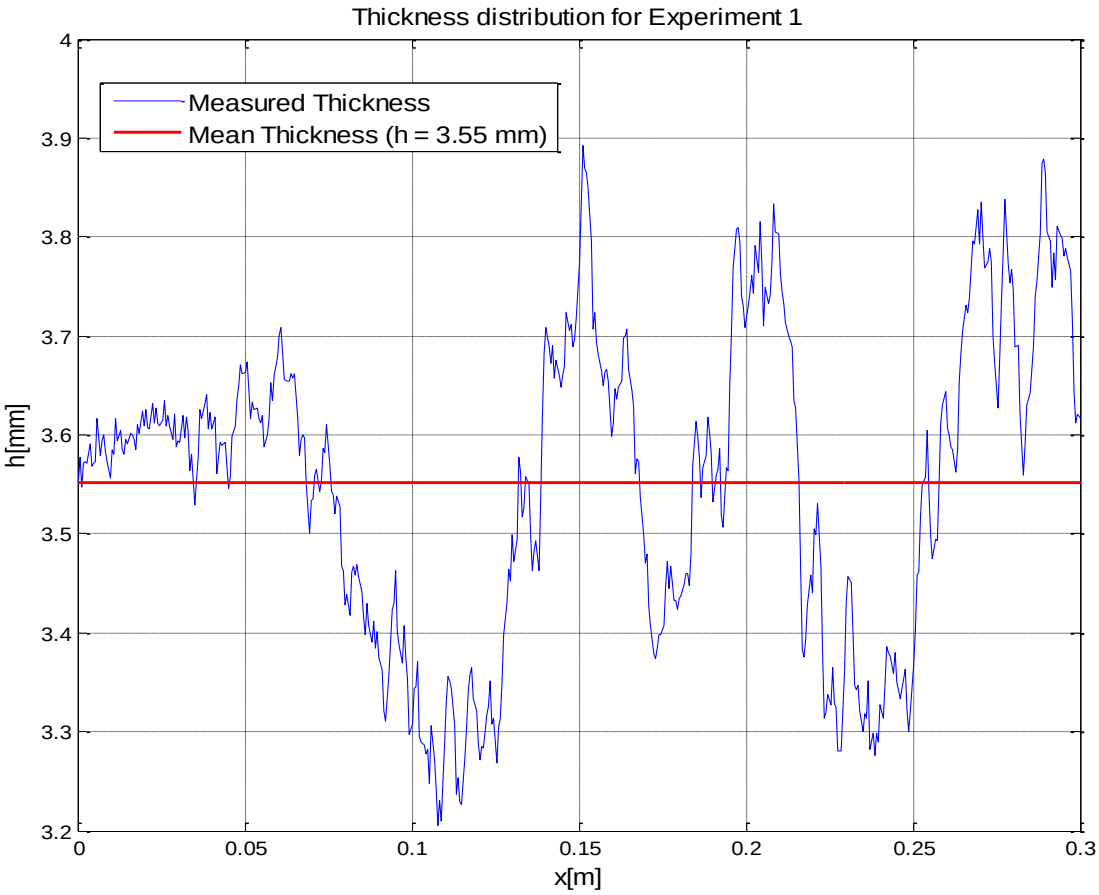

Figure 3.15 *Thickness distribution of the fabric preform at 80 kPa compaction pressure.*

3.3.2. The Pros and Cons of the RTM Setup

The pros and cons of this RTM setup can be listed as follows.

Pros:

- The thickness, h_{RTM} can be adjusted to a specific value readily by using the clamp system. Compared to conventional lab-scale RTM molds, which may have a set of spacer frames to change the thickness with a finite increment, in this study, h_{RTM}

does not have to be set to one of those incremental values. That means, continuously varying thickness can be set with good precision, and its accuracy can be controlled by using the dial gages.

- Transparent upper mold lid made of acrylic allows monitoring of resin flow. Thus, the validity of experiment (i.e., whether the flow front propagates as 1D, or not) can be visualized. Also, the resin arrival times to particular locations (x = 2, 4, 6, …, 28, 30 cm) are recorded for tracking purpose.
- Racetracking phenomenon is avoided in this mold setup. The vacuum bag covers the edges of the specimen very tightly due to vacuuming and tacky tape used in this approach. Thus, potential racetracking channels between the specimen and rigid walls in a conventional RTM mold are eliminated here. This also eliminates the requirement of tight dimensional tolerances during fabric cutting. However, one should still keep in mind that all the edges should be neat and overlapping; otherwise, the flow may not develop as 1D due to nonuniform density and effective permeability along the edges.

Cons:

- Tacky tape has to be peeled off and replaced with a new one before each experiment.
- h_{RTM} is set to the average thickness of the initial VI setup: $h_{RTM} = h_{VI,average} = \int_0^L h_{VI}(x,0)\,dx$. This approach causes a problem: some regions of the initial VI and RTM molds will have h(x,t) thinner than the average (statistically speaking, almost half of the length), whereas the other regions will be thicker than the average (see Figure 3.166). When the upper lid of the RTM mold is clamped to generate a fixed gap thickness, unfortunately, those thin sections will not be compacted by the upper lid. Thus, the effective thickness at those sections will not be exactly equal to $h_{VI,average}$. This may seem to form an unfair comparison between

VI and RTM. But, actually this approach is even better than having the specimen placed within a conventional RTM mold cavity (i.e., with no vacuum bag). Because, the two setups used here have the same initial compaction pressure (more fair treatment for the sake of comparison than in conventional RTM). More importantly, even if one considers this feature of the RTM mold setup (i.e., use of vacuum bag and applying vacuum within a doubled sided mold), the following fact should not be forgotten. As the flow front propagates in the mold cavity, the increasing local pressure in the resin-covered region causes decreasing the compaction pressure with time. Thus, the thickness will start increasing as it was observed in the literature [3]. But, due to the rigid upper mold, its thickness is limited to the desired average thickness. Therefore, even though this item is listed under the cons list here, it may even be considered as another pros item. At least, it is not a major shortcoming of the setup.

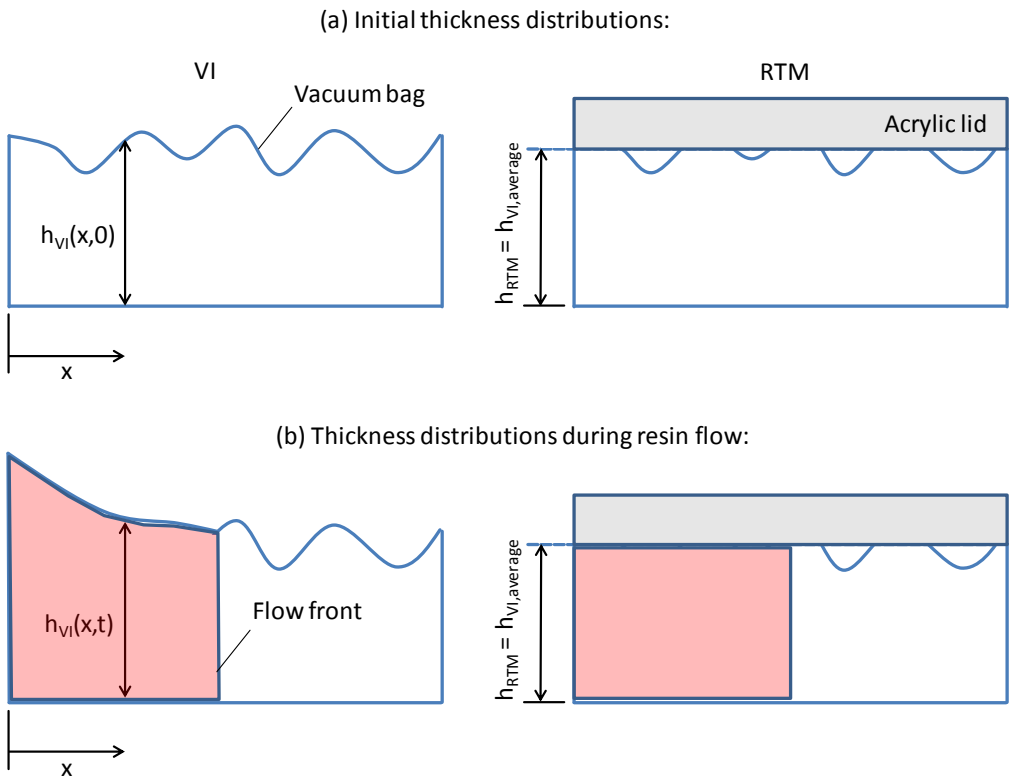

Figure 3.16 *The thickness distributions in the two setups: (a) at the beginning of the injection, and (b) during mold filling. Note that the drawing is not scaled, but exaggeratedly drawn to illustrate how the thickness evolves in both setups.*

3.3.3. Mold Filling Experiments

The injection of test fluid was started simultaneously in both setups. The flow front position, $x_f(t)$, was monitored by recording the arrival times to x = 0, 2, 4, …., 28, 30 cm. To investigate the statistical variation due to fabric preform preparation and placement, five sets of experiments were conducted, and an example of these experiments is presented in Figure 3.17. The rest of the results is given in Chapter 5 and Appendix B.

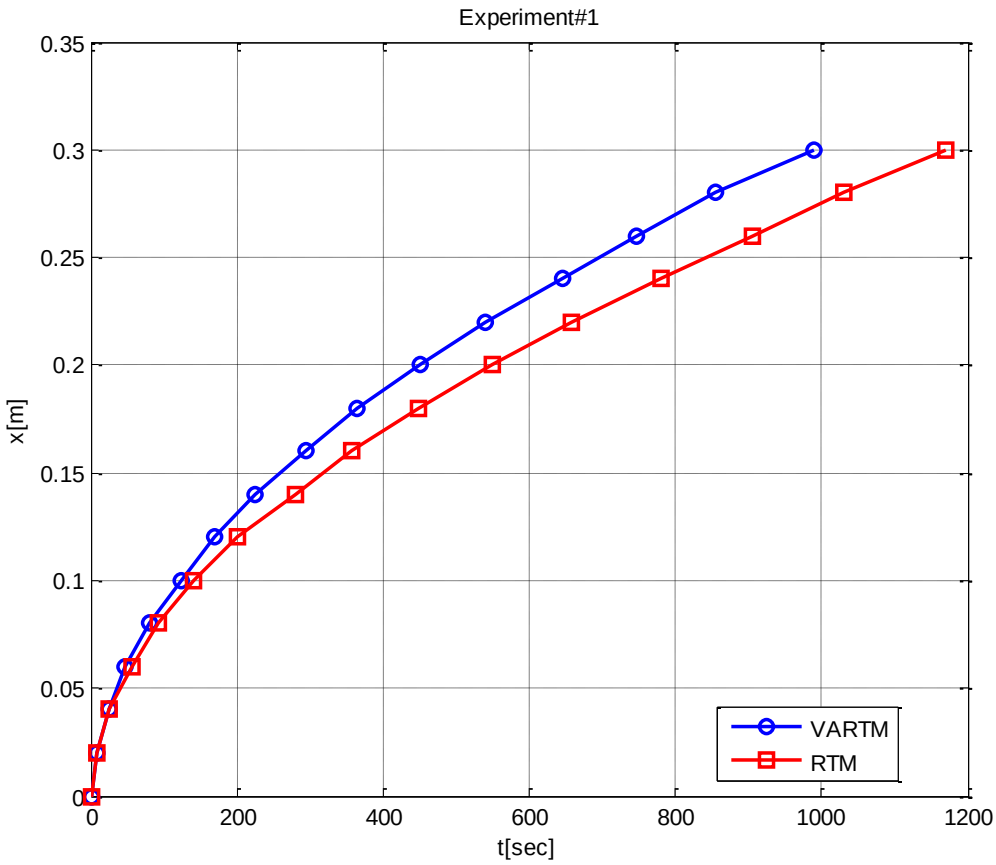

Figure 3.17 *Mold filling times for Experiment 1*

Part thickness in the VI setup, $h_{VI}(x,t)$, was monitored with time, and presented in Figure 3.18 at the instants of resin arrival times to L/4, L/2, and 3L/4 where L is the mold length which is 0.30 m.

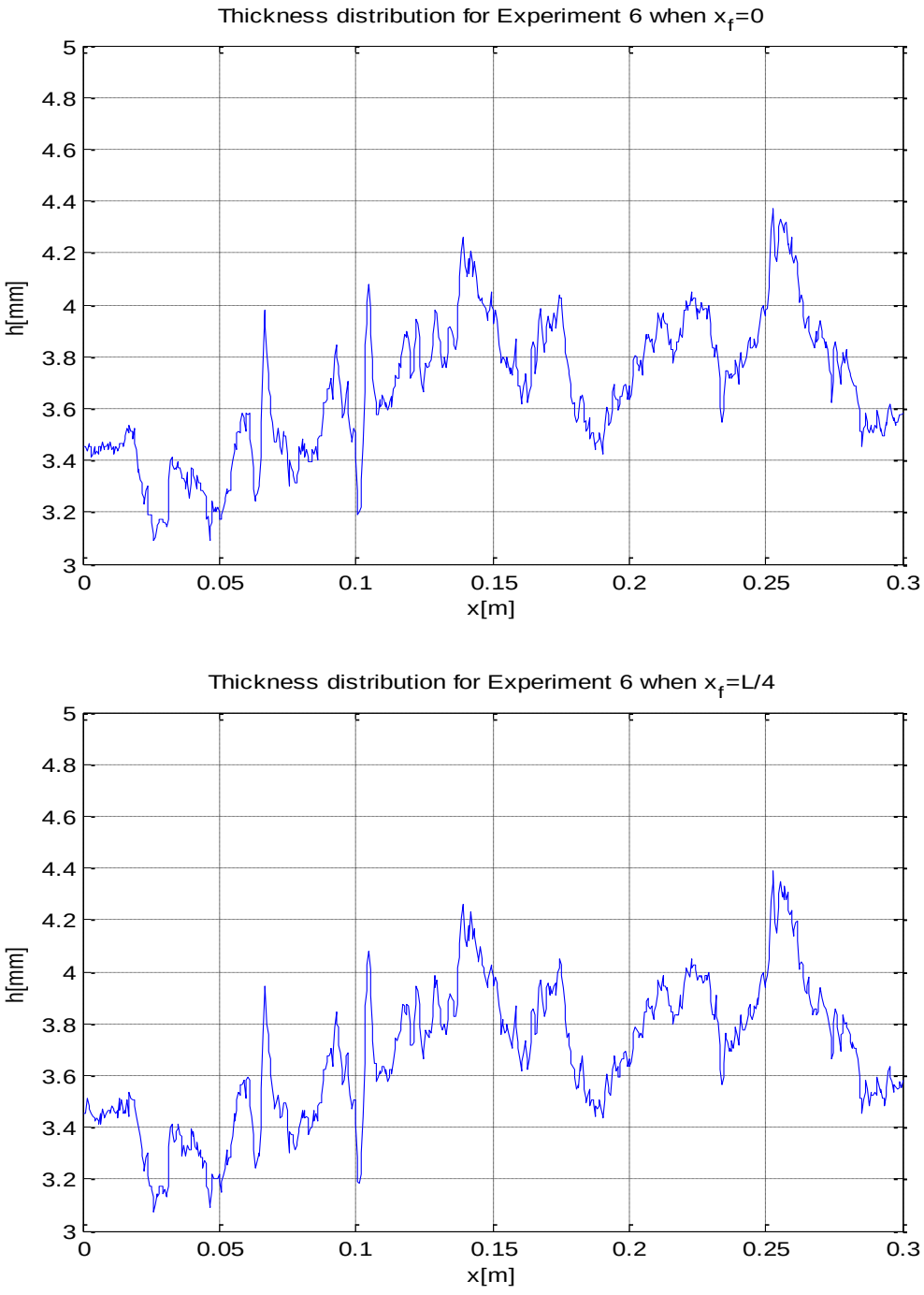

Figure 3.18 (continued on the next page) *Thickness measurement when the flow front reaches x_f = 0, L/4, L/2, 3L/4, and L*

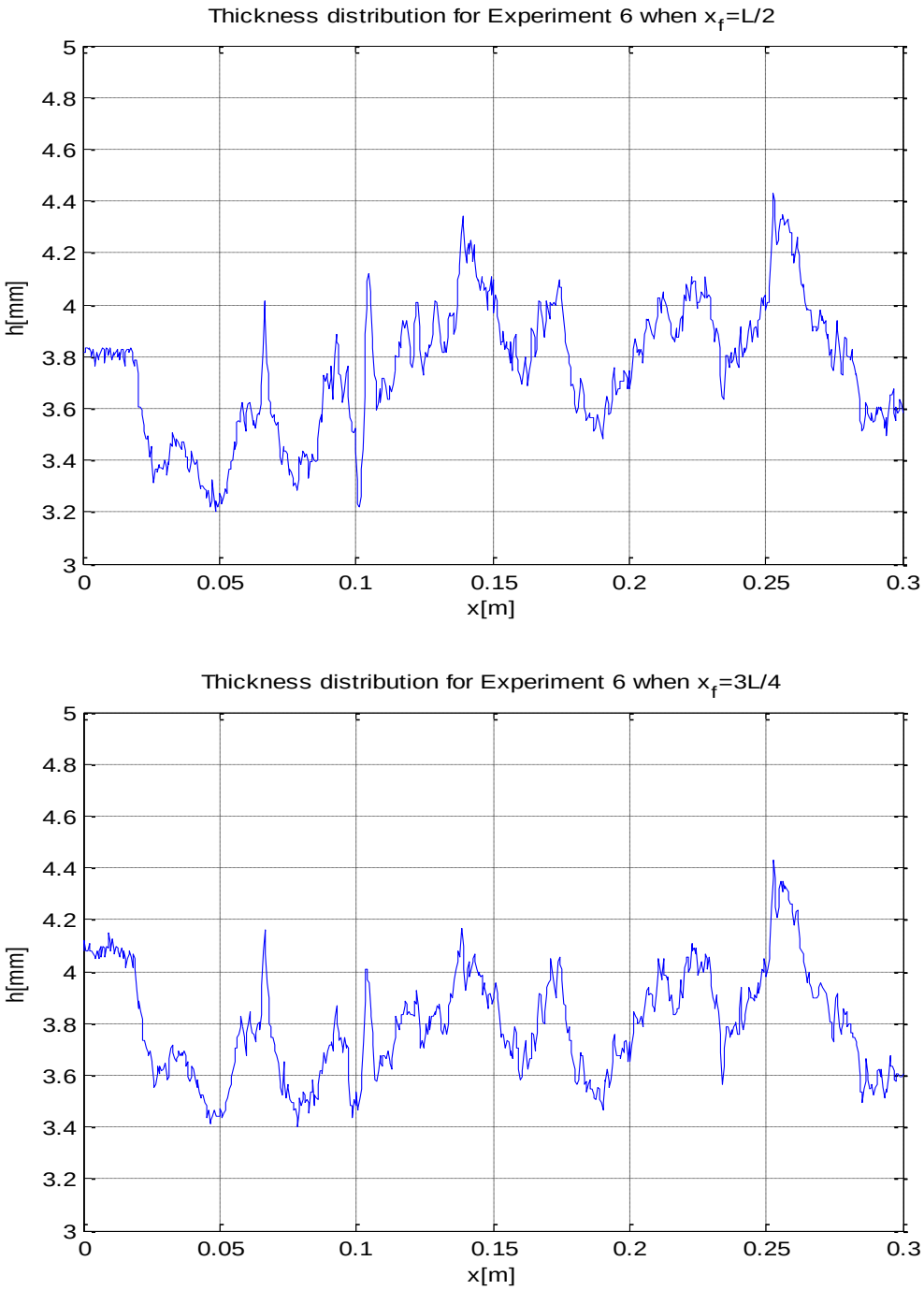

Figure 3.18 (continued on the next page) *Thickness measurement when the flow front reaches x_f = 0, L/4, L/2, 3L/4, and L*

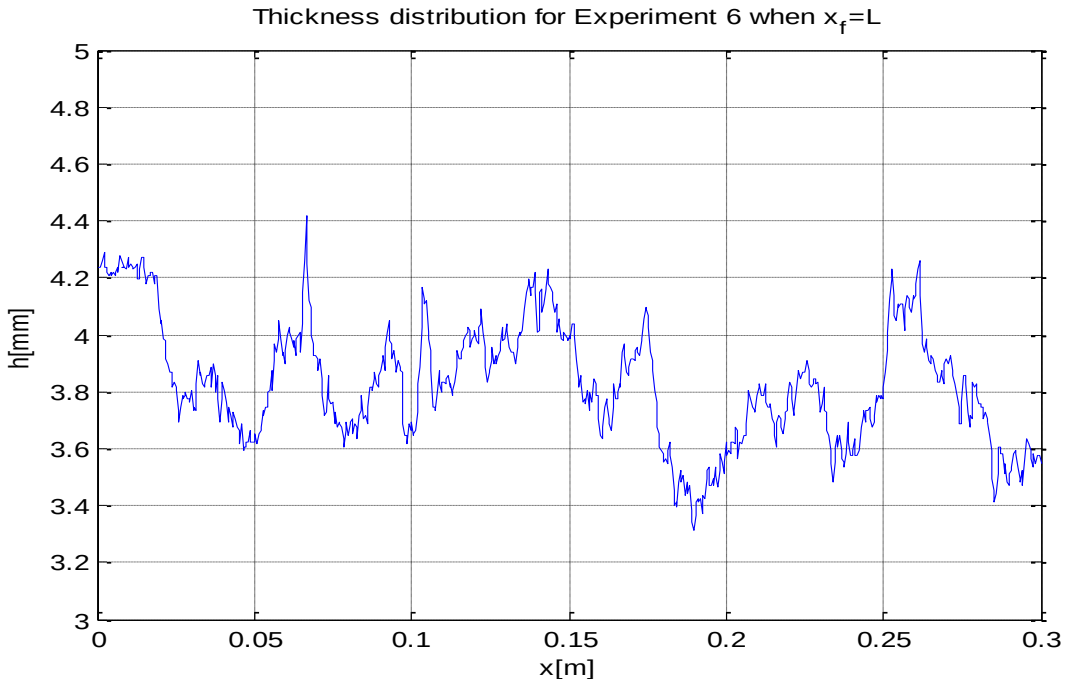

Figure 3.18 *Thickness measurement when the flow front reaches x_f = 0, L/4, L/2, 3L/4, and L*

4. Modeling

4.1. Modeling of the Mold Filling in VI

The VI process is modeled by using conservation of mass in an infinitesimal control volume (see Figure 4.1). It is assumed that the flow is one-dimensional in x direction, hence 1D Darcy law is used to calculate the velocity of the fluid flowing through the fabric preform.

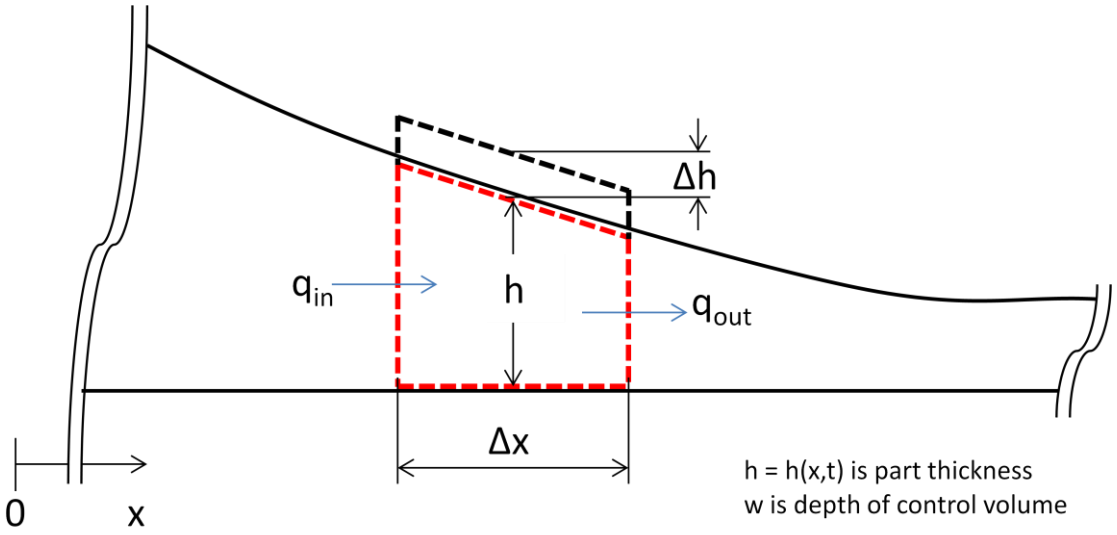

Figure 4.1 *Control volume for conservation of mass*

The conservation of mass equation in a control volume is given in Eq. 4.1.

$$\begin{aligned} \rho q_x - \rho q_{x+\Delta x} &= \rho \frac{\partial (hw\Delta x)}{\partial t} \\ &= \rho w \Delta x \frac{\partial (h)}{\partial t} \end{aligned} \qquad 4.1$$

Since ρ, w, and Δx are constants, they were taken out of $\frac{\partial ( )}{\partial x}$. Here $q_x = u_x h_x w$ and $q_{x+\Delta x} = u_{x+\Delta x} h_{x+\Delta x} w$. Substitutions result in Eq. 4.2.

$$\rho u_x h_x w - \rho u_{x+\Delta x} h_{x+\Delta x} w = \rho w \Delta x \frac{\partial h}{\partial t} \tag{4.2}$$

Dividing both sides of Eq. 4.2 by ρw results in

$$u_x h_x - u_{x+\Delta x} h_{x+\Delta x} = \frac{\partial h}{\partial t} \Delta x \tag{4.3}$$

Darcy law is used for the velocity terms, u_x and $u_{x+\Delta x}$,

$$\left(-\frac{K}{\mu} \frac{\partial P}{\partial x} \right)_x h_x - \left(-\frac{K}{\mu} \frac{\partial P}{\partial x} \right)_{x+\Delta x} h_{x+\Delta x} = \frac{\partial h}{\partial t} \Delta x \tag{4.4}$$

Equation 4.4is rewritten by leaving $\frac{\partial h}{\partial t}$ alone

$$\frac{\partial h}{\partial t} = \frac{1}{\mu \Delta x} \left[\left(Kh \frac{\partial P}{\partial x} \right)_{x+\Delta x} - \left(Kh \frac{\partial P}{\partial x} \right)_x \right] \tag{4.5}$$

As Δx approaches to zero, Eq. 4.5 becomes

$$\frac{\partial h}{\partial t} = \frac{1}{\mu} \frac{\partial}{\partial x} \left(Kh \frac{\partial P}{\partial x} \right) \tag{4.6}$$

Correia et al. [1] used Eq. 4.6 and derived a time independent model (Eq. 2.4) which was mentioned earlier in Chapter 2. In this study, it is assumed that the thickness change with respect to time is negligible compared to the terms on the right hand side of Eq. 4.6. Thus $\frac{\partial h}{\partial t}$ term in Eq. 4.6 is dropped, and it results in

$$\frac{\partial}{\partial x} \left(Kh \frac{\partial P}{\partial x} \right) = 0 \tag{4.7}$$

that means

$$Kh \frac{\partial P}{\partial x} \neq f(x) = \text{constant} \tag{4.8}$$

at all x locations. K is assumed to be a function of fiber volume fraction, V_f, and h is a function of compaction pressure, P_c.

Sarioglu [36] conducted permeability measurement experiments for the same fabric preform used in this study. Among four different methods, the one with constant pressure boundary condition mimics the VI process due to the injection boundary condition; and the corresponding results (see Figure 4.2) will be used here.

In that study, permeability, K was related to fiber volume fraction, V_f, by assuming an exponential fit:

$$K = Ce^{-DV_f} \tag{4.9}$$

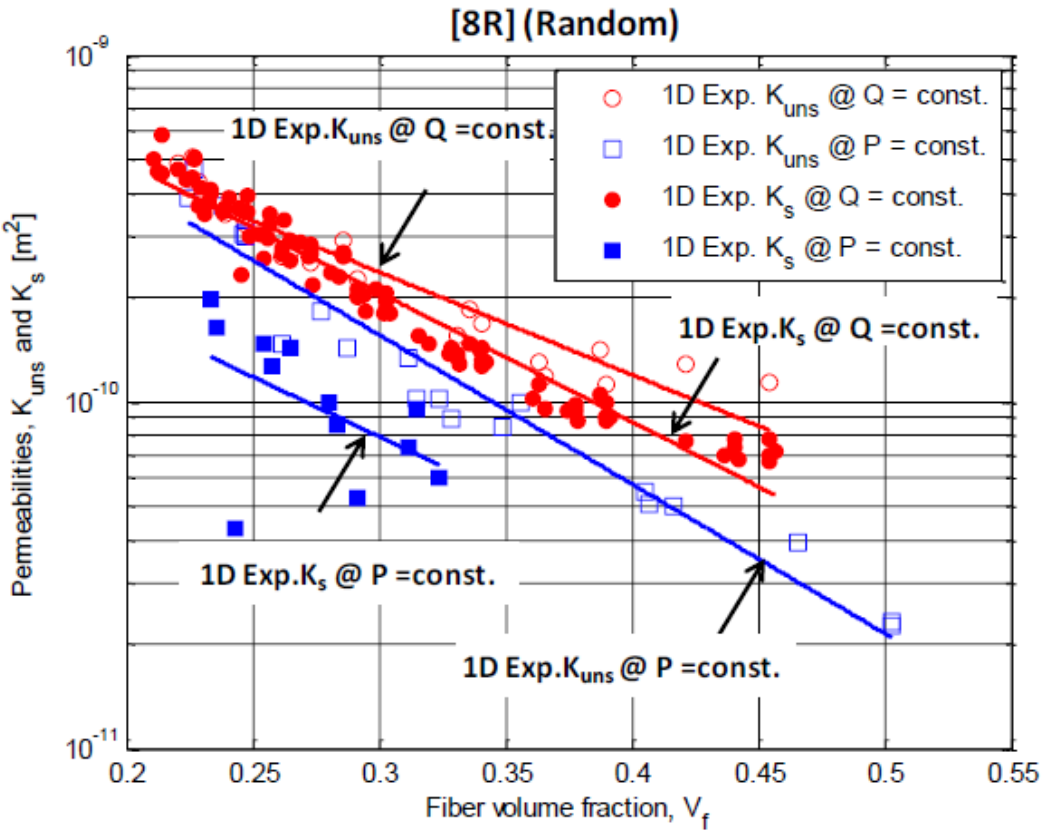

Figure 4.2 *Curve fit of experimental permeability values taken from Sarioglu's recent study [36]*

The constants C and D were calculated by using least square method; and they are tabulated in Table 4.2.

Thickness $h(x,t)$ and fiber volume fraction, $V_f(x,t)$ are related by using the following formula

$$h = \frac{N\rho_{\text{sup}}}{\rho_f}\frac{1}{V_f} \tag{4.10}$$

where N is the number of layers in the preform, ρ_{sup} is the superficial (a.k.a. areal) density of a single fabric layer, and ρ_f is the fiber density

V_f and compaction pressure, P_c, are related experimentally using specially designed compaction/decompaction characterization on specimens by mimicking different stages of VI.

As commonly used in the literature, P_c and V_f are empirically related by using an exponential function

$$P_c = Ae^{BV_f} \tag{4.11}$$

Constants A and B are determined as follows. By taking logarithm of both sides of Eq. 4.11 results in

$$\begin{aligned} V_f &= \frac{1}{B}\left[-\ln(A) + \ln(P_c)\right] \\ &= E + F\ln(P_c) \end{aligned} \tag{4.12}$$

where $E = -\ln(A)/B$ and $F = 1/B$.

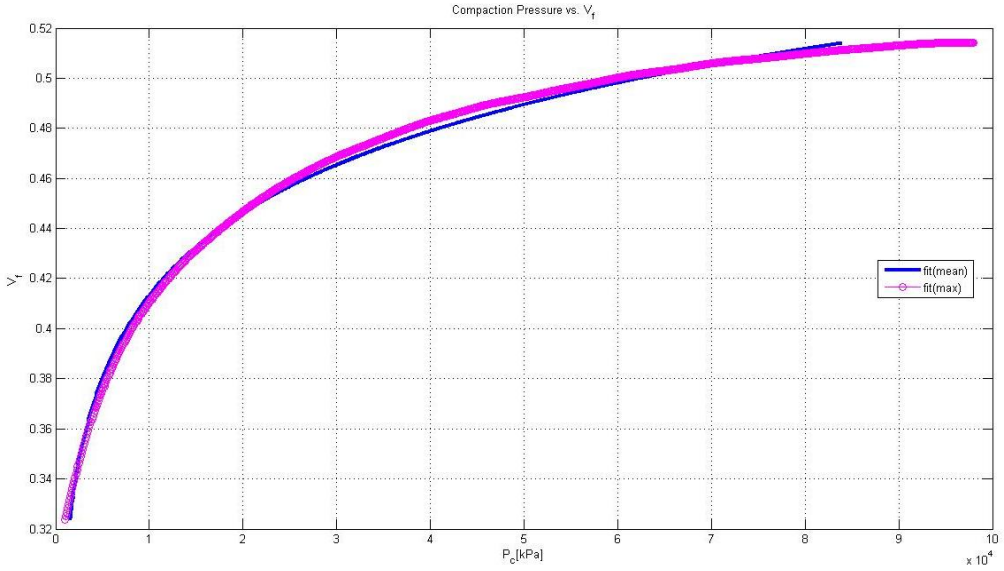

Figure 4.3 *Exponential curve fit of experimental compaction pressure and volume fraction data by Yenilmez* [38]

One can now apply least square method by using Matlab's built-in function polyfit after an algebraic transformation as done in Table 4.1. Recall that the experimental data is valid in the domain of $1kPa \le P_c \le 100kPa$.

Table 4.1 First order polynomial fit algortithm

$z = \log(P_c)$	log( ) is ln in Matlab	4.13
$U = polyfit(z, V_f, 1)$	The third argument, 1, is used for a 1st order polynomial fit; U is the vector containing the coefficients of polynomial fit	4.14
$F = U(1)$		4.15
$E = U(2)$		4.16
$B = 1/F$	see Table 4.2 for the values of A and B	4.17
$A = \exp(-D * B)$		4.18

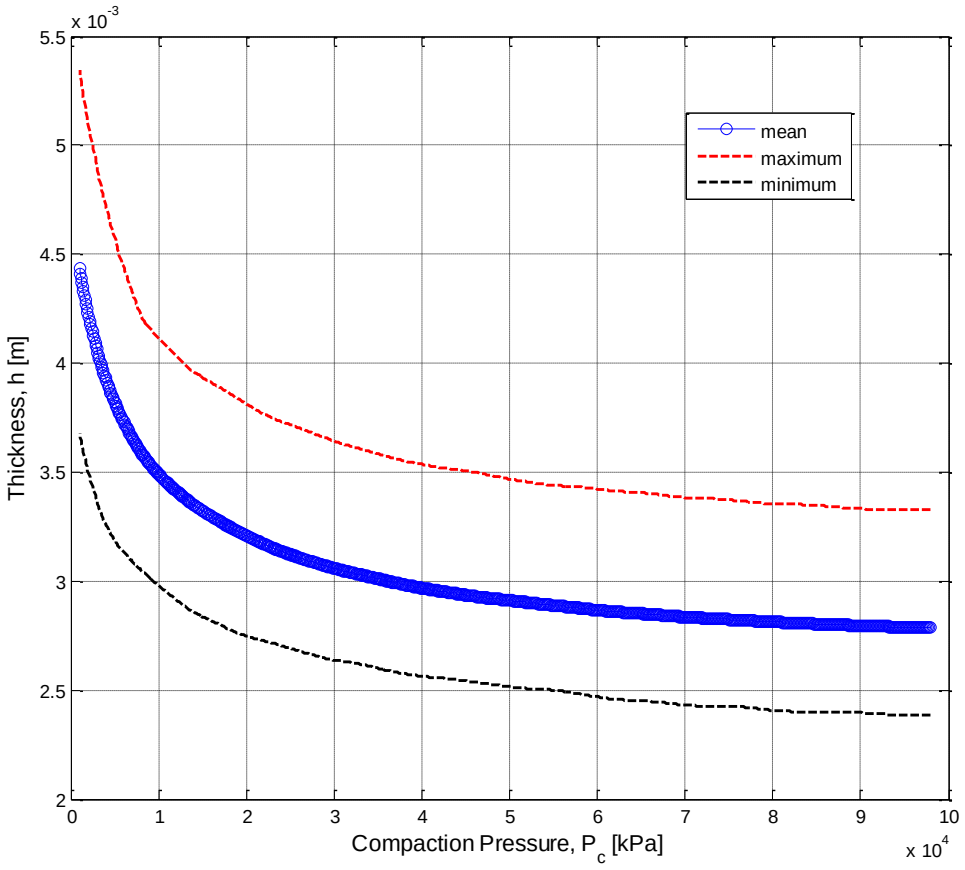

Figure 4.4 *Experimental compaction data of Yenilmez* [38]

Table 4.2 Emprical constants obtained by curve-fitting to experimental data of Sarioglu [36] and Yenilmez [38]

A	2.04 [kPa]
B	19.42
C	3.06e-9 [m^2]
D	9.91

4.2. Numerical Solution

Eq. 4.7 is solved at the end of mold filling by using finite difference method (FDM) in the 0.3 m preform which is divided into N equally-spaced nodes. Replacing the first order derivative, $\frac{\partial}{\partial x}\left(Kh\frac{\partial P}{\partial x} \right)$ with a central finite difference results in

$$\frac{\left(Kh\frac{\partial P}{\partial x} \right)_{i+1} - \left(Kh\frac{\partial P}{\partial x} \right)_{i-1}}{2\Delta x} = 0 \qquad 4.19$$

The pressure gradient term, $\frac{\partial P}{\partial x}$, is also expressed numerically using central finite difference

$$\left.\frac{\partial P}{\partial x}\right|_i = \frac{P_{i+1} - P_{i-1}}{2\Delta x} \qquad 4.20$$

Eq. 4.20 is substituted into Eq. 4.19, and the following expression is obtained for fluid pressure at node i

$$P_i = \frac{P_{i-2}(K_{i-1}h_{i-1}) + P_{i+2}(K_{i+1}h_{i+1})}{K_{i+1}h_{i+1} + K_{i-1}h_{i-1}} \qquad 4.21$$

For the elements i = 2 and i = N-1, forward and backward finite differences are used, respectively, to express $\frac{\partial P}{\partial x}$ term which result in the following

$$P_2 = \frac{1}{4}\left[\frac{K_2 h_2(-P_5 + 4P_4 - 3P_3)}{K_1 h_1} + P_3 + 3P_1 \right] \qquad 4.22$$

$$P_{N-1} = \frac{1}{4}\left[\frac{K_{N-2} h_{N-2}(-P_{N-4} + 4P_{N-3} - 3P_{N-2})}{K_N h_N} + P_{N-2} + 3P_N \right] \qquad 4.23$$

The numerical solution is used to obtain the pressure, permeability, thickness, and fiber volume fraction distributions at the end of the mold filling. The iterations are

continued as the term, $Kh\frac{\partial P}{\partial x}$, approaches to a constant value with a small error tolerance.

The results are seen in Figure 4.5.

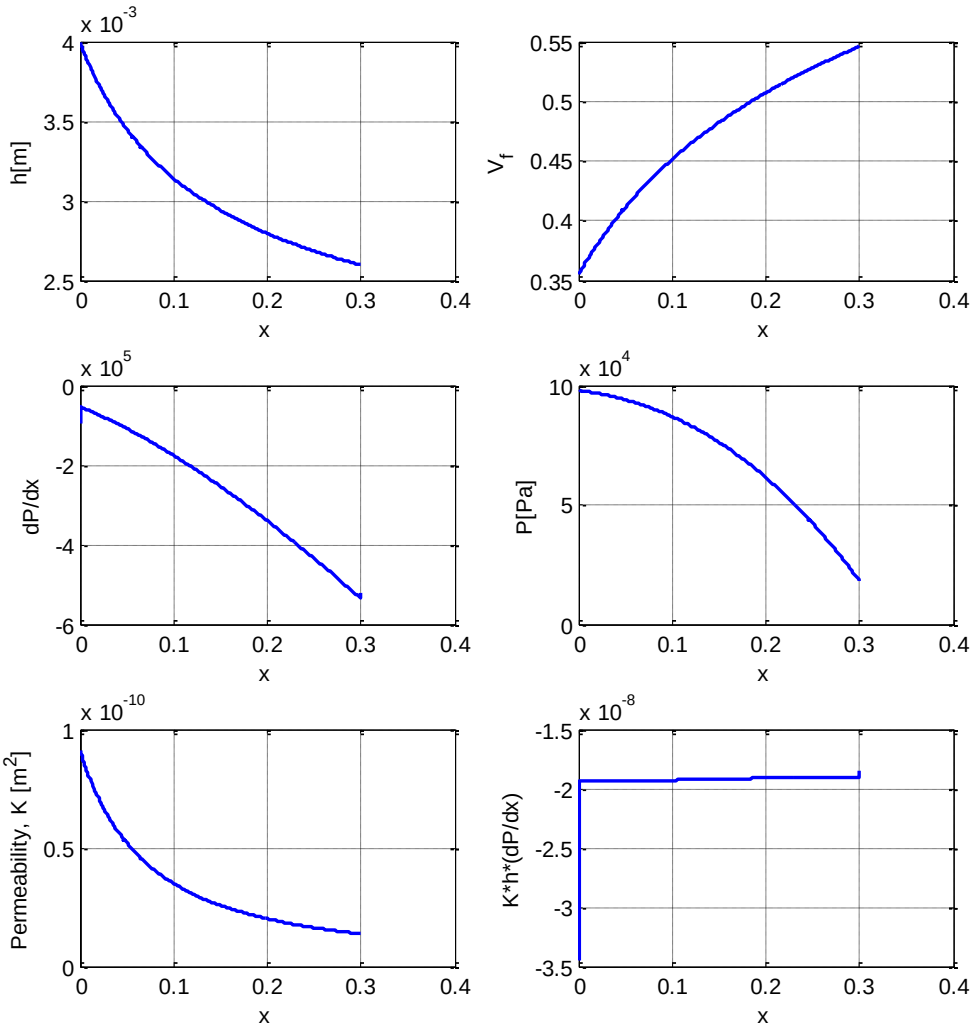

Figure 4.5 *K, h, dP/dx, V_f, P, and Kh(dP/dx) distributions at the end of mold filling*

The distributions of P, h, V_f, and K can be scaled in the x direction to the resin filled domain, $0 \le x \le x_f$, where x_f is the flow front position. That means, x domain

of $0 \le x \le 0.3\text{m}$ in Figure 4.5 is replaced with $0 \le x^* = \frac{x_f}{L} \le 1$ assuming that P, h, V_f, and K distributions in $0 \le \frac{x}{x_f} \le 1$ are constants at all times, similar to Correia et al.'s [1] conclusion. The flow front velocity is calculated using Darcy law since the term, $\frac{\partial P}{\partial x}$, is known at $x = x_f$. The scaling is applied to all elements by using the built in function, "spline", of Matlab as follows

Table 4.3 Algorithm for use of spline function of Matlab

$S = x_f / L$	Eq. 4.24
$P_{resinfilled} = spline\,(S * x, P_{moldfill}, x_{resinfilled})$	Eq. 4.25
$P_{dry} = P_{vent}$	Eq. 4.26

Here $P_{resinfilled}$ is the fluid pressure distribution in the wetted region of the preform, $P_{moldfill}$ is the fluid pressure distribution at the mold filling, P_{dry} is the pressure in the dry region.

As seen in Figure 4.6, one can calculate pressure gradient at the flow front, $x = x_f$, using finite difference, and use it to calculate the time step to advance the flow front from $x_f = x_i$ to $x_f = x_{i+1}$ by using the following algorithm:

Flow front velocity, u_{f_i}, is calculated as follows:

$$u_i = -\left(\frac{K_i}{\mu} \frac{\partial P}{\partial x} \right)\Bigg|_i \qquad 4.27$$

where,

$$u = u_f \phi \rightarrow u_f = \frac{u}{\phi} = \frac{u}{1-v_f} \tag{4.28}$$

$$u_{f_i} = -\frac{K_i}{\mu \phi_i}\left(\frac{\partial P}{\partial x}\right)_i \tag{4.29}$$

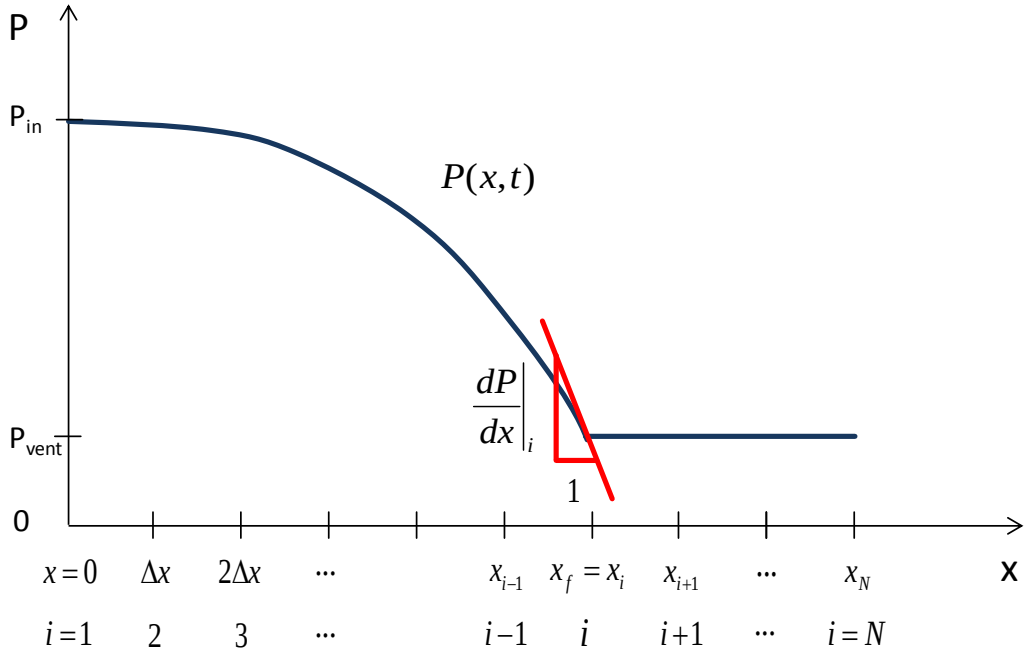

Figure 4.6 $P(x,t)$ and $\left.\frac{\partial P}{\partial x}\right|_{x_f}$

Note that $\left.\frac{\partial P}{\partial x}\right|_{x_f}$ is needed to calculate the speed of flow front.

Eq. 4.29 is re-written in terms of finite difference formula:

$$u_{f\,i} = -\frac{K_i}{\phi u_i}\left(\frac{-P_{i-2} + 4P_{i-1} - 3P_i}{2\Delta x}\right) \tag{4.30}$$

$$\Delta t_{x_f : x_i \rightarrow x_{i+1}} = \frac{\Delta x}{u_{f_i}} \tag{4.31}$$

The error in finite difference term in Eq. 4.30 is large at early stages of mold filling because of smaller number of data points in x vs P curve. Instead of using Eq. 4.30, the following approach was used.

Using the pressure distribution at the end of mold filling which was calculated by using the numerical solution presented in this chapter;

$$\left.\frac{dP_{moldfill}}{dx}\right|_{i=N} = \frac{-P_{moldfill_{i-2}} + 4P_{moldfill_{i-1}} - 3P_{moldfill_i}}{2\Delta x} \tag{4.32}$$

$$u_{f_N} = -\frac{K_N}{\phi\mu_N}\left(\frac{-P_{moldfill_{N-2}} + 4P_{moldfill_{N-1}} - 3P_{moldfill_N}}{2\Delta x}\right) \tag{4.33}$$

During resin flow, i.e., when $x_f = x_i \neq x_N$;

$$u_{f_i} = u_{f_N}\frac{L}{x_f} \tag{4.34}$$

Note that we start the simulation with $x_f = x_3$; otherwise $\frac{1}{x_f}$ will be singular at $x_1 = 0$.

By using a numerical time integration with a time step given in Eq. 4.31, the evolution of *h*, *K*, *P*, and P_c are tracked until $x_f = x_i = x_N$.

The evolution of graphs are given in Figure 4.7 at times corresponding to $x_f = \frac{1}{4}L, \quad \frac{1}{2}L, \quad \frac{3}{4}L,$ and L.

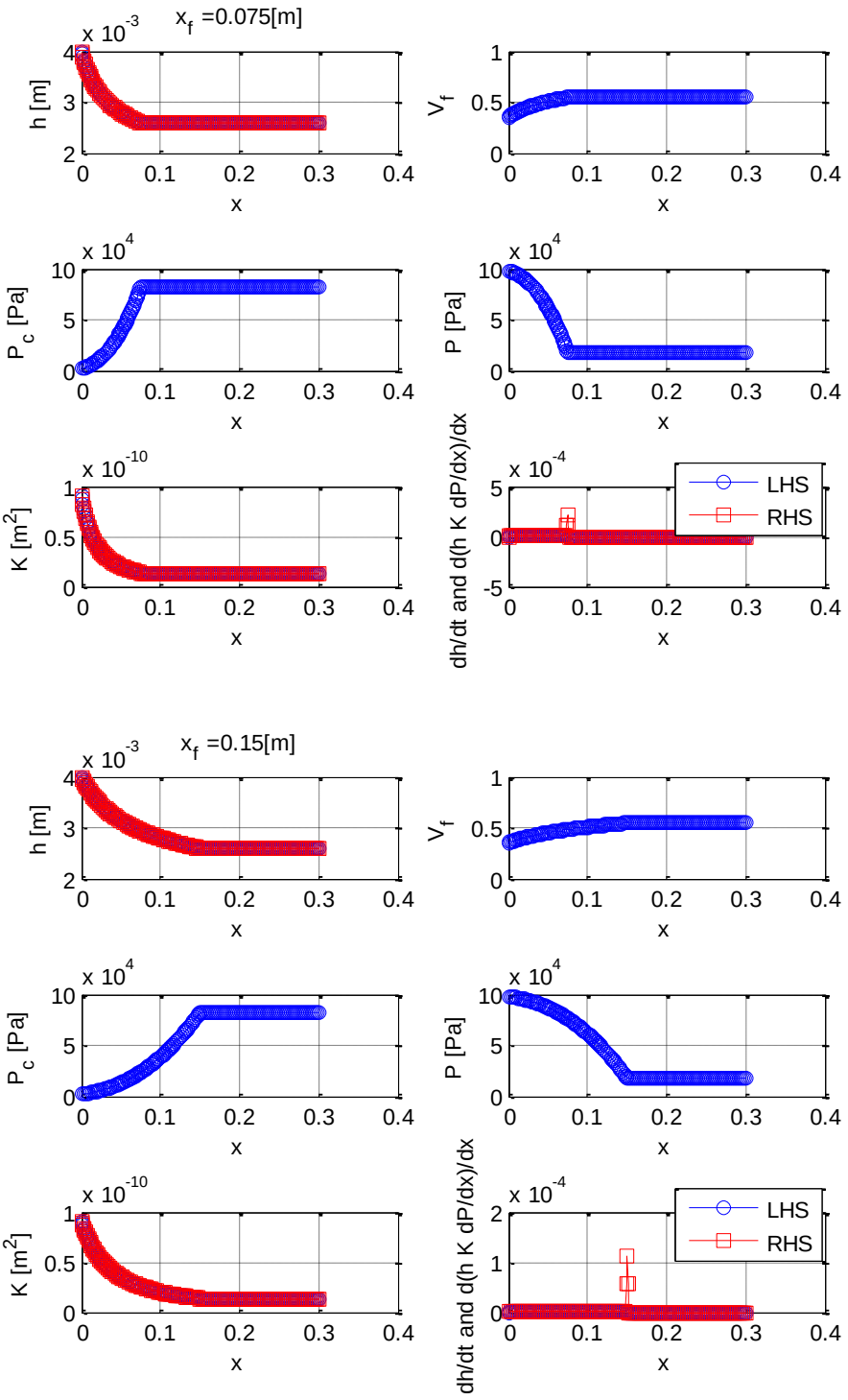

Figure 4.7 *(continued on the next page) Evolution of h, V_f, P, P_c, and K at x = L/4, L/2, 3L/4, and L*

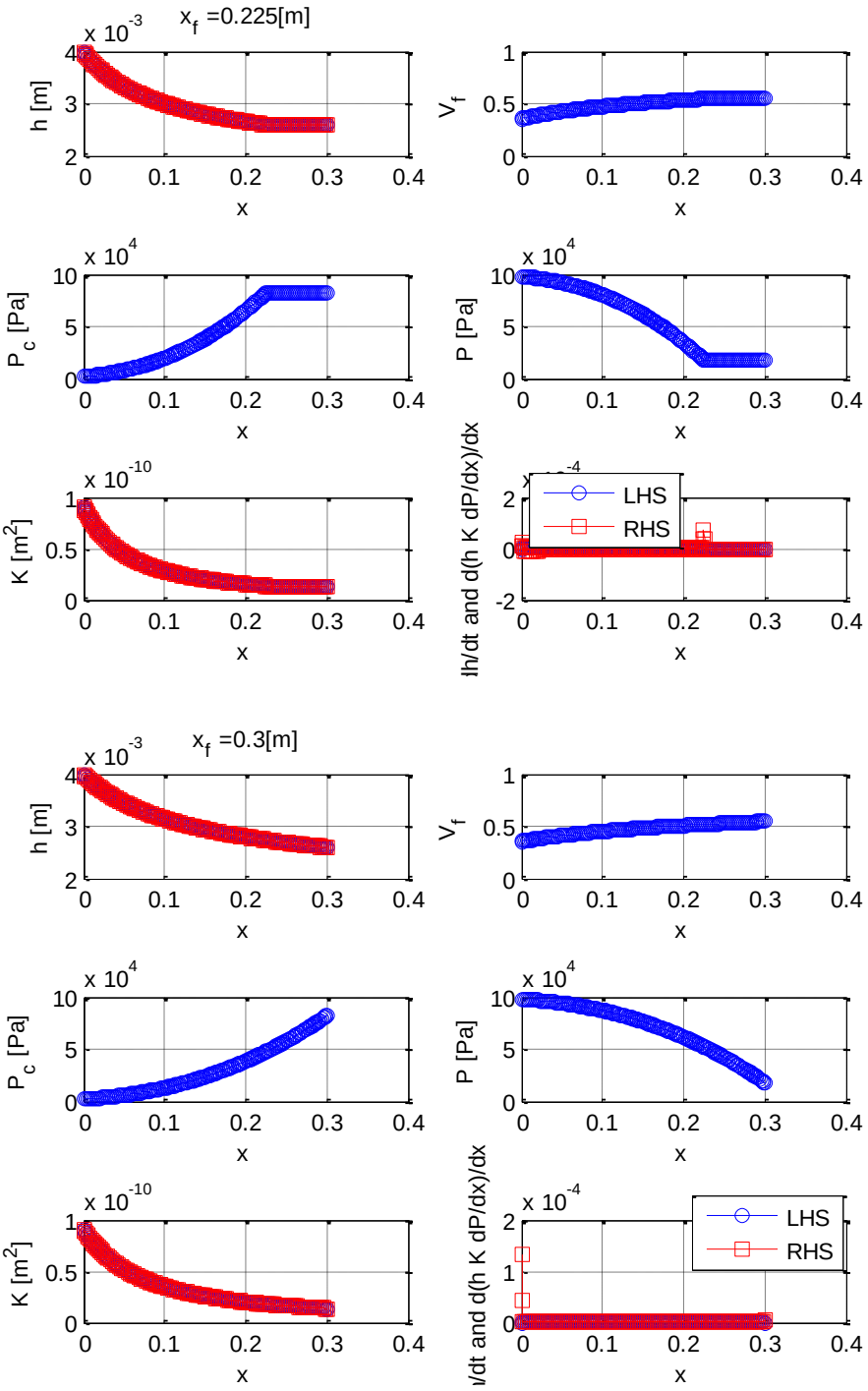

Figure4.7 *Evolution of h, V_f, P, P_c, and K at x = L/4, L/2, 3L/4, and L*

4.3. Analytical Solution for Mold Filling Time in RTM

The analytical formulation for the mold filling time for RTM process is derived by using Darcy law which is given in Eq. 2.5 [39]. In Darcy law, $\frac{\partial P}{\partial x}$ can be expressed as $\frac{P_{exit} - P_{inlet}}{x_f}$ because the injection pressure is constant and the fluid pressure is linearly distributed along the wetted region. Thus, Darcy law can be written as

$$u = -\frac{K}{\mu}\frac{P_{exit} - P_{inlet}}{x_f} \tag{4.35}$$

The flow front velocity, u_f, can be expressed as

$$\begin{aligned} u_f &= \frac{u}{\phi} = -\frac{K}{\phi\mu}\frac{P_{exit} - P_{inlet}}{x_f} \\ &= \frac{dx_f}{dt} \end{aligned} \tag{4.36}$$

Eq.4.36 is rearranged as follows

$$\frac{dx_f}{dt} = -\frac{K}{\phi\mu}\frac{P_{exit} - P_{inlet}}{x_f} \tag{4.37}$$

Eq. 4.37 is rearranged as

$$x_f\, dx_f = -\frac{K(P_{exit} - P_{inlet})}{\phi\mu}\, dt \tag{4.38}$$

The mold filling time, t_{fill}, is obtained by integration of Eq. 4.38.

$$\int_0^L x_f\, dx_f = \int_0^{t_{fill}} -\frac{K(P_{exit} - P_{inlet})}{\phi\mu}\, dt \tag{4.39}$$

$$\frac{{x_f}^2}{2} - \frac{0^2}{2} = -\frac{K(P_{exit} - P_{inlet})}{\phi\mu} t_{fill} - 0 \tag{4.40}$$

$$t_{fill} = -\frac{L^2 \phi \mu}{2K(P_{exit} - P_{inlet})} \qquad 4.41$$

5. Results

5.1. Results of the Experiments

Five sets of experiments are conducted and the results are given in Table **5.1**.

Table 5.1 Experimental mold filling times of experiments 1 to 5

Position [m]	Time [s]									
	Experiment 1		Experiment 2		Experiment 3		Experiment 4		Experiment 5	
	VI	RTM	VI	RTM	VI	RTM	VI	RTM	VI	RTM
0	0	0	0	0	0	0	0	0	0	0
0.02	9	8	9	12	13	12	21	22	9	8
0.04	25	25	21	32	27	26	41	46	25	25
0.06	47	56	48	64	55	55	72	82	47	56
0.08	81	92	82	105	90	91	110	125	81	92
0.1	123	140	120	155	133	138	160	185	123	140
0.12	169	200	175	217	185	195	212	252	169	200
0.14	225	279	230	290	249	260	276	336	225	279
0.16	294	357	310	373	323	333	352	422	294	357
0.18	365	448	395	461	400	422	430	525	365	448
0.2	450	550	505	562	487	515	518	625	450	550
0.22	540	658	605	675	580	626	613	755	540	658
0.24	645	780	725	793	690	740	716	885	645	780
0.26	746	905	850	918	800	880	825	1032	746	905
0.28	855	1030	985	1055	925	990	946	1187	855	1030
0.3	990	1170	1110	1180	1025	1150	1085	1323	990	1170

The mean values of the experiments are plotted in Figure 5.1. In this figure the maximum and the minimum values of resin arrival times are also shown.

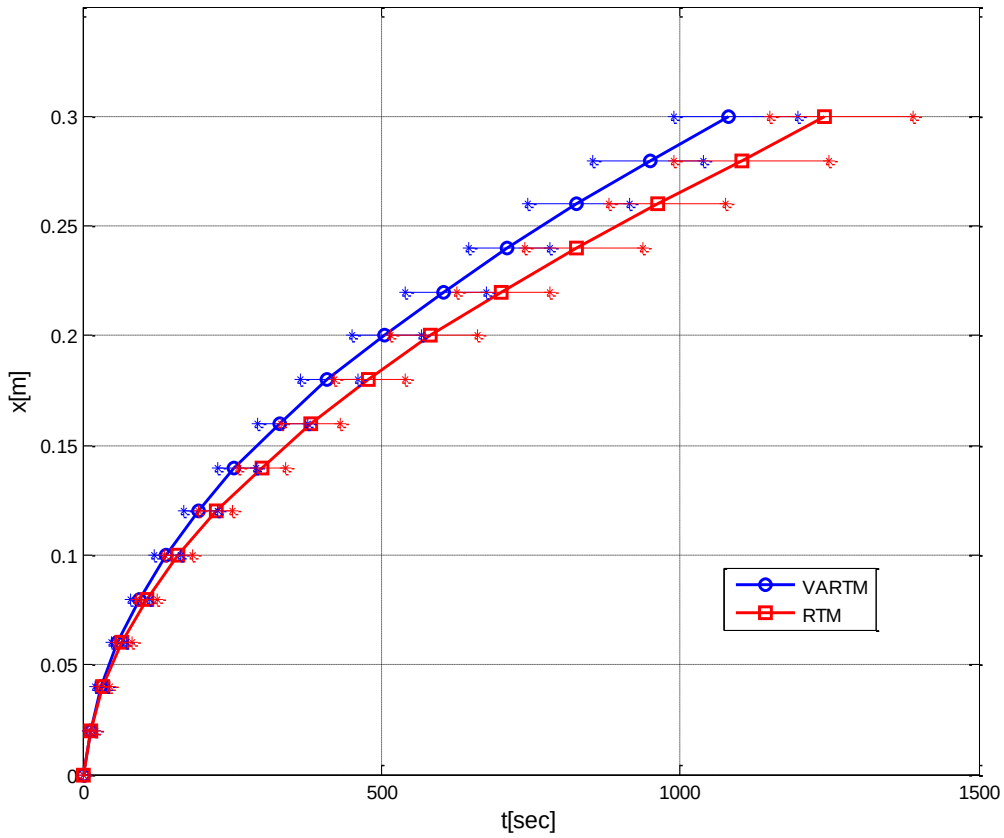

Figure 5.1 *Flow front propagation in VI and RTM setup for experiments 1 to 5*

The solid lines are the mean values of the five experiments; and the maximum and minimum of the resin arrival times are also shown with the horizontal bars.The results of the experiments show that VI mold filling times are always shorter than RTM mold filling times. The difference between the average mold filling times is 13 %.

5.2. Results of the Model

Using the numerical model explained in Chapter 4 in combination with the permeability and compaction data taken from Sarıoğlu [36] and Yenilmez [38], a result for the mold filling time in VI is obtained. On the other hand, the analytical solution given in Chapter 4 is used to calculate the mold filling time in RTM. The flow front position vs. time graph is shown in Figure 5.2.

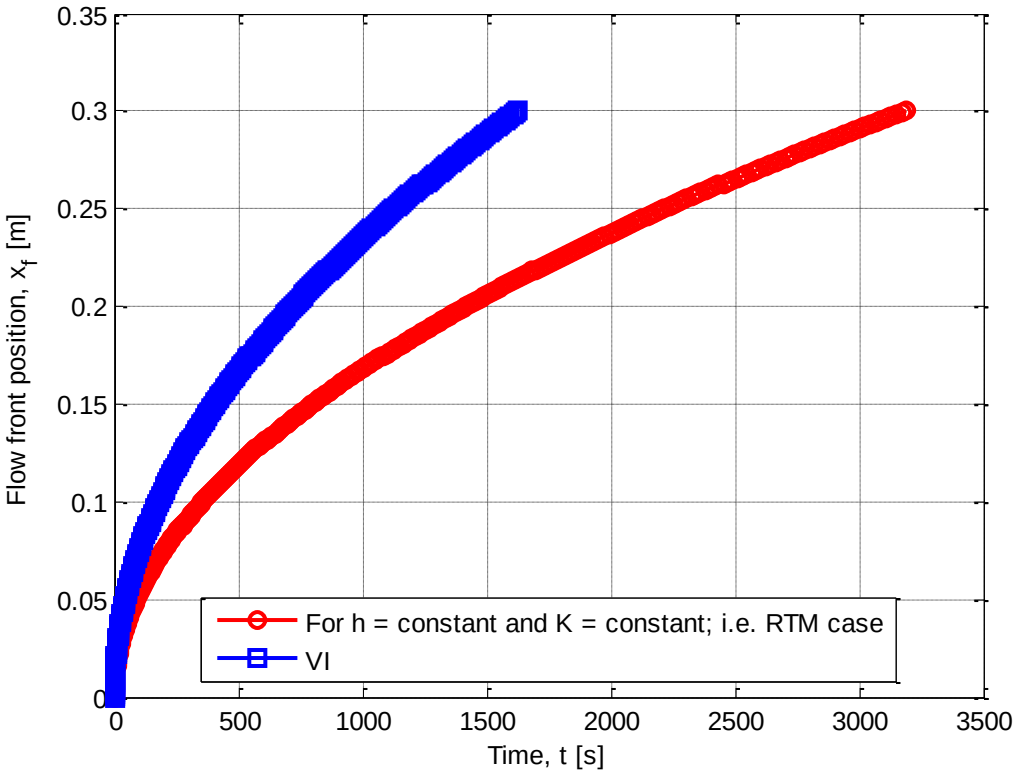

Figure 5.2 *Numerically obtained results for the mold filling times in VI and RTM using the compaction data of Yenilmez*[38]

The difference in the experimental average mold filling time is 13% (i.e., $(t_{fill_{RTM}} - t_{fill_{VI}}) / t_{fill_{RTM}} = 0.13$). Calculated filling time for VI and RTM is 1626 and 3191 seconds respectively which corresponds to a difference of 49%.

The experimental results for mold filling are normalized with respect to the average mold filling time in RTM. The model is also normalized with the same approach. Figure 5.3 and 5.4 shows the dimensionless flow front position versus time.

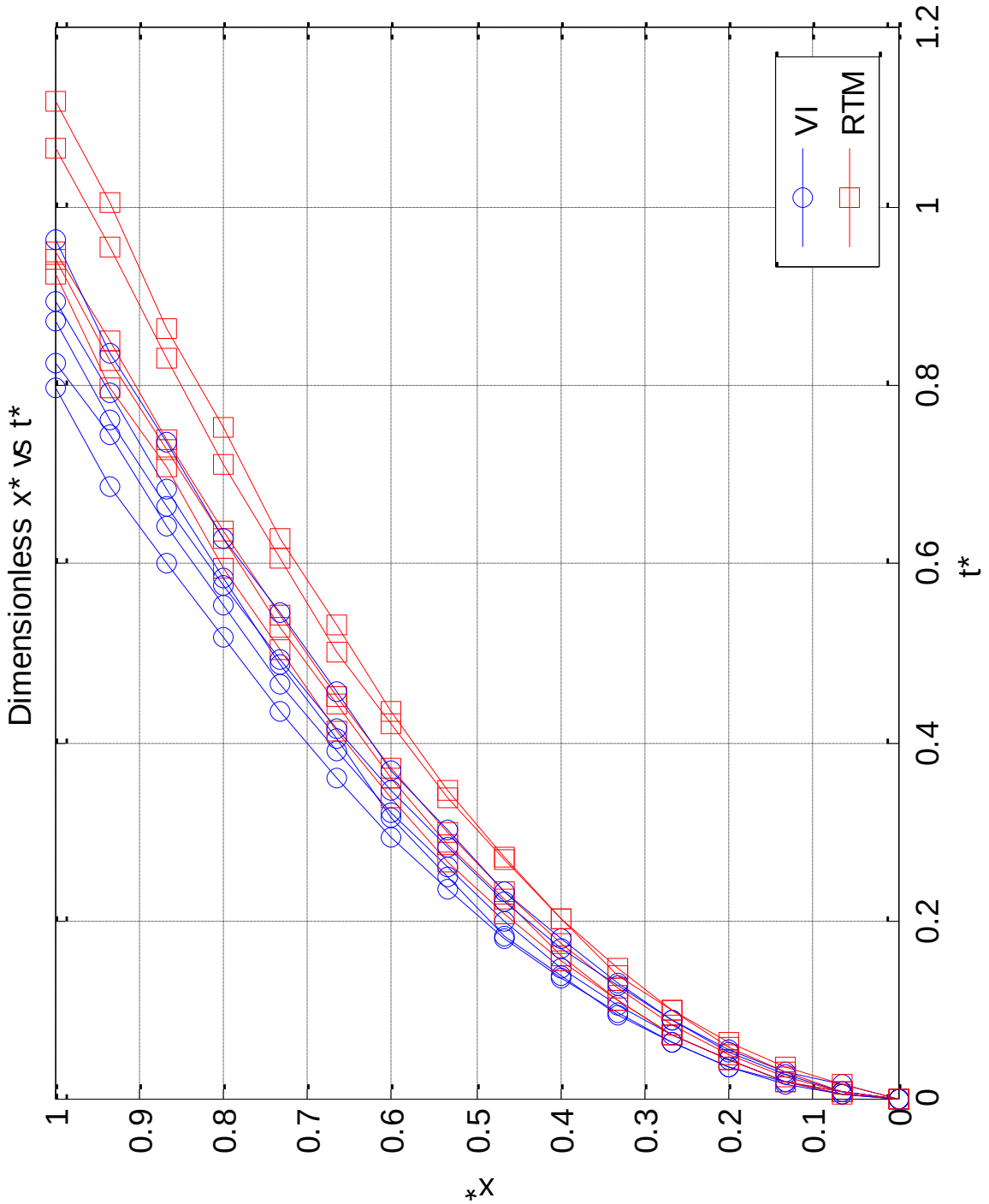

Figure 5.3 *Normalized experimental flow front propagation for experiments 1 to 5*

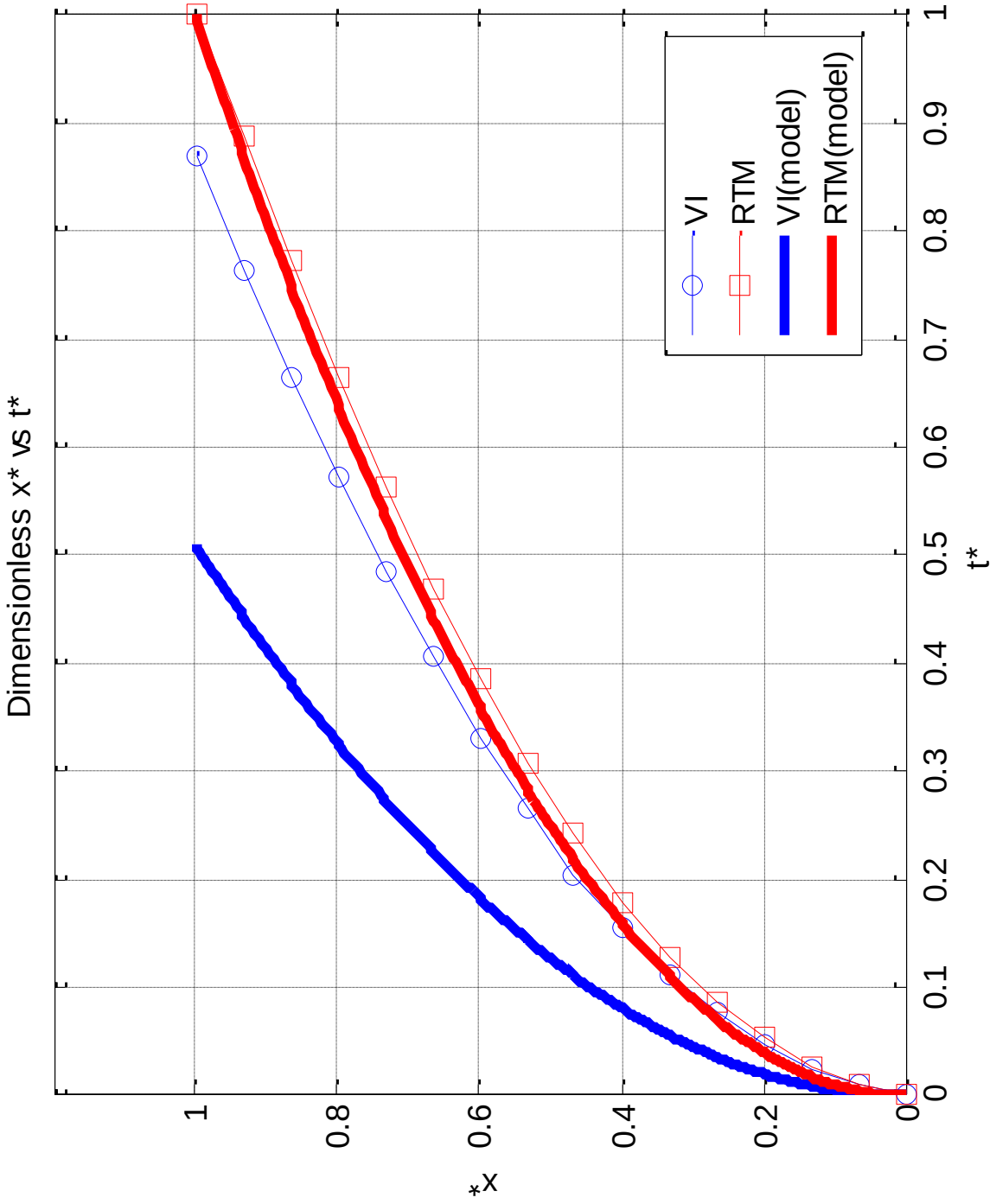

Figure 5.4 *Normalized average mold filling times and model results using the compaction data of Yenilmez [38]*

5.3. Use of the VI Experimental Setup for Compaction Characterization Experiments

In the previous chapters and sections, it was illustrated that the VI setup and the thickness scanner system were successfully used to do the followings: (1) measure the thickness distributions before and during the resin injection; and (2) monitor the resin propagation and thus determine the mold filling time.

Recall that in the earlier chapters and sections of this study, compaction database of Yenilmez [38] was used in the coupled model of flow and compaction. Here in this section, it will also be shown that this straightforward design of the system (i.e., the mold, vacuuming with pressure regulator, and thickness scanner) allows performing one more important task additional to the two items given in the previous paragraph; (3) conducting compaction characterization experiments on the dry fabric specimen as described below.

- After vacuuming the VI mold at its highest level (approximately zero vacuum pressure which corresponds to approximately 100 kPa compaction pressure on the specimen) for a while (10 minutes), then h is scanned and the compaction pressure is reduced to 80 kPa controlling the pressure regulator via a PC.
- At Pc = 80 kPa, the thickness, h is scanned using the scanner system, and recorded. An example of the thickness measurement at Pc = 80 kPa is shown in Figure 5.5.

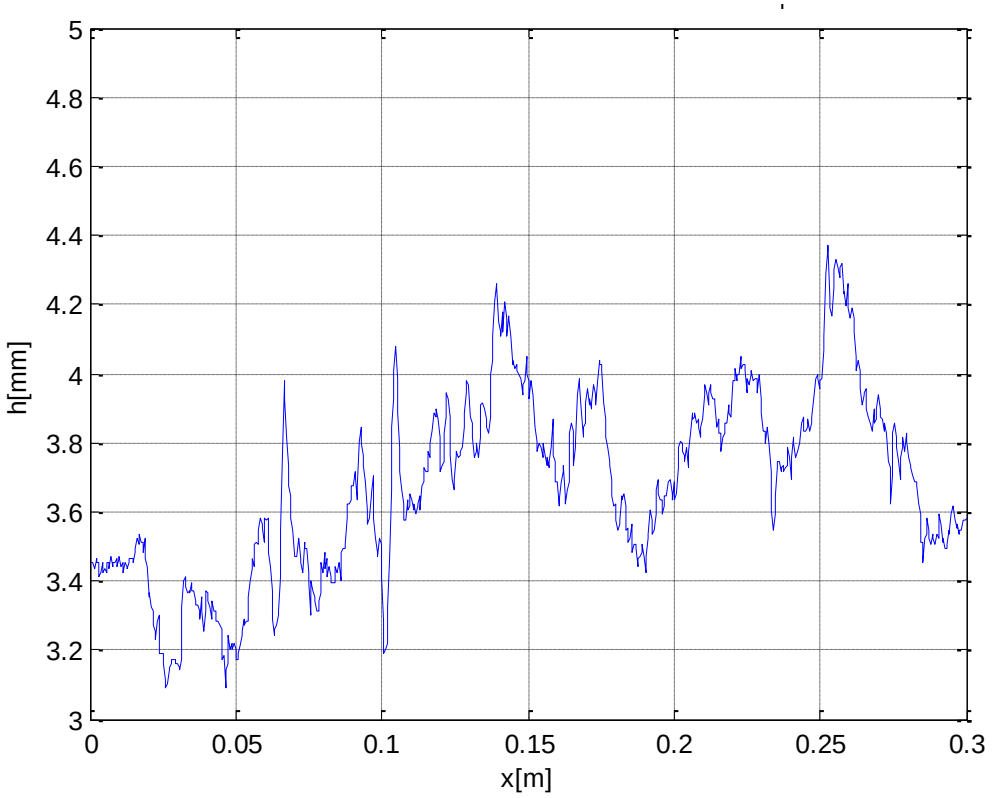

Figure 5.5 *Thickness measurement at Pc = 80 kPa*

- The thickness scanning step is repeated after adjusting the compaction pressure to 78, 76, 74, … , 6, 4, 2, 1 kPa. In Figure 5.6 and 5.7, an example for a compaction characterization experiment is shown. The rest of the figures for experiments is given in Appendix B.

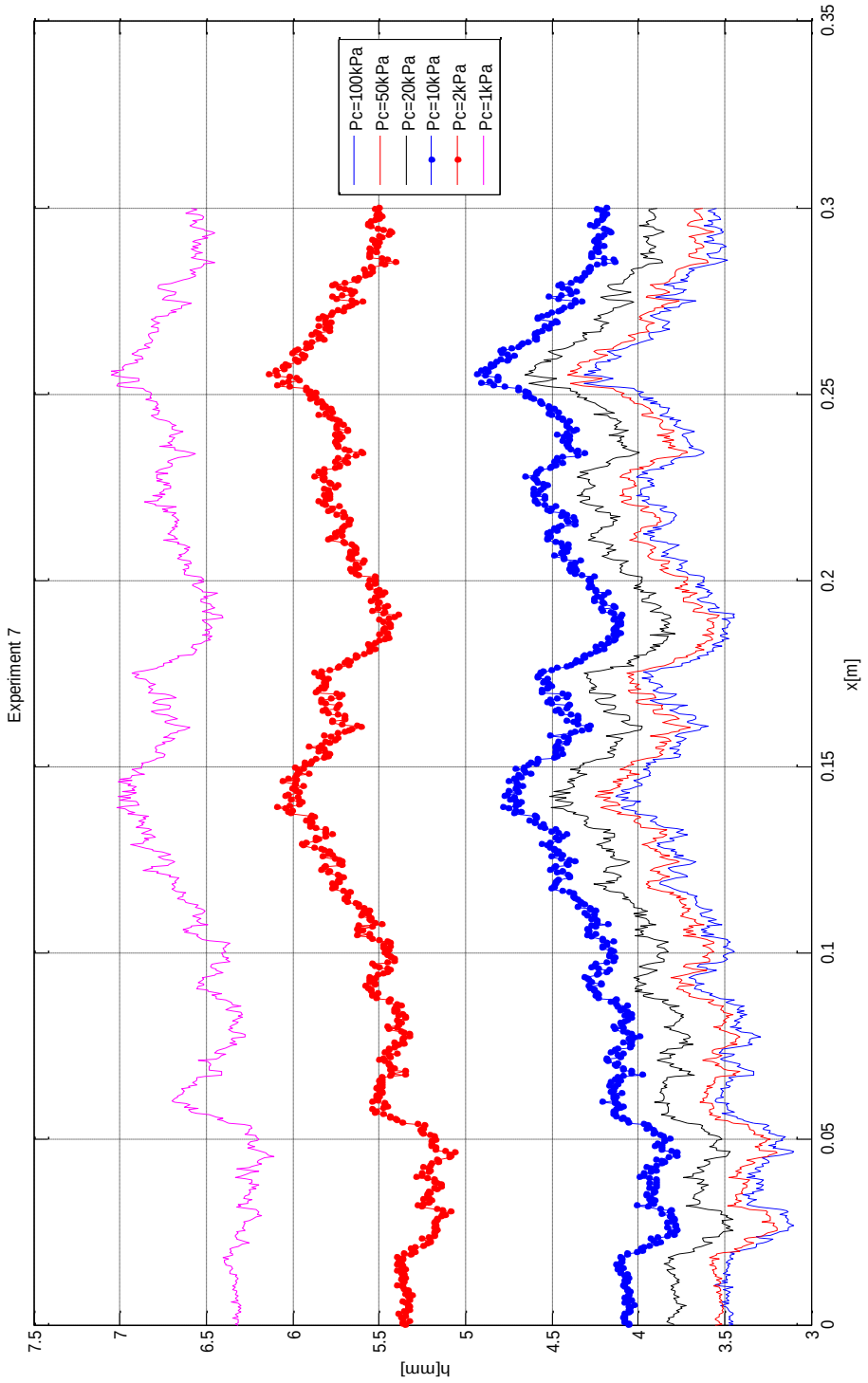

Figure 5.6 *Change in thickness as the compaction pressure decreases from 80 to 1kPa*

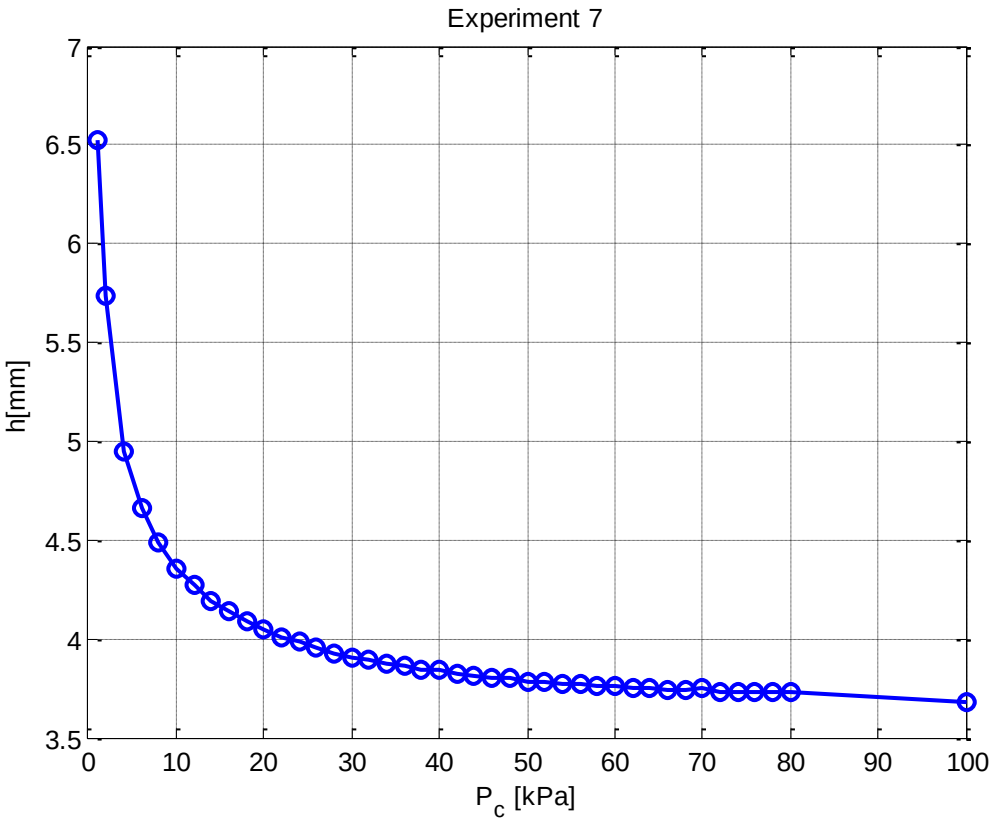

Figure 5.7 *Compaction Characterization Experiment*

- The compaction database is constructed in the PC; and it will be used to determine the two constants in the empirical compaction formula used earlier, $P_C = Ae^{BV_f}$. Figure 5.8 shows the experimental data and the curve fit.

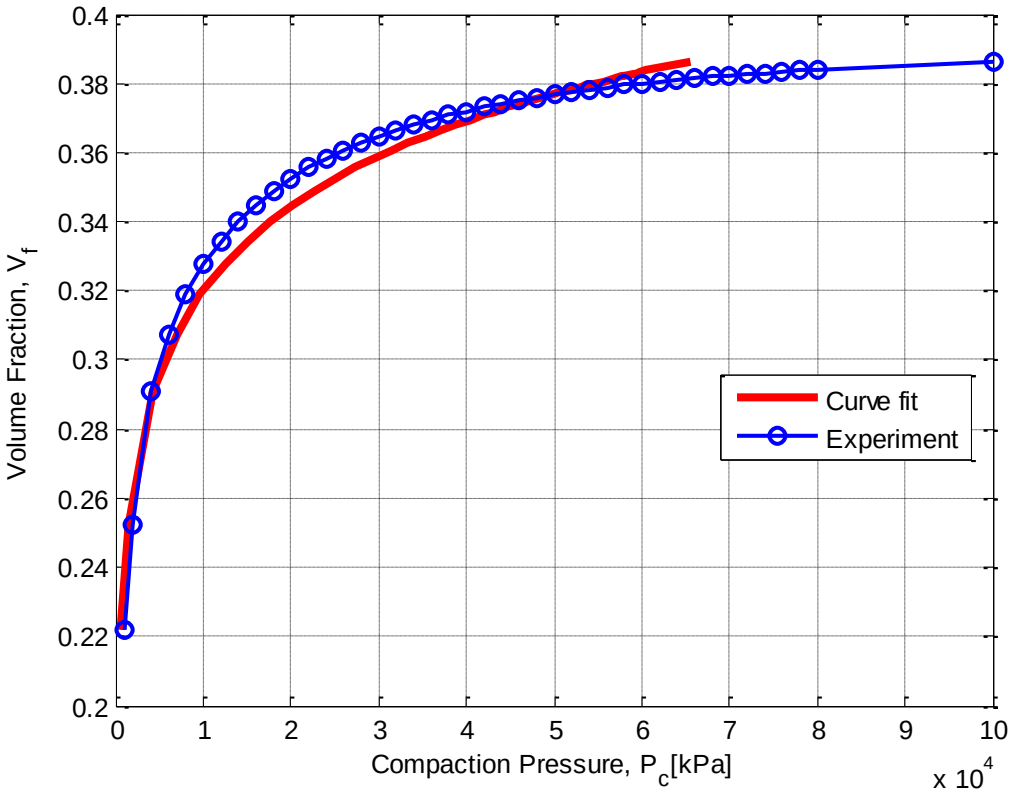

Figure 5.8 *Exponential curve fit of experimental compaction pressure and volume fraction data obtained in five compaction experiments*

Using the compaction experiments which are conducted as explained above, the constants A and B are calculated as 1.14 [kPa] and 28.35, respectively. These constants are implemented in the Matlab code and the following results which are shown in Figures 5.9 and 5.10 are obtained.

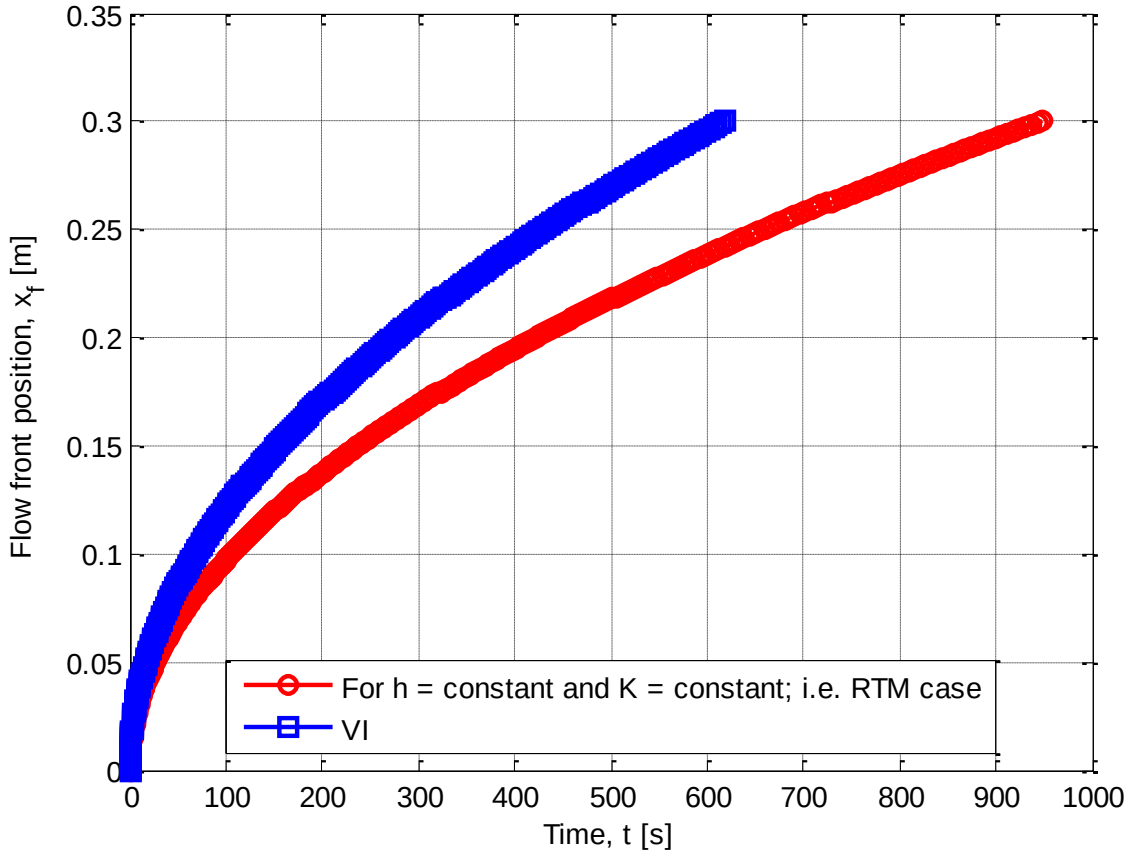

Figure 5.9 *Numerically obtained results using the compaction experiments of the setup used in this study (A=1.14 [kPa], B=28.35)*

Calculated filling time for VI and RTM is 619 and 949 seconds respectively which corresponds to a difference of 35%.

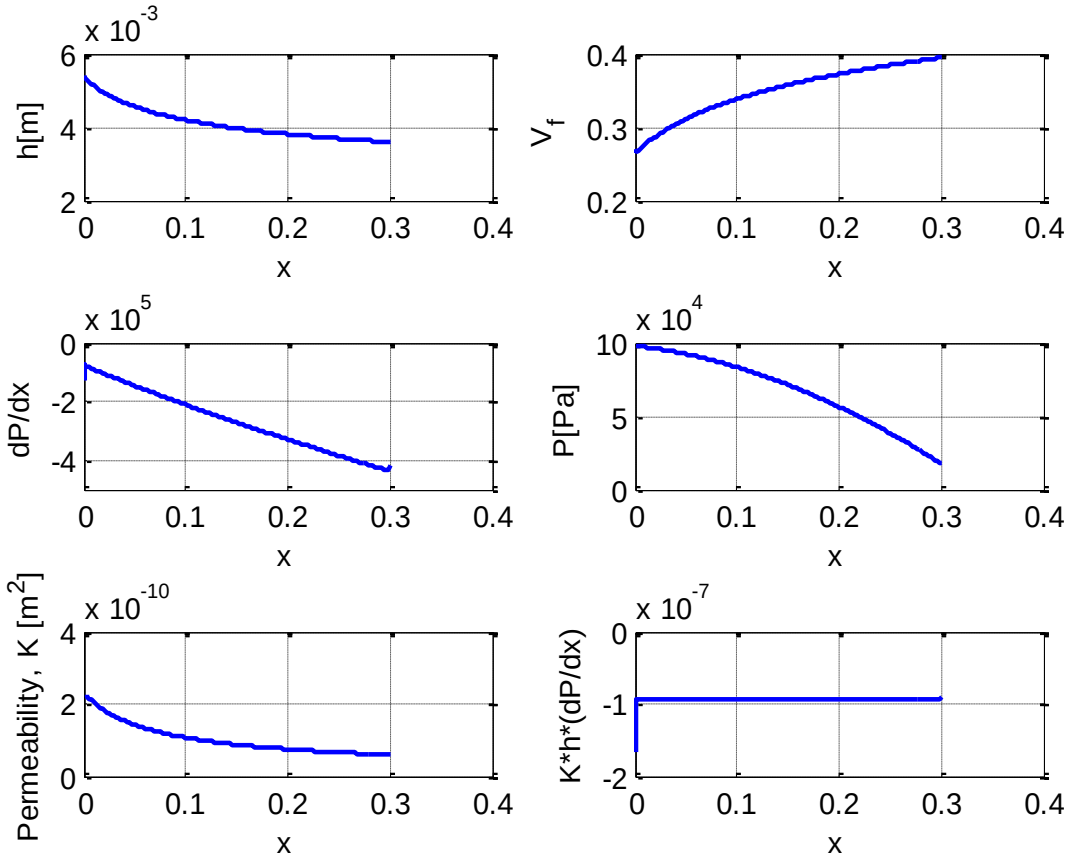

Figure 5.10 *K, h, dP/dx, V_f, P, and Kh(dP/dx) distributions at the end of mold filling using the constants derived in compaction experiments*

After conducting the compaction experiments, injections are made and five more mold filling experiments are performed. The results are presented in Table 5.2 and Figure 5.11. Notice that the major difference between this set of five experiments and the previous set of five experiments is that, here the compaction characterization was performed in such a way that the fabric perform is compacted from zero to 100 kPa during the loading stage, and then the unloading stage was continued in a compaction pressure domain of 80-1 kPa. Differently in the previous section, the loading stage had been conducted in a domain of 0-80 kPa, but not 0-100 kPa.

Table 5.2 Experimental mold filling times of experiments 6 to 10

Position [m]	Time [s]									
	Experiment 6		Experiment 7		Experiment 8		Experiment 9		Experiment 10	
	VI	RTM	VI	RTM	VI	RTM	VI	RTM	VI	RTM
0	0	0	0	0	0	0	0	0	0	0
0.02	12	11	10	9	10	11	13	14	9	15
0.04	33	33	47	40	29	37	34	38	28	43
0.06	61	68	88	81	58	73	67	77	55	86
0.08	102	115	140	129	99	120	111	132	93	138
0.1	150	172	202	195	150	170	166	195	140	205
0.12	207	248	270	260	200	243	230	275	192	285
0.14	283	332	352	348	273	325	313	363	263	375
0.16	366	423	452	453	362	427	395	470	334	485
0.18	460	535	550	555	455	545	493	575	416	590
0.2	573	652	663	685	565	680	590	705	517	720
0.22	687	789	782	815	678	807	732	837	610	850
0.24	818	939	910	955	800	962	835	990	725	1000
0.26	953	1093	1044	1104	920	1120	957	1140	840	1150
0.28	1096	1266	1195	1267	1054	1290	1084	1316	964	1315
0.3	1232	1476	1318	1405	1195	1427	1218	1552	1110	1497

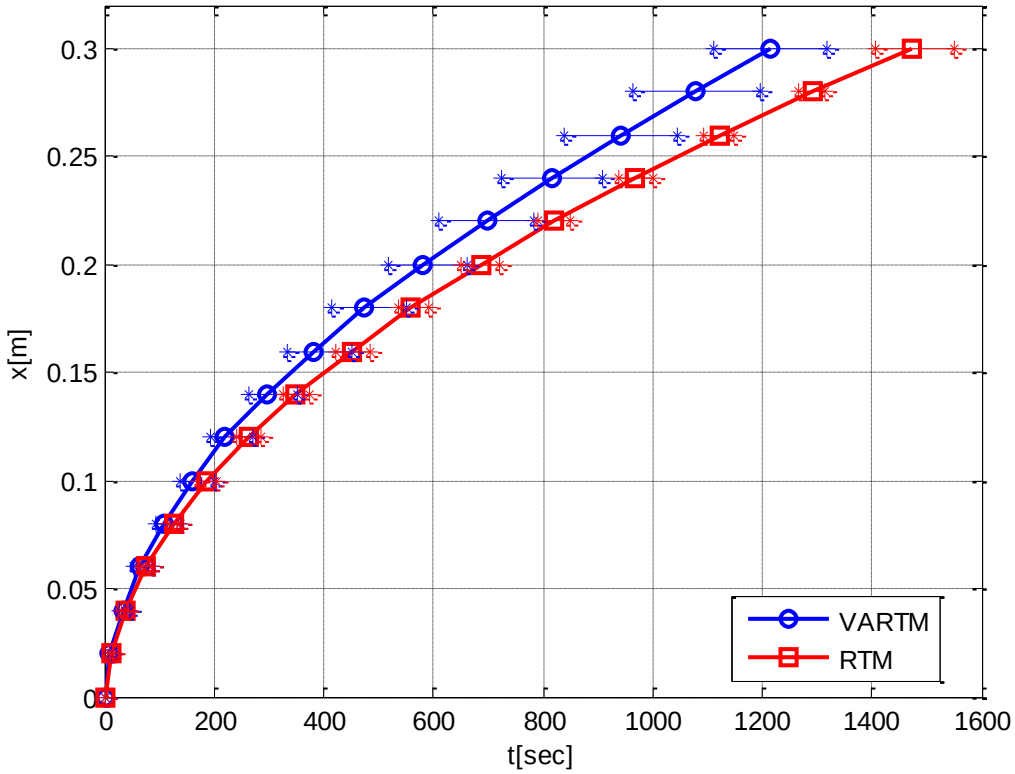

Figure 5.11 *Flow front propagation in VI and RTM setup for experiments 6 to 10*

Experiments 6 to 10 are also in a similar trend with the first five experiments. Mold filling in VI is faster than in RTM. The difference in the experimental average mold filling time is 17% (i.e., $(t_{fill_{RTM}} - t_{fill_{VI}}) / t_{fill_{RTM}} = 0.17$).

The experimental results for mold filling times are normalized with respect to the average mold filling time in RTM. The model is also normalized with the same approach. Figures 5.12 and 5.13 show the dimensionless flow front propagation.

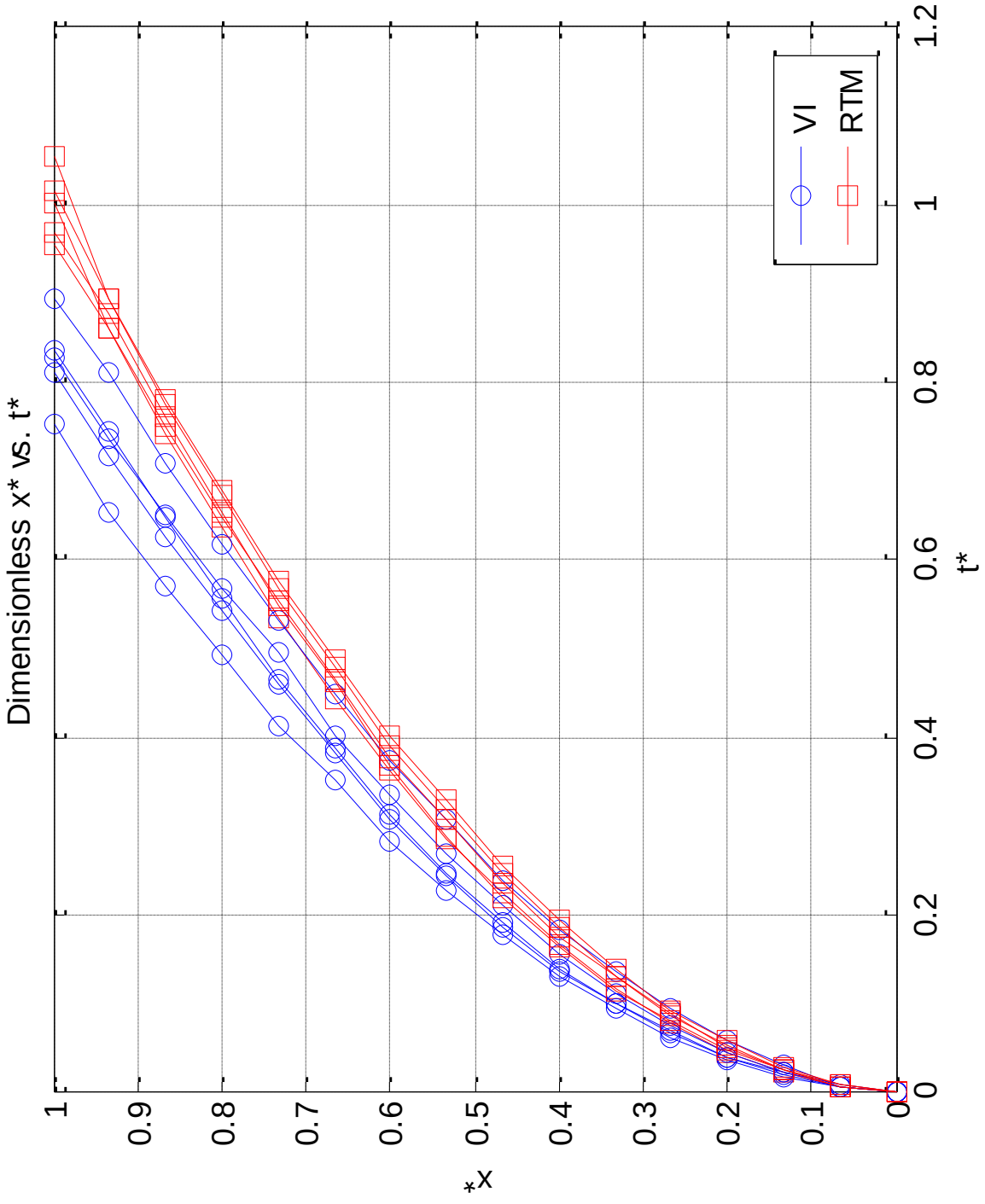

Figure 5.12 *Normalized experimental flow front propagation for experiments 6 to 10*

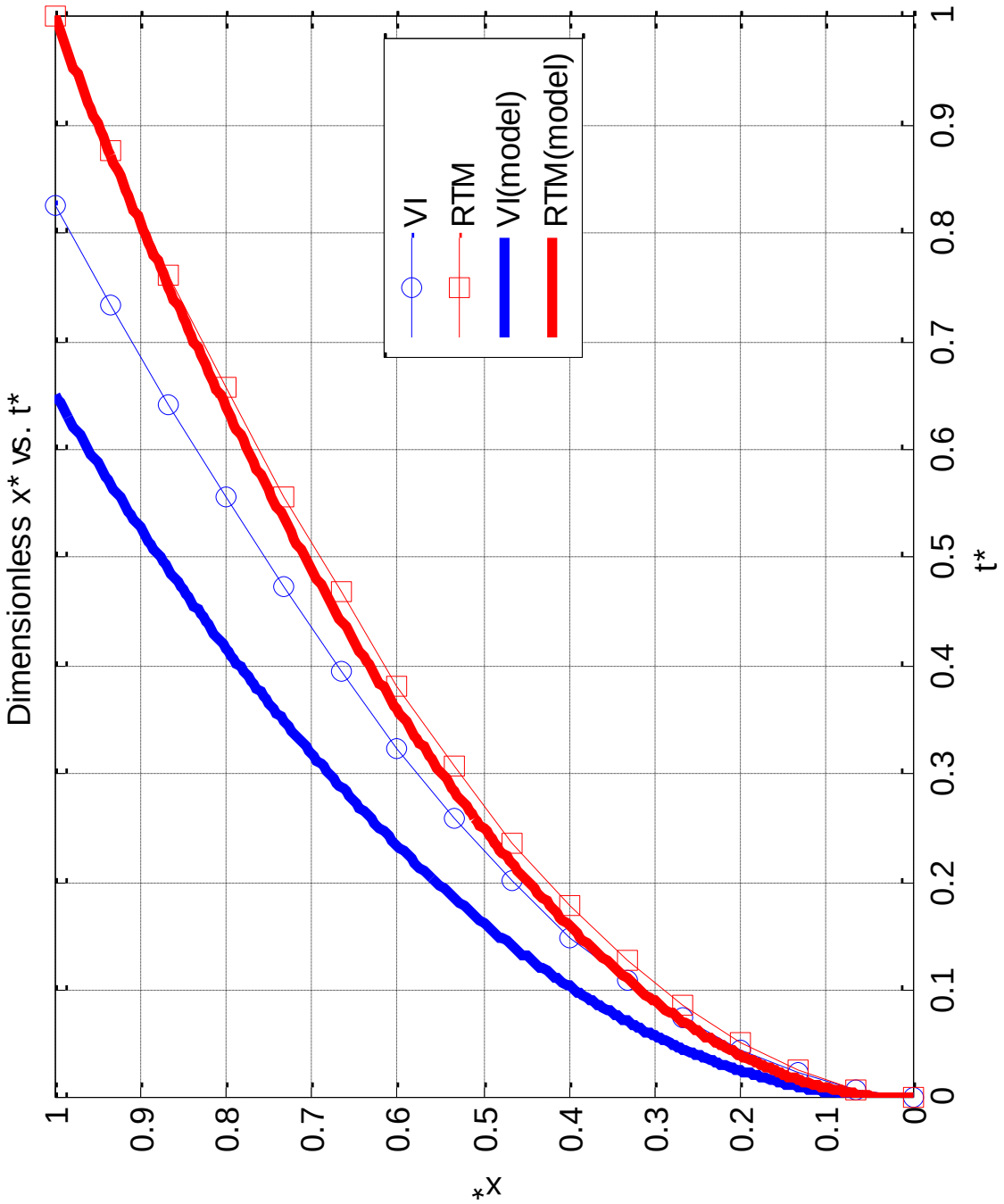

Figure5.13 *Normalized flow front propagation obtained with the compaction characterization performed using the setup used in this study.*

In Figure 5.13, blue and red lines represent VI and RTM, respectively. The thin lines with the symbols attached are the average of experimental data (Experiments 6-10); and the thick solid lines are the model results

6. Conclusion

The results obtained in Chapter 5, are compared and the following comments are made:

- Experimental results show that, flow front propagates faster in VI than in RTM since the thickness in the wetted upstream region increases in VI and hence the effective permeability increases as well. Recalling that the permeability is analogues to the "inverse of the resistance" (i.e., conductance) to the flow, this result is in agreement with the expectations. As discussed at the beginning of this thesis, one could doubt if the change in the part thickness would result in a significant change in the mold filling times, or not. Because, especially in the industrial environment in which the variations in the material parameters is significantly high, tedious material characterization and process modeling may not be valuable unless they correspond to a significant improvement in the simulated results. Otherwise, use of simple RTM formulation, which does not require to track the time-dependent change in part thickness while calculating the mold filling, could be alternatively used by accepting the small error involves in it. Experimental mold filling time in VI was 13 % shorter than in RTM, in average, for Experiments 1-5. It was 17 % for Experiments 6-10. The only difference between the two five-experiment sets was the loading stage: it was in 0-80 kPa and 0-100 kPa for Experiments 1-5 and 6-10, respectively.
- Although the difference between the model and the experiments is too big when the compaction data from Yenilmez [38] is used in the model, it is still in good agreement when the VI versus RTM comparison is done. The mold filling time in VI is shorter (49 %) than in RTM. However, the difference between the filing time values (1626 s and 3191 s in VI and RTM, respectively) is much greater than the experiments (1081 s and 1247 s in VI and RTM, respectively as the average of the five experiments). This can be explained with large scatter in both permeability and compaction databases of [36] and [38], respectively. The superficial density per layer was 338-550 g/m^2 in [38] and it is 470-491 g/m^2 in

this study. However, the superficial density of the fabric is given as 450g/m^2 in the datasheet of the fabric. The specimens in [38] were prepared a larger spectrum of the fabric roll, while the specimens of this study was carefully cut, stacked and selected to have a small variation in the superficial density as well as the other related properties such as thickness and permeability. This could be another major cause of large deviation between the experimental and simulated mold filling times.

- The second set (Experiments 6-10) was used for a second purpose in mind. Pre-injection compaction characterization could be achieved to illustrate that this straightforward setup can be independent of any other database or setup; and allows conducting self characterization experiments as well as actual VI/RTM experiments.
- Using the compaction experiments conducted in the VI setup, the numerical solution is conducted again, and the results of the model showed a similar trend with the experiments. However the difference is still too much. The reason of this difference can be the inconsistencies in the fiber perform speciemens used here and in the permeability characterization database by Sarioglu [36]. Also, the viscosity of the diluted corn syrup had time-varying characteristics if not mixed well; and it may have contributed to the error in the simulated results.
- As a future work, not only the fabric compaction characterization, but also permeability characterization will be conducted using the RTM side of the setup itself. This task can be conducted by varying the gap of RTM part in multiple experiments using multiple specimens. The thickness domain will correspond to the thickness domain observed in the VI experiments. Each injection will be used as a permeability measurement experiment under constant pressure boundary condition, and the flow front position will be monitored to calculate permeability at different thicknesses and thus fiber volume fractions. This will enable the user to construct the permeability database.

- This will allow achieving two things for the current setup: (1) a straightforward but yet totally independent of any other setup or material property database to perform VI/RTM experiments and material characterization involves in the process modeling; and (2) use of consistent scatters in the VI/RTM experiments and material characterization so that the simulated results will realistically model the experiments.

7. References

[1] N. C. Correia, F. Robitaille, a. C. Long, C. D. Rudd, P. Šimáček, and S. G. Advani, "Analysis of the vacuum infusion moulding process: I. Analytical formulation," *Composites Part A: Applied Science and Manufacturing*, vol. 36, no. 12, pp. 1645–1656, Dec. 2005.

[2] B. Yenilmez, M. Senan, and E. Murat Sozer, "Variation of part thickness and compaction pressure in vacuum infusion process," *Composites Science and Technology*, vol. 69, no. 11–12, pp. 1710–1719, Sep. 2009.

[3] B. Yenilmez and E. M. Sozer, "Compaction of e-glass fabric preforms in the Vacuum Infusion Process, A: Characterization experiments," *Composites Part A: Applied Science and Manufacturing*, vol. 40, no. 4, pp. 499–510, Apr. 2009.

[4] B. Yenilmez and E. M. Sozer, "Compaction of Coupled flow and compaction model for e-glass fabric preforms in the vacuum infusion process : (i) use of characterization database in a model and (ii) experiments," *In Progress*, no. i, pp. 1–22, 2012.

[5] F. Robxtaille and R. Gauvin, "Compaction of textile reinforcements for composites manufacturing. I: Review of experimental results," *Polymer composites*, vol. 19, no. 2, 1998.

[6] M. Haboğlu, "Strain rate controlled compaction characterization of e-glass fabrics and investigation of the effects of process parameters on the results," Koç University, 2012.

[7] K. M. Pillai and S. G. Advani, "Numerical simulation of unsaturated flow in woven fiber preforms during the resin transfer molding process," *Polymer Composites*, no. 1, 1998.

[8] Y. Kuan and a. S. El-Gizawy, "Numerical characterization of mold injection in resin transfer molding process," *Advances in Polymer Technology*, vol. 19, no. 3, pp. 173–179, 2000.

[9] J. M. Lawrence, K.-T. Hsiao, R. C. Don, P. Simacek, G. Estrada, E. M. Sozer, H. C. Stadtfeld, and S. G. Advani, "An approach to couple mold design and on-line control to manufacture complex composite parts by resin transfer molding," *Composites Part A: Applied Science and Manufacturing*, vol. 33, no. 7, pp. 981–990, Jul. 2002.

[10] N. C. Correia, F. Robitaille, a. C. Long, C. D. Rudd, P. Šimáček, and S. G. Advani, "Use of Resin Transfer Molding Simulation to Predict Flow, Saturation, and Compaction in the VARTM Process," *Journal of Fluids Engineering*, vol. 126, no. 2, p. 210, 2004.

[11] A. Hammami and B. R. Gebart, "Analysis of the vacuum infusion molding process," *Polymer Composites*, vol. 21, no. 1, pp. 28–40, Feb. 2000.

[12] H. M. Andersson, T. S. Lundström, and B. R. Gebart, "Numerical model for vacuum infusion manufacturing of polymer composites," *International Journal of Numerical Methods for Heat & Fluid Flow*, vol. 13, no. 3, pp. 383–394, 2003.

[13] R. Mathur, D. Heider, C. Hoffma, J. W. G. Jr, and B. K. Fink, "Flow Front Measurements and Model Validation," vol. 22, no. 4, 2001.

[14] R. Chen, C. Dong, Z. Liang, C. Zhang, and B. Wang, "Flow modeling and simulation for vacuum assisted resin transfer molding process with the equivalent permeability method," *Polymer Composites*, vol. 25, no. 2, pp. 146–164, Apr. 2004.

[15] K.-T. Hsiao, M. Devillard, and S. G. Advani, "Simulation based flow distribution network optimization for vacuum assisted resin transfer moulding process," *Modelling and Simulation in Materials Science and Engineering*, vol. 12, no. 3, pp. S175–S190, May 2004.

[16] X. Sun, S. Li, and L. J. Lee, "Mold filling analysis in vacuum-assisted resin transfer molding. Part I: SCRIMP based on a high-permeable medium," *Polymer Composites*, vol. 19, no. 6, pp. 807–817, Dec. 1998.

[17] M. K. Kang, W. I. Lee, and H. T. Hahn, "Analysis of vacuum bag resin transfer molding process," *Composites Part A: Applied Science and Manufacturing*, vol. 32, no. 11, pp. 1553–1560, Nov. 2001.

[18] J. a. Acheson, P. Simacek, and S. G. Advani, "The implications of fiber compaction and saturation on fully coupled VARTM simulation," *Composites Part A: Applied Science and Manufacturing*, vol. 35, no. 2, pp. 159–169, Feb. 2004.

[19] S. Lopatnikov, P. Simacek, J. GillespieJr, and S. G. Advani, "A closed form solution to describe infusion of resin under vacuum in deformable fibrous porous media," *Modelling and Simulation in Materials Science and Engineering*, vol. 12, no. 3, pp. S191–S204, May 2004.

[20] R. Arbter, J. M. Beraud, C. Binetruy, L. Bizet, J. Bréard, S. Comas-Cardona, C. Demaria, a. Endruweit, P. Ermanni, F. Gommer, S. Hasanovic, P. Henrat, F. Klunker, B. Laine, S. Lavanchy, S. V. Lomov, a. Long, V. Michaud, G. Morren, E. Ruiz, H. Sol, F. Trochu, B. Verleye, M. Wietgrefe, W. Wu, and G. Ziegmann, "Experimental determination of the permeability of textiles: A benchmark exercise," *Composites Part A: Applied Science and Manufacturing*, vol. 42, no. 9, pp. 1157–1168, Sep. 2011.

[21] R. S. Parnas, K. M. Flynn, and M. E. Dal-Favero, "A permeability database for composites manufacturing," *Polymer Composites*, vol. 18, no. 9, pp. 623–633, 1997.

[22] H. Stadtfeld, M. Erninger, S. Bickerton, and S. G. Advani, "An experimental method to continuously measure permeability of fiber preforms as a function of fiber volume fraction," *Journal of reinforced …*, vol. 21, no. 10, 2002.

[23] J. Alms, N. Correia, S. G. Advani, and E. Ruiz, "Experimental Procedures to Run Longitudinal Injections to Measure Unsaturated Permeability of LCM Reinforcements," *cchp.meca.polymtl.ca*, 1995.

[24] V. Antonucci, M. Esposito, M. R. Ricciardi, M. Raffone, M. Zarrelli, and M. Giordano, "Permeability characterization of stitched carbon fiber preforms by fiber optic sensors," *Express Polymer Letters*, vol. 5, no. 12, pp. 1075–1084, Oct. 2011.

[25] R. Gauvin, F. Trochu, Y. Lemenn, and L. Diallo, "Permeability Measurement and Flow Simulation," vol. 17, no. 1, pp. 34–42, 1996.

[26] E. Sozer, B. Chen, P. Graham, S. Bickerton, T.-W. Chou, and S. G. Advani, "Characterization and prediction of compaction force and preform permeability of woven fabrics during the resin transfer molding process," *Proceedings of the …*, 1999.

[27] Q. Liu, R. S. Parnas, and H. S. Giffard, "New set-up for in-plane permeability measurement," *Composites Part A: Applied Science and Manufacturing*, vol. 38, no. 3, pp. 954–962, Mar. 2007.

[28] K. Hoes, D. Dinescu, H. Sol, M. Vanheule, R. S. Parnas, Y. Luo, and I. Verpoest, "New set-up for measurement of permeability properties of fibrous reinforcements for RTM," *Composites Part A: Applied Science and Manufacturing*, vol. 33, no. 7, pp. 959–969, Jul. 2002.

[29] J. Weitzenböck, R. Shenoi, and W. PA, “Radial flow permeability measurement. Part A: Theory,” *... Part A: Applied Science and ...*, vol. 30, pp. 781–796, 1999.

[30] S. Comas-Cardona, C. Binetruy, and P. Krawczak, “Unidirectional compression of fibre reinforcements. Part 2: A continuous permeability tensor measurement,” *Composites Science and Technology*, vol. 67, no. 3–4, pp. 638–645, Mar. 2007.

[31] M. J. Buntain and S. Bickerton, “Compression flow permeability measurement: a continuous technique,” *Composites Part A: Applied Science and Manufacturing*, vol. 34, no. 5, pp. 445–457, May 2003.

[32] M. Um, I. Daniel, and B. Childs, “A gas flow method for determination of in-plane permeability of fiber preforms,” *Polymer composites*, vol. 22, no. 1, pp. 47–56, 2001.

[33] S. U. N. K. Kim, J. G. Opperer, D. Kim, and I. M. Daniel, “Determination of In-Plane Permeability of Fiber Preforms by the Gas Flow Method,” *Polymer Composites*, vol. 24, no. 1, pp. 34–44, 2003.

[34] T. Lundström, R. Stenberg, R. Bergström, H. Partanen, and P. Birkeland, “In-plane permeability measurements: a nordic round-robin study,” *Composites Part A: ...*, vol. 31, pp. 29–43, 2000.

[35] S. Sharma and D. a. Siginer, “Permeability Measurement Methods in Porous Media of Fiber Reinforced Composites,” *Applied Mechanics Reviews*, vol. 63, no. 2, p. 020802, 2010.

[36] A. Sarıoğlu, “Permeability Measurement Experiments for Fabric Preform Using LCM Processes,” Koc University, 2012.

[37] P. Simacek, S. G. Advani, R. Transfer, and M. Rtm, *Handbook of Polymer Matrix Composite Manufacturing*, no. September. 2011.

[38] B. Yenilmez, “Vacuum Infusion (VI) Process Modeling and Material Characterization with Viscoelastic Compaction Models,” Koc University, 2012.

[39] S. Bickerton, “Modeling and control of flow during impregnation of heterogeneous porous media, with application to composite mold filling processes,” University of Delaware, 1999.

8. Vita

Mehmet Akif Yalçınkaya was born in Istanbul, Turkey on October 11, 1987. He received his B.Sc. degree in Mechanical Engineering from Istanbul Technical University in 2010. Since then, he has enrolled in the M.Sc. program in Mechanical Engineering at Koc University, Istanbul with full scholarship, as both a teaching and a research assistant. His recent study, "Effect of Part Thickness Variation on the Mold Filling in Vacuum Infusion Process" is the M.Sc. thesis of him which is completed in 2012. Upon completion of his Masters Degree, Mehmet Akif Yalçınkaya plans to study further, with a view to achieving a PhD.

9. Appendix A

Detailed photos of the setup

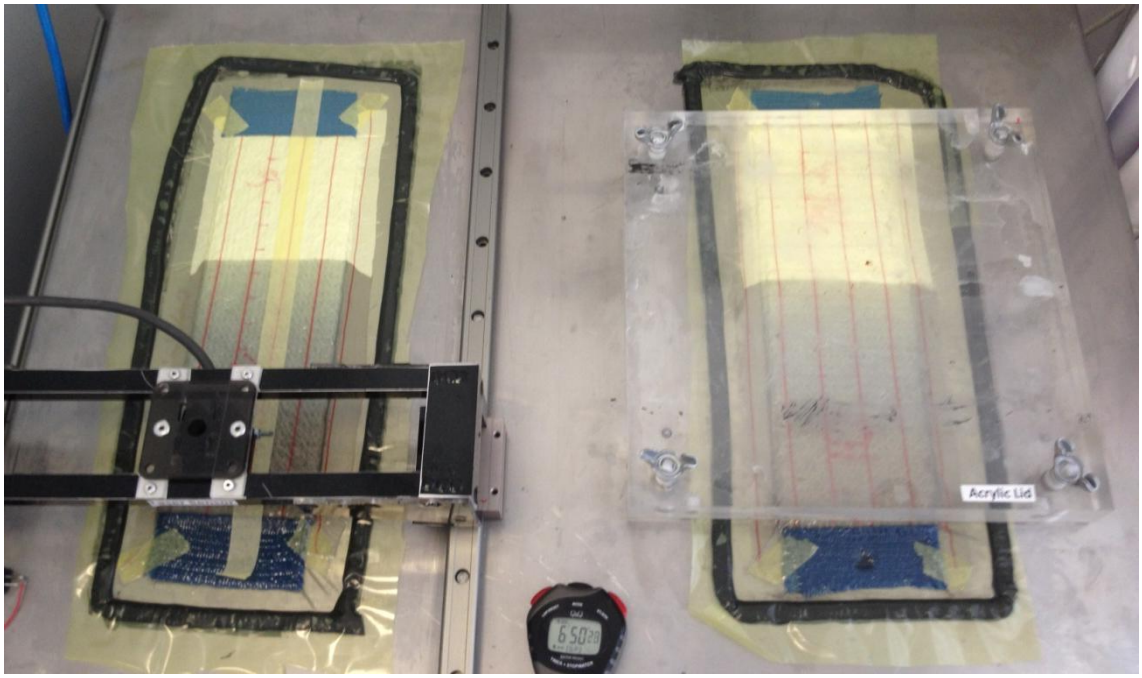

Arduino Code

```
static int PinDirection = 3;
static int PinStep = 2;
static int Switch = 4;
static int PinLaser = 0;
int cycle = 400*2;
int val = 0;
void setup() {
  // put your setup code here, to run once:
pinMode(PinStep,OUTPUT); //
pinMode(PinDirection,OUTPUT); //
pinMode(Switch,INPUT);//
digitalWrite(Switch,HIGH);
Serial.begin(1000000); //analog read baud rate 1000000
}
void loop() {
  // put your main code here, to run repeatedly:
  if (Serial.available() > 0) commandreceived();
}
//Receiving a Command
void commandreceived(){
  byte cmd;
  cmd=Serial.read();
  switch (cmd) {
    case 'A':  // zero position
    homelaser();
    break;
    case 'B': // start scanning
    startscan();
    break;
}
}
// Laser homing
void homelaser() {
    digitalWrite(PinDirection,LOW);
    while(digitalRead(Switch) == LOW)    Step(4);
    digitalWrite(PinDirection,HIGH);
    while(digitalRead(Switch) == HIGH)   Step(10);
    for (int i=0;i<20;i++)               Step(4);
}
// Move motor a PinStep without laser measurement with delay in ms
void Step(int pausetime){
      digitalWrite(PinStep,HIGH);
      delay(pausetime);
      val = analogRead(PinLaser);
      digitalWrite(PinStep,LOW);
      Serial.write(lowByte(val));
      Serial.write(highByte(val));
      delay(pausetime);
}
void forward(){
      digitalWrite(PinDirection,HIGH);
      Step(2);
}
void backward(){
  if (digitalRead(Switch)) return;
```

```
  digitalWrite(PinDirection,LOW);
  Step(2);
}
void startscan(){
  int count=0;
  for(count=0; count<cycle; count++)  {
  forward();
  }
  delay(200);
  for(count=0; count<cycle; count++){
  backward();
  }
}
```

Matlab Code for the Simulation

```
clear all, close all, clc
%%%Constants from Comp. Experiments
% a =  1.14;
% b = 28.35;
%%%Constants from Yenilmez
a =  2.04;
b = 19.42;
%%%Constants from Sarioglu calculated!!
% c = 3.65e-9;
% d = 10.44;

%%%Constants from Sarioglu's thesis!
c = 3.06e-9;
d = 9.91;

Pin  =  98000;
Pvac =  80000;
Patm = 100000;
Pout = Pin-Pvac;

L = 0.3;
N = 301;
x = linspace(0,L,N);
rosup = 8*0.45;
rof = 2540;
dx = x(2)-x(1);
err = 1;
P = Pin-(Pvac/L)*x;
finit = 0;
index = 0;
Pnew = P;

while err >0.000001

   Pc = Patm-P;
   vf = (1/b)*(-log(a)+log(Pc));
   K  = c*exp(-d*vf);
   h  = (rosup/rof)./vf;

   dpdx     = zeros(1,N);
   dpdx(1)  = (-P(3)+4*P(2)-3*P(1))       / (2*dx);
   dpdx(N)  = -(-P(N-2)+4*P(N-1)-3*P(N))   / (2*dx);
   for i = 2:1:N-1
   dpdx(i)  = ( P(i+1)-P(i-1))            / (2*dx);
   end

   f = K.*h.*dpdx;

   Pnew(2) = (K(1)*h(2)*(-Pnew(5)+4*Pnew(4)-3*Pnew(3))/(K(1)*h(1))+Pnew(3)+3*Pnew(1))/4;
   Pnew(end-1) = (K(end-2)*h(end-2)*(-Pnew(end-4)+4*Pnew(end-3)-3*Pnew(end-2))/(K(end)*h(end))+Pnew(end-
2)+3*Pnew(end))/4;
   for j = 3:1:N-2
      Pnew(j) = (Pnew(j-2)*K(j-1)*h(j-1) + Pnew(j+2)*K(j+1)*h(j+1))/(K(j+1)*h(j+1)+K(j-1)*h(j-1));
   end
```

```
%     figure(1)
%     subplot(3,2,1), plot(x,K,'b-','linewidth',2), grid on, xlabel('x'), ylabel('Permeability, K [m^2]')
%     subplot(3,2,2), plot(x,vf, 'b-','linewidth',2),grid on, xlabel('x'), ylabel('V_f')
%     subplot(3,2,3), plot(x,h, 'b-','linewidth',2),grid on, xlabel('x'), ylabel('h[m]')
%     subplot(3,2,4), plot(x,P, 'b-','linewidth',2),grid on, xlabel('x'), ylabel('P[Pa]')
%     subplot(3,2,5), plot(x,dpdx, 'b-','linewidth',2),grid on, xlabel('x'), ylabel('dP/dx')
%     subplot(3,2,6), plot(x,f, 'b-','linewidth',2),grid on, xlabel('x'), ylabel('K*h*(dP/dx)')
% %     pause(0.01)
    index=index+1;
    err = norm(abs(Pnew-P))/norm(P);
    P = Pnew;

end
    figure(1)
    subplot(3,2,5), plot(x,K,'b-','linewidth',2), grid on, xlabel('x'), ylabel('Permeability, K [m^2]')
    subplot(3,2,2), plot(x,vf, 'b-','linewidth',2),grid on, xlabel('x'), ylabel('V_f')
    subplot(3,2,1), plot(x,h, 'b-','linewidth',2),grid on, xlabel('x'), ylabel('h[m]')
    subplot(3,2,4), plot(x,P, 'b-','linewidth',2),grid on, xlabel('x'), ylabel('P[Pa]')
    subplot(3,2,3), plot(x,dpdx, 'b-','linewidth',2),grid on, xlabel('x'), ylabel('dP/dx')
    subplot(3,2,6), plot(x,f, 'b-','linewidth',2),grid on, xlabel('x'), ylabel('K*h*(dP/dx)')

 index

%%%%%%%%%%% Mold filling simulation:  %%%%%%%%%%%%%%%%%%%%%%%%%%%%%%%%%%%
mu       = 0.171;
H        = h(N)*ones(size(x));

u_tfill  = -(K(N)/mu)*dpdx(N);
uf_tfill = u_tfill/(1-vf(N));

M      = 3;
t(1:M) = 0;
while M < N

xf     = x(M);
s      = xf/L;

HPREV  = H;

uf     = uf_tfill/s;
dt     = dx/uf;

M      = M+1;
xf     = x(M);
s      = xf/L;
t(M)   = t(M-1)+dt;

X1     = x(  1:1:M);
X2     = x(M+1:1:N);
X      = [X1 X2];

p1     = spline(x*s,P,X1);
p2     = Pout*ones(size(X2));
p      = [p1 p2];
pc     = Patm-p;

k1     = spline(x*s,K,X1);
```

```
k2     = K(N)*ones(size(X2));
k      = [k1 k2];
 H1     = spline(x*s,h,X1);
H2     = h(N)*ones(size(X2));
H      = [H1 H2];

dhdt   = (H-HPREV)*(1/dt);

    dPdX     = zeros(1,N);
    dPdX(1)  = (-p(3)+4*p(2)-3*p(1))        / (2*dx);
    dPdX(N)  = -(-p(N-2)+4*p(N-1)-3*p(N))   / (2*dx);
    for i = 2:1:N-1
    dPdX(i)  = ( p(i+1)-p(i-1))             / (2*dx);
    end

f      = k.*H.*dPdX;

    dfdX     = zeros(1,N);
    dfdX(1)  = (-f(3)+4*f(2)-3*f(1))        / (2*dx);
    dfdX(N)  = -(-f(N-2)+4*f(N-1)-3*f(N))   / (2*dx);
    for i = 2:1:N-1
    dfdX(i)  = ( f(i+1)-f(i-1))             / (2*dx);
    end

%%% alternative calculations of h and K:
VF = (1/b)*(-log(a)+log(pc));
kk = c*exp(-d*VF);
HH = (rosup/rof)./VF;
st = num2str(round(t(M)));
str= ['Time, t = ',st,' seconds'];

%     figure(2)
%     subplot(3,2,5), plot(X,k, 'b-o',x,kk,'r-s'    ),  grid on, xlabel('x'), ylabel('Permeability, K [m^2]'), title(str);
%     subplot(3,2,2), plot(X,VF,'b-o'               ),  grid on, xlabel('x'), ylabel('Fiber volume fraction, V_f')
%     subplot(3,2,1), plot(X,H, 'b-o',x,HH,'r-s'    ),  grid on, xlabel('x'), ylabel('Thickness, h [m]')
%     subplot(3,2,4), plot(X,p, 'b-o'               ),  grid on, xlabel('x'), ylabel('Resin pressure, P [Pa]')
%     subplot(3,2,3), plot(X,pc,'b-o'               ),  grid on, xlabel('x'), ylabel('Compaction pressure, P_c [Pa]')
%     subplot(3,2,6), plot(X,dhdt,'b-o',X,dfdX/mu,'r-s'),  grid on, xlabel('x'), ylabel('dh/dt and d(h K dP/dx)/dx'),
legend('LHS','RHS',0)
%     pause(0.1)

    if (M == 76) ||(M == 151)||(M == 226)||(M == 301)
     %% x=L/4, L/2, 3L/4
    jj = ['x_f =' num2str((M-1)/1000) '[m]'];
    figure()
    subplot(3,2,5), plot(X,k, 'b-o',x,kk,'r-s'    ),  grid on, xlabel('x'), ylabel('K [m^2]')
    subplot(3,2,2), plot(X,VF,'b-o'               ),  grid on, xlabel('x'), ylabel('V_f')
    subplot(3,2,1), plot(X,H, 'b-o',x,HH,'r-s'    ),  grid on, xlabel('x'), ylabel('h [m]'),  title(jj)
    subplot(3,2,4), plot(X,p, 'b-o'               ),  grid on, xlabel('x'), ylabel('P [Pa]'),
    subplot(3,2,3), plot(X,pc,'b-o'               ),  grid on, xlabel('x'), ylabel('P_c [Pa]')
    subplot(3,2,6), plot(X,dhdt,'b-o',X,dfdX/mu,'r-s'),  grid on, xlabel('x'), ylabel('dh/dt and d(h K dP/dx)/dx'),
legend('LHS','RHS',0)
    end
end

t_analytical = (x.^2*mu*(1-vf(N)))./(2*K(N)*Pvac);
figure(3)
```

```
plot(t_analytical,x,'r-o', t,x,'b-s', 'linewidth',2), grid on, xlabel('Time, t [s]'), ylabel('Flow front position, x_f [m]')
legend('For h = constant and K = constant; i.e. RTM case','VI',0)
 file = fopen('simulation.txt','w');
for i = 1:1:301
fprintf(file,'%6.2f   %6.2f  \n', t(i), t_analytical(i));
end
fclose(file);

difference= (t_analytical(end)-t(end))/t_analytical(end)*100
t(end)
t_analytical(end)
```

Matlab Code for the Control of the Experimental Setup

```
function varargout = akif_gui(varargin)
% AKIF_GUI MATLAB code for akif_gui.fig
%      AKIF_GUI, by itself, creates a new AKIF_GUI or raises the existing
%      singleton*.
%
%      H = AKIF_GUI returns the handle to a new AKIF_GUI or the handle to
%      the existing singleton*.
%
%      AKIF_GUI('CALLBACK',hObject,eventData,handles,...) calls the local
%      function named CALLBACK in AKIF_GUI.M with the given input arguments.
%
%      AKIF_GUI('Property','Value',...) creates a new AKIF_GUI or raises the
%      existing singleton*.  Starting from the left, property value pairs are
%      applied to the GUI before akif_gui_OpeningFcn gets called.  An
%      unrecognized property name or invalid value makes property application
%      stop.  All inputs are passed to akif_gui_OpeningFcn via varargin.
%
%      *See GUI Options on GUIDE's Tools menu.  Choose "GUI allows only one
%      instance to run (singleton)".
%
% See also: GUIDE, GUIDATA, GUIHANDLES

% Edit the above text to modify the response to help akif_gui

% Last Modified by GUIDE v2.5 23-Aug-2012 18:13:36

% Begin initialization code - DO NOT EDIT
gui_Singleton = 1;
gui_State = struct('gui_Name',       mfilename, ...
   'gui_Singleton',  gui_Singleton, ...
   'gui_OpeningFcn', @akif_gui_OpeningFcn, ...
   'gui_OutputFcn',  @akif_gui_OutputFcn, ...
   'gui_LayoutFcn',  [] , ...
   'gui_Callback',   []);
if nargin && ischar(varargin{1})
   gui_State.gui_Callback = str2func(varargin{1});
end

if nargout
   [varargout{1:nargout}] = gui_mainfcn(gui_State, varargin{:});
else
   gui_mainfcn(gui_State, varargin{:});
end
% End initialization code - DO NOT EDIT

 % --- Executes just before akif_gui is made visible.
function akif_gui_OpeningFcn(hObject, eventdata, handles, varargin)
% This function has no output args, see OutputFcn.
% hObject    handle to figure
% eventdata  reserved - to be defined in a future version of MATLAB
% handles    structure with handles and user data (see GUIDATA)
% varargin   command line arguments to akif_gui (see VARARGIN)
```

```
% Choose default command line output for akif_gui
handles.output = hObject;

% Update handles structure
guidata(hObject, handles);

global command scantimer ghandles zerotimer tstart

ghandles=handles;
%seri portu commanda at

if ~isempty(instrfind('Name','Serial-COM7','status','open'))
   command=instrfind('Name','Serial-COM7','status','open');
else
   command = serial('COM7', 'BaudRate', 1000000);
   command.InputBufferSize=10240;
   fopen(command);
end

zerotimer=timer('ExecutionMode','fixedRate','Period',7,'TasksToExecute',3,'TimerFcn',@zero_thickness);
tstart = tic;

% --- Outputs from this function are returned to the command line.
function varargout = akif_gui_OutputFcn(hObject, eventdata, handles)
% varargout  cell array for returning output args (see VARARGOUT);
% hObject    handle to figure
% eventdata  reserved - to be defined in a future version of MATLAB
% handles    structure with handles and user data (see GUIDATA)

% Get default command line output from handles structure
varargout{1} = handles.output;

% --- Executes on button press in akif_scan.
function akif_scan_Callback(hObject, eventdata, handles)
datafile = fopen('compaction.txt','a');
global Data command ghandles DataCount datatime tstart time
DataCount=command.BytesAvailable/2; % 1 integer = 2bytes
time = toc(tstart);
if DataCount==1600;
   Data=uint8(fread(command,DataCount*2,'uint8'));
   Data=reshape(Data,2,DataCount);
   Data=typecast(Data(:),'int16');
   Data=double(Data);
   Data = Data/49.6599;
   datatime = [time Data'];
   fprintf(datafile,'%f\t', datatime);
   fprintf(datafile,'\n');
else
   fread(command,DataCount*2);
   Data=[];
end
% Data=typecast(Data(:),'double');

sendcmd('B');
```

```
%axes(handles.thickness)

L = length(Data)/2;
%Data = Data(1:L);
plot(ghandles.thickness,1:L,Data(1:L)),
axis([0 800 0 1024]), axis autoy1
fclose(datafile)

function zero_thickness(hObject, eventdata, handles)
datafile = fopen('zerothickness.txt','a');
global Data command ghandles DataCount datatime tstart time
DataCount=command.BytesAvailable/2; % 1 integer = 2bytes
time = toc(tstart);
if DataCount==1600;
    Data=uint8(fread(command,DataCount*2,'uint8'));
    Data=reshape(Data,2,DataCount);
    Data=typecast(Data(:),'int16');
    Data=double(Data);
    Data = Data/49.6599;
    datatime = [time Data'];
    fprintf(datafile,'%f\t', datatime);
    fprintf(datafile,'\n');
else
    fread(command,DataCount*2);
    Data=[];
end
% Data=typecast(Data(:),'double');
 sendcmd('B');
%axes(handles.thickness)
 L = length(Data)/2;
%Data = Data(1:L);
plot(ghandles.thickness,1:L,Data(1:L)),
axis([0 800 0 1024]), axis autoy1
fclose(datafile)
 % --- Executes on button press in akif_home.
function akif_home_Callback(hObject, eventdata, handles)
sendcmd('A');
 function sendcmd(data)
global command
fwrite(command,uint8(data));
  % --- Executes on button press in zero_thickness.
function zero_thickness_Callback(hObject, eventdata, handles)
global zerotimer tstart time
start(zerotimer);
 % --- Executes on button press in injection.
function injection_Callback(hObject, eventdata, handles)
datafile = fopen('injection.txt','a');
global Data command ghandles DataCount datatime tstart time
DataCount=command.BytesAvailable/2; % 1 integer = 2bytes
time = toc(tstart);
if DataCount==1600;
    Data=uint8(fread(command,DataCount*2,'uint8'));
    Data=reshape(Data,2,DataCount);
    Data=typecast(Data(:),'int16');
    Data=double(Data);
    Data = Data/49.6599;
    datatime = [time Data'];
```

```
    fprintf(datafile,'%f\t', datatime);
    fprintf(datafile,'\n');
else
    fread(command,DataCount*2);
    Data=[];
end

sendcmd('B');
%axes(handles.thickness)

L = length(Data)/2;
%Data = Data(1:L);
plot(ghandles.thickness,1:L,Data(1:L)),
axis([0 800 0 1024]), axis autoy1
fclose(datafile)
```

Datasheet for the Stepper Motor (Leadshine 57HS22)

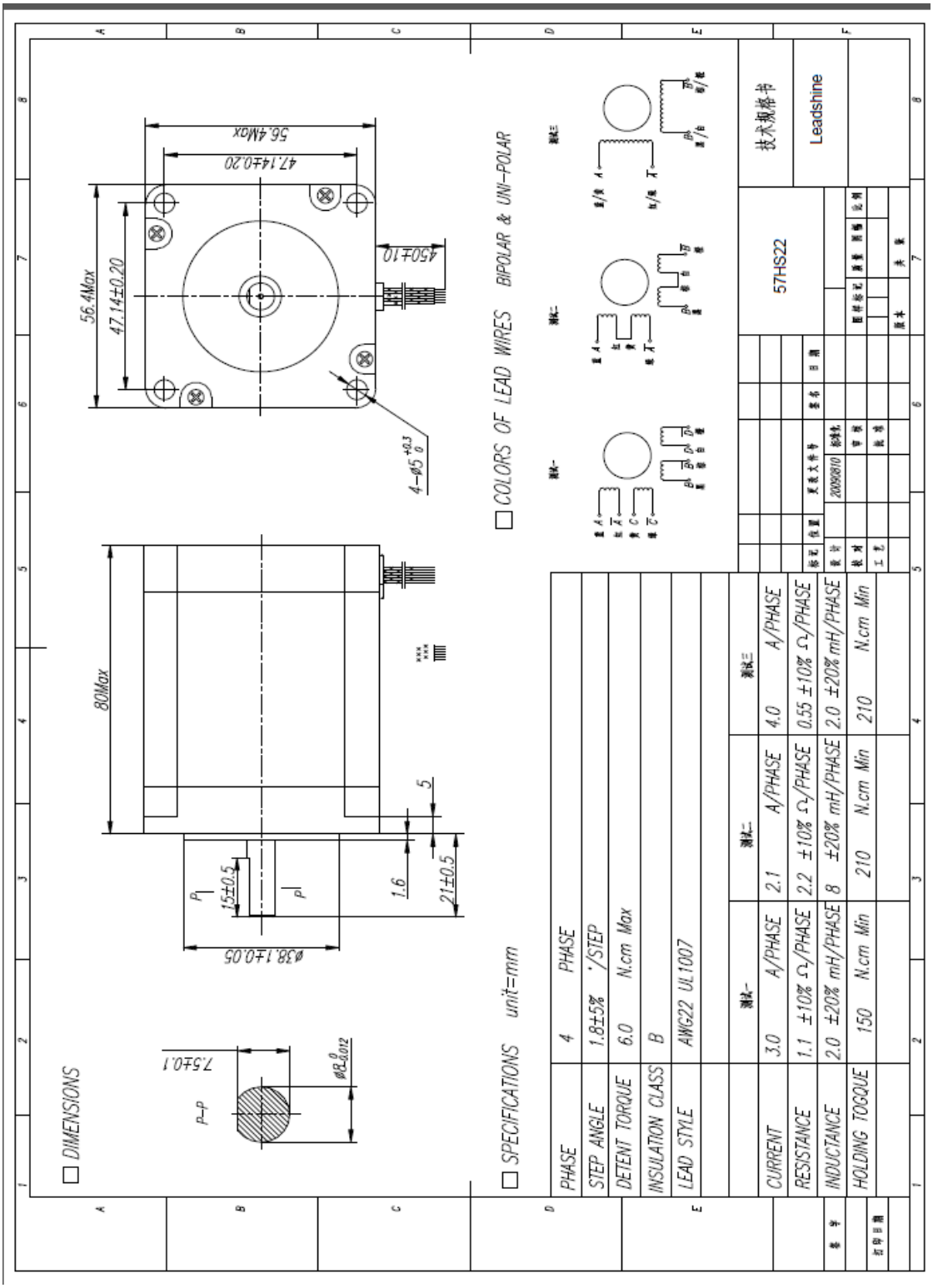

Laser Sensor

OMRON Z4M-W40RA Laser Displacement Sensor (Resolution 1.5 micrometers)

Specifications

■ Ratings

Item	Z4M-W40RA	Z4M-W100RA	Z4M-W40	Z4M-W100
Measurement range	±10 mm	±40 mm	±10 mm	±40 mm
Measurement point	40 mm	100 mm	40 mm	100 mm
Offset adjustment range	±10 mm	±40 mm	±10 mm	±40 mm
Span adjustment range	0.8 mA/mm ±10%	0.2 mA/mm ±10%	0.4 V/mm ±30%	0.1 V/mm ±30%
Light source	Visible-light semiconductor lasers with a wavelength of 670 nm and an output of 1.2 mW max.; class 2 (IEC), class II (FDA)		Infrared semiconductor laser with a wavelength of 780 nm and an output of 3 mW max., class 3B (IEC), class IIIb (FDA)	
Spot diameter (see note 2)	1 mm dia. max. (at measurement point)	1 x 2 mm max. (at measurement point)	1 mm dia. max. (at measurement point)	1 x 2 mm max. (at measurement point)
Resolution (see note 3)	3 µm (60 ms), 20 µm (2 ms), 80 µm (0.15 ms)	16 µm (500 ms), 60 µm (20 ms), 300 µm (0.7 ms)	1.5 µm (60 ms), 10 µm (2 ms), 40 µm (0.15 ms)	8 µm (500 ms), 30 µm (20 ms), 150 µm (0.7 ms)
Linearity (see note 4)	1% FS	1.5% FS	1% FS	1.5% FS
Response time (see note 5)	0.15 ms/2 ms/60 ms switch-selectable	0.7 ms/20 ms/500 ms switch-selectable	0.15 ms/2 ms/60 ms switch-selectable	0.7 ms/20 ms/500 ms switch-selectable
Sensitivity selector	WHITE/BLACK/AUTO switch-selectable			
Temperature characteristics (at measurement point)	Sensor: 0.03% FS/°C max. Amplifier: 0.03% FS/°C max.	Sensor: 0.02% FS/°C max. Amplifier: 0.03% FS/°C max.	Sensor: 0.03% FS/°C max. Amplifier: 0.03% FS/°C max.	Sensor: 0.02% FS/°C max. Amplifier: 0.03% FS/°C max.
Range indicators (sensor and amplifier) also used as laser warning lights (green)	Outside range, abnormal volume of light: NEAR indicator and FAR indicator flash. Near: NEAR indicator is lit. Measurement point: NEAR indicator and FAR indicator are lit. Far: FAR indicator is lit.			
Stability indicator (amplifier)	Stable operating range: Green Possible operating range: Not lit Insufficient or excessive light: Red			
Linear output (see note 6)	4 to 20 mA/30 to 50 mm Permissible load resistance: 0 to 300 Ω	4 to 20 mA/60 to 140 mm Permissible load resistance: 0 to 300 Ω	–4 to 4 V/30 to 50 mm Output impedance: 100 Ω Permissible load resistance: 10 kΩ min.	–4 to 4 V/60 to 140 mm Output impedance: 100 Ω Permissible load resistance: 10 kΩ min.
Enable output	NPN open collector, 50 mA max. at 40 VDC, residual voltage: 1 V max.			
Laser emission OFF input	Short-circuited with the 0-V terminal (residual voltage: 2 V max.): Laser emission is turned off. Open (current leakage: 0.1 mA max.): Laser emission is turned on. Linear output, indicators, and enable output holding function incorporated.			

Note: 1. The FS (full scale) value is calculated as follows:
Example: 1% FS on the Z4M-W40RA
Distance full scale conversion: 20 mm x 0.01 = 0.2 mm
Current full scale conversion: 16 mA x 0.01 = 0.16 mA

Item	Z4M-W40RA	Z4M-W100RA	Z4M-W40	Z4M-W100
Distance full scale	20 mm	80 mm	20 mm	80 mm
Voltage full scale*	---	---	8 V ±30%	8 V ±30%
Current full scale*	16 mA ±10%	16 mA ±10%	---	---

*The value changes according to the span to be adjusted.

2. The spot diameter is defined by $1/e^2$ (13.5%) of the sensor's laser beam center. There is light leakage outside the defined spot and the environment of the object may influence sensing accuracy. Reduce the influence of the environment as much as possible.

Datasheet for Arduino Uno

Arduino Uno

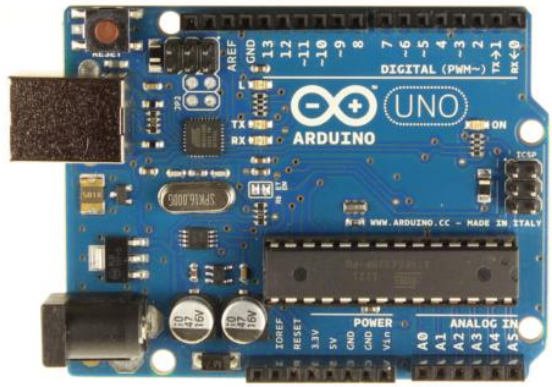

Arduino Uno R3 Front

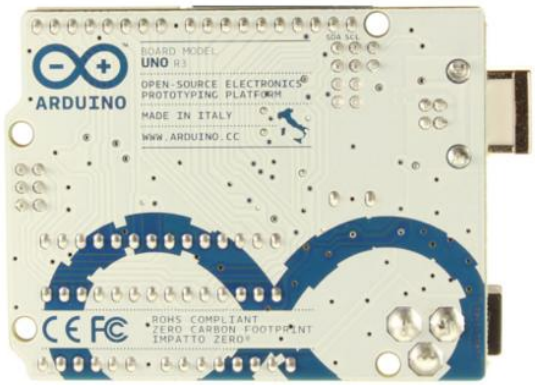

Arduino Uno R3 Back

Arduino Uno R2 Front

Arduino Uno SMD

Arduino Uno Front

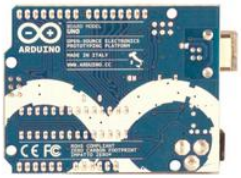

Arduino Uno Back

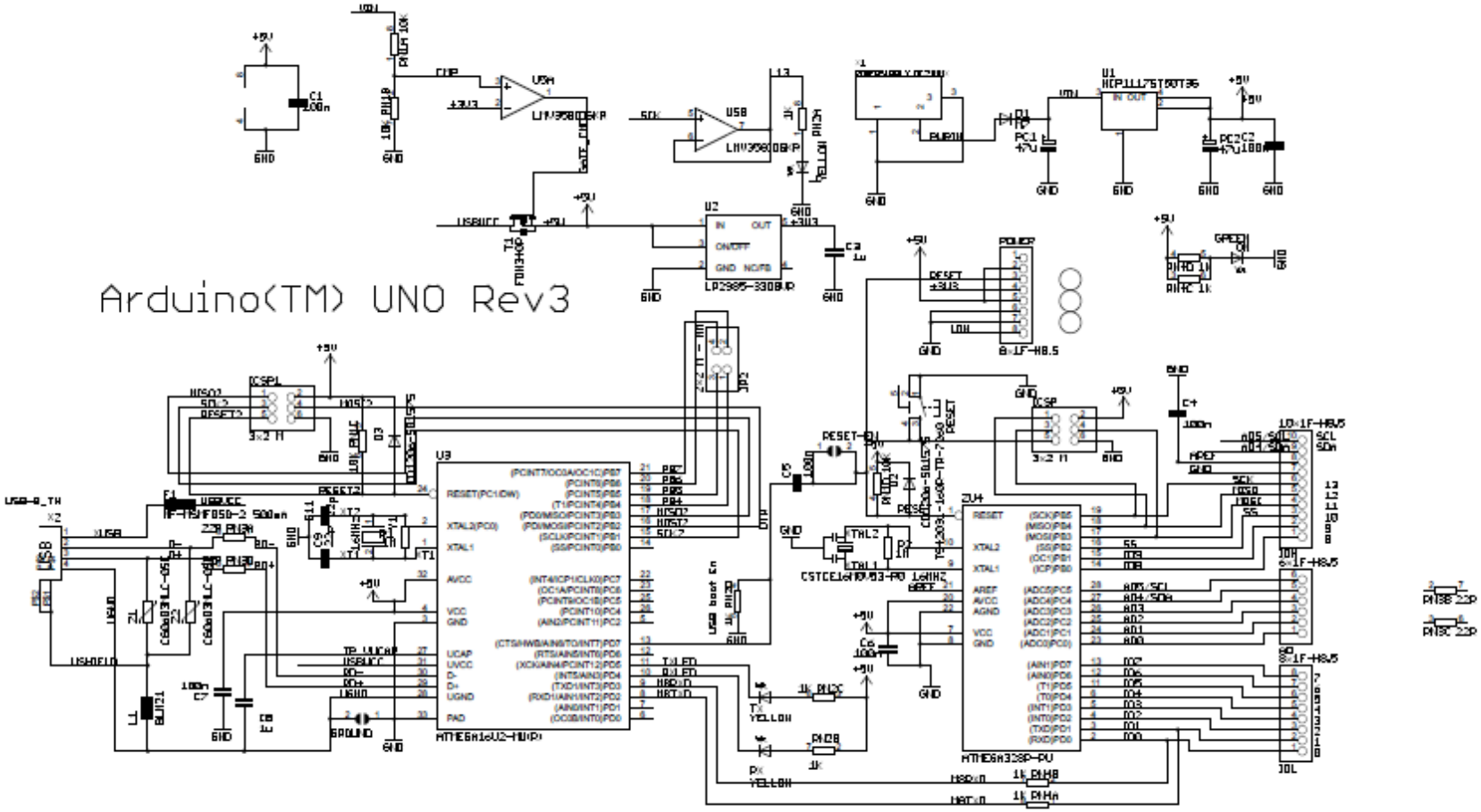

10. Appendix B

Experimental mold filling results

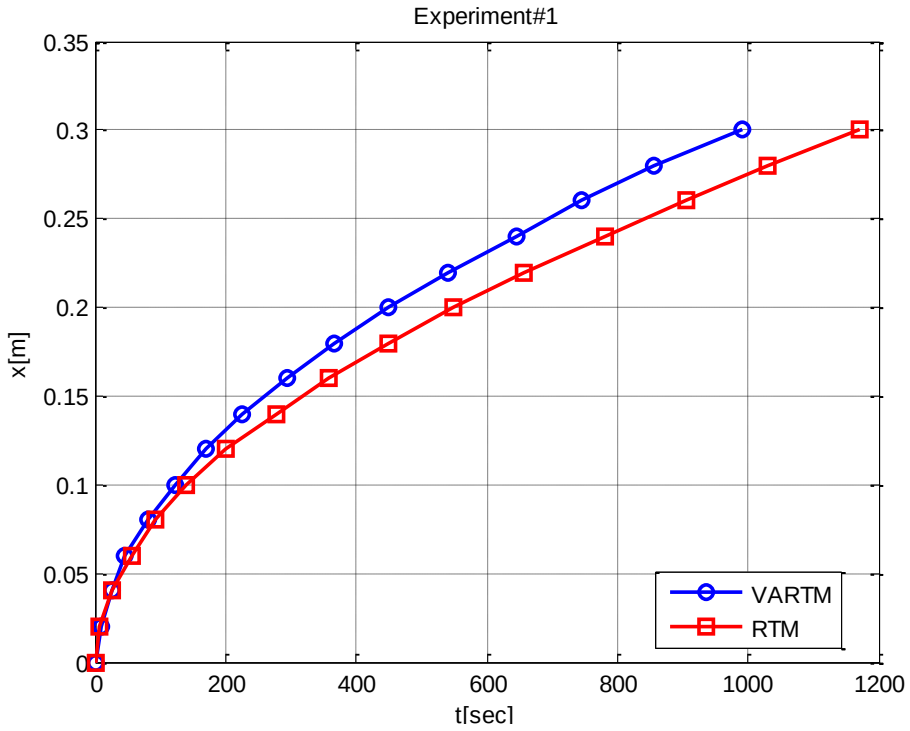

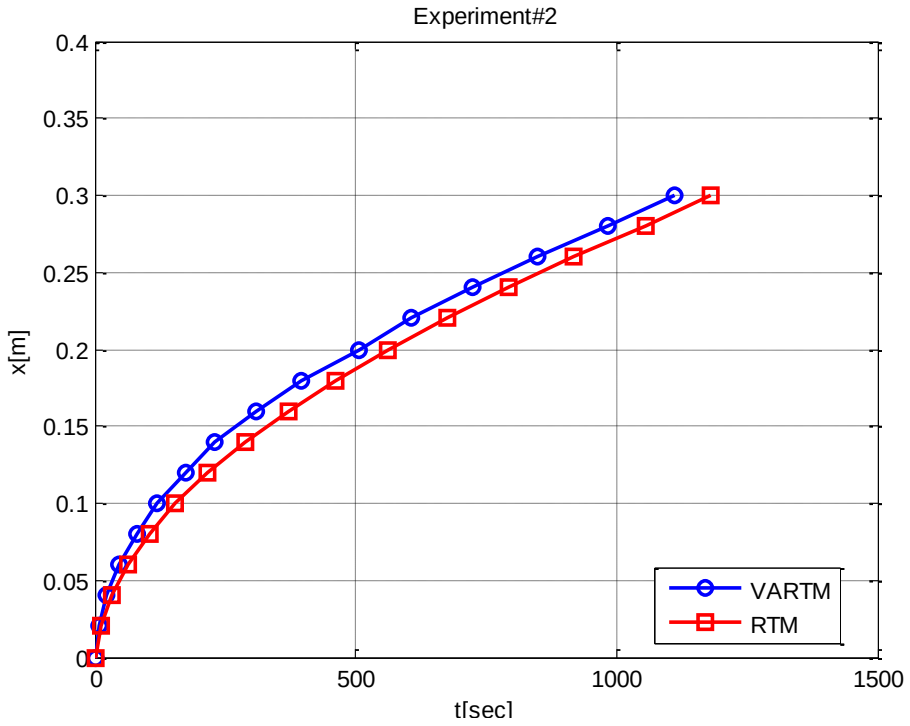

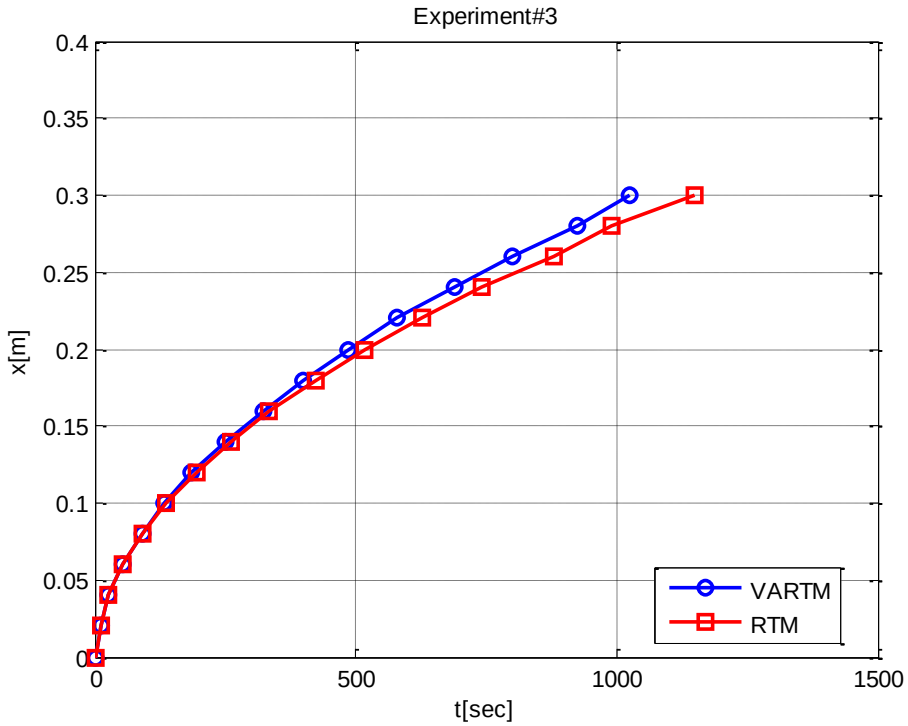
Experiment#3
0.4
0.35
0.3
0.25
0.2
0.15
0.1
0.05
0
x[m]
0
500
1000
1500
t[sec]
VARTM
RTM

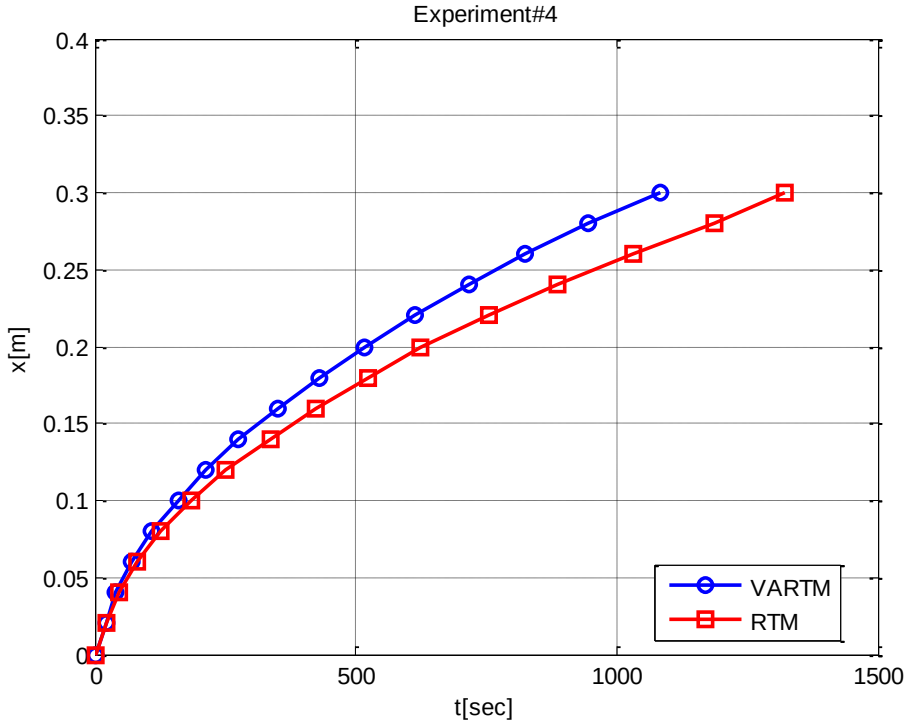
Experiment#4
0.4
0.35
0.3
0.25
0.2
0.15
0.1
0.05
0
x[m]
0
500
1000
1500
t[sec]
VARTM
RTM

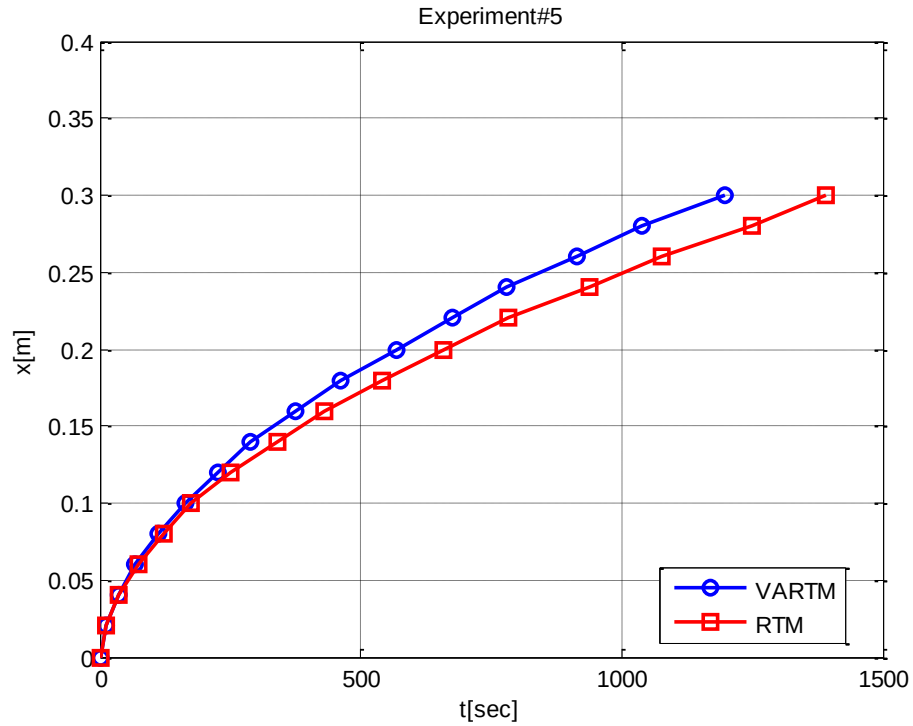
Experiment#5
x[m]
t[sec]
VARTM
RTM
0
0.05
0.1
0.15
0.2
0.25
0.3
0.35
0.4
0
500
1000
1500

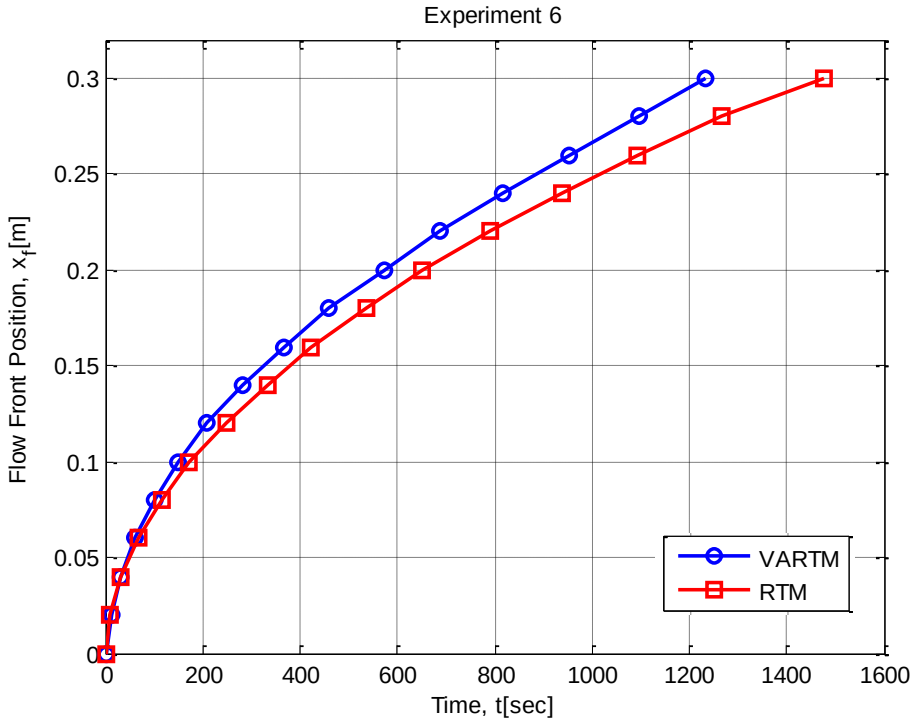
Experiment 6
Flow Front Position, x_f[m]
Time, t[sec]
VARTM
RTM
0
0.05
0.1
0.15
0.2
0.25
0.3
0
200
400
600
800
1000
1200
1400
1600

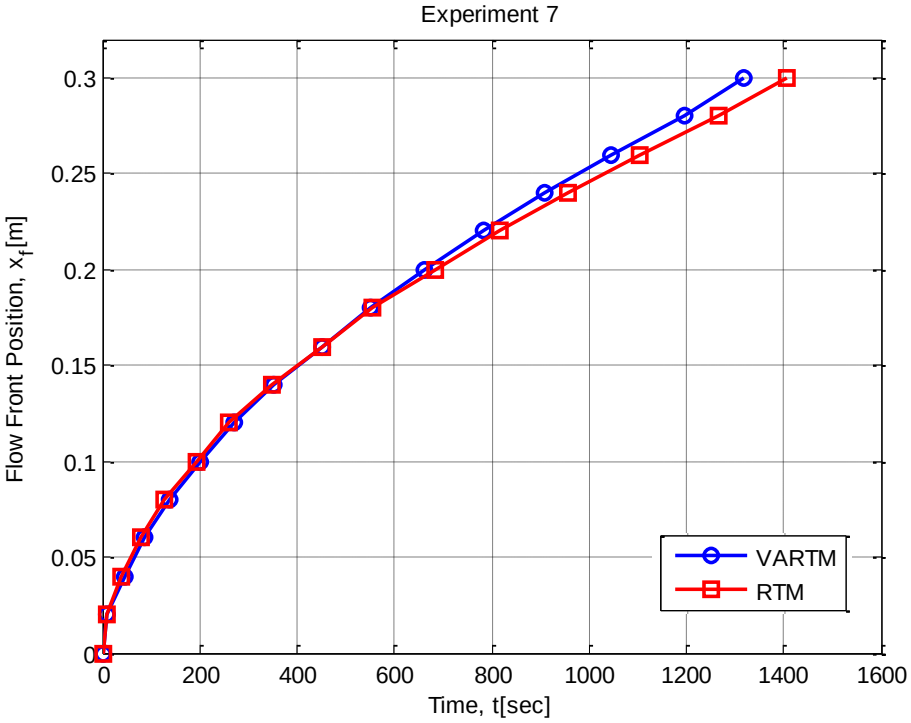
Experiment 7
Flow Front Position, x_f[m]
Time, t[sec]
VARTM
RTM
0
0.05
0.1
0.15
0.2
0.25
0.3
0
200
400
600
800
1000
1200
1400
1600

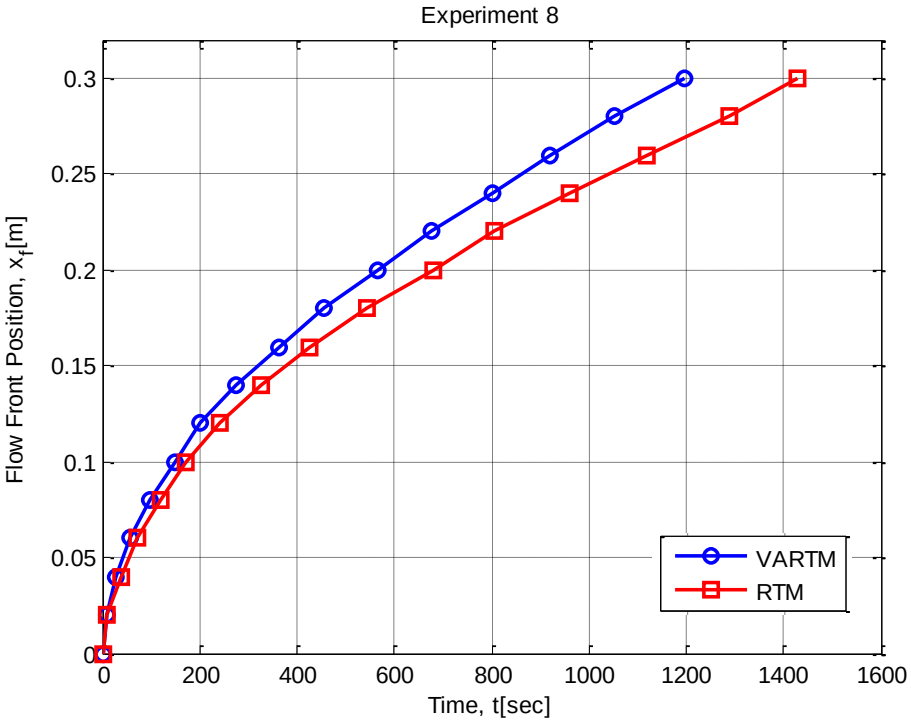
Experiment 8
Flow Front Position, x_f[m]
Time, t[sec]
VARTM
RTM
0
0.05
0.1
0.15
0.2
0.25
0.3
0
200
400
600
800
1000
1200
1400
1600

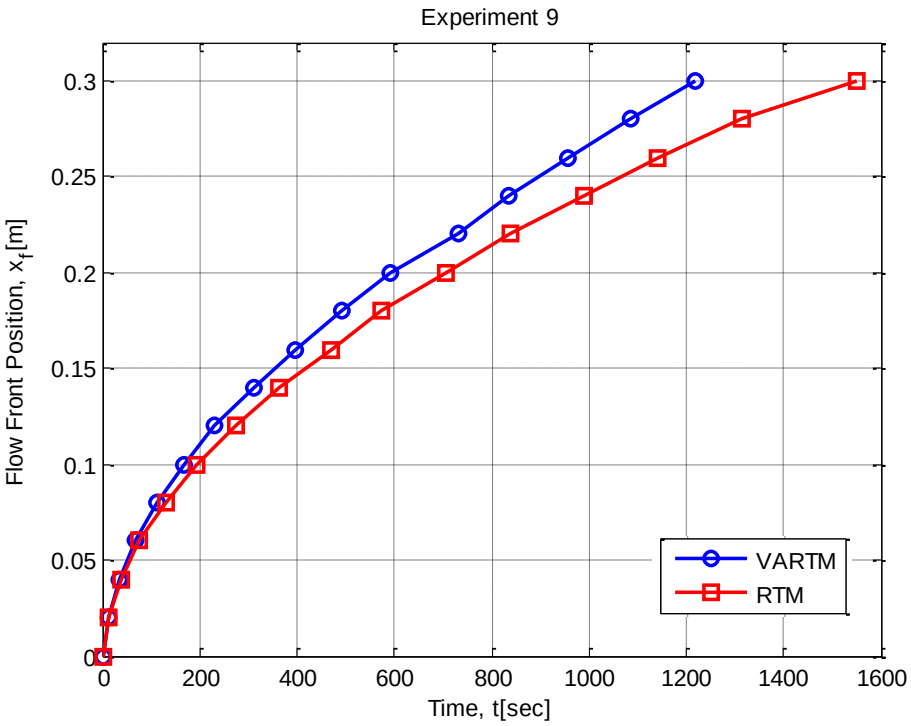
Experiment 9
Flow Front Position, x_f[m]
Time, t[sec]
VARTM
RTM
0
0.05
0.1
0.15
0.2
0.25
0.3
0
200
400
600
800
1000
1200
1400
1600

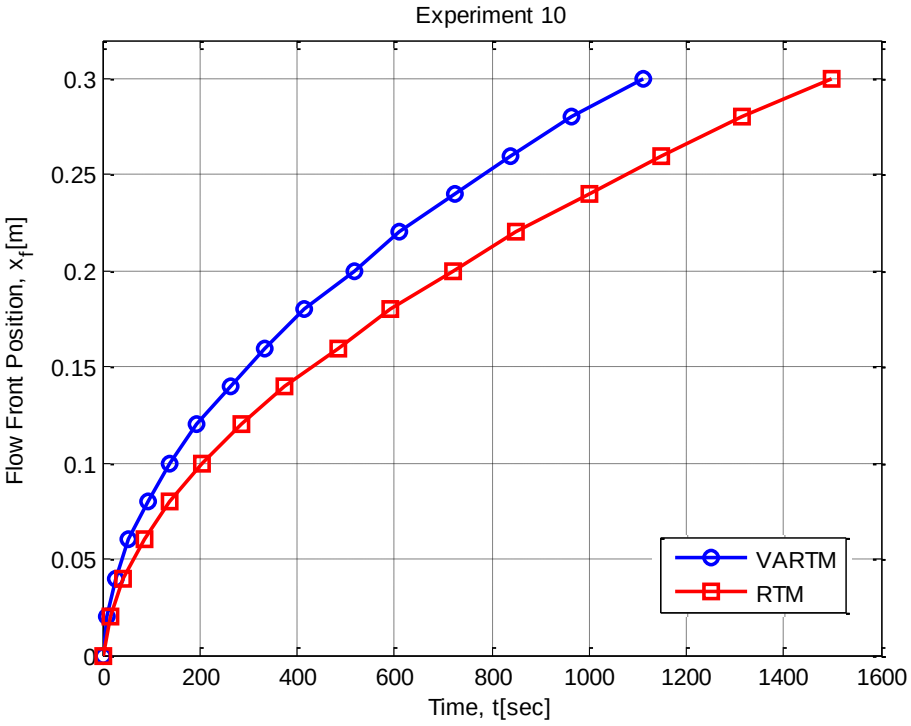
Experiment 10
Flow Front Position, x_f[m]
Time, t[sec]
VARTM
RTM
0
0.05
0.1
0.15
0.2
0.25
0.3
0
200
400
600
800
1000
1200
1400
1600

Thickness Distribution of the Preform at Pc=80 kPa (just before the injection)

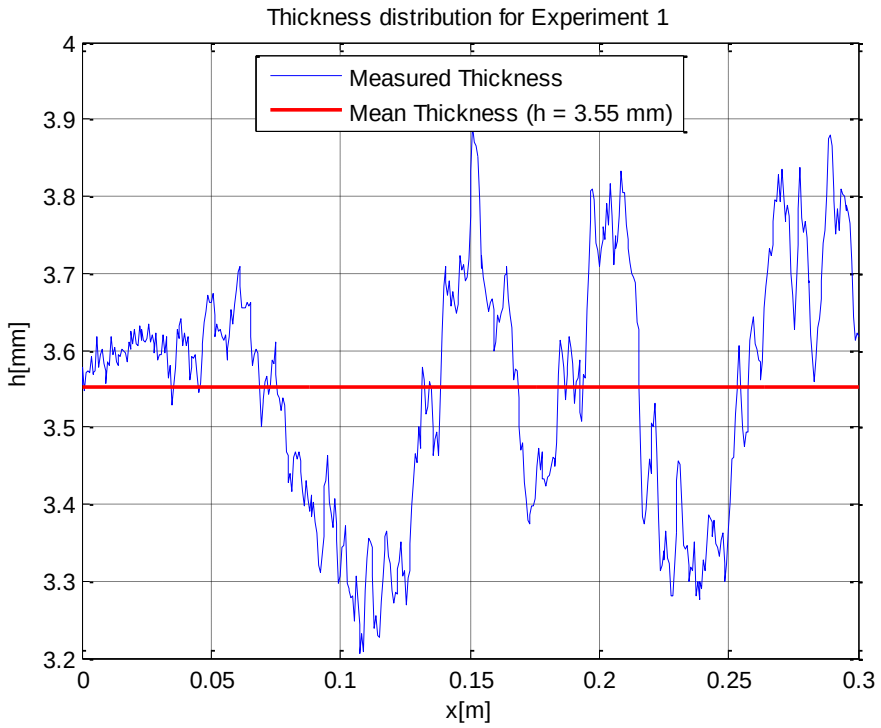

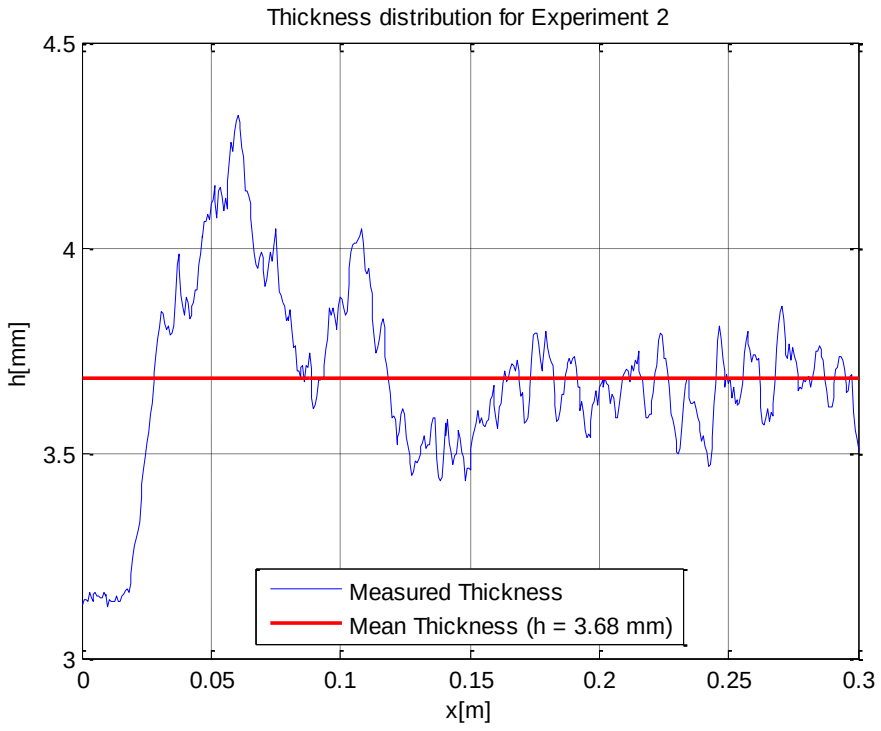

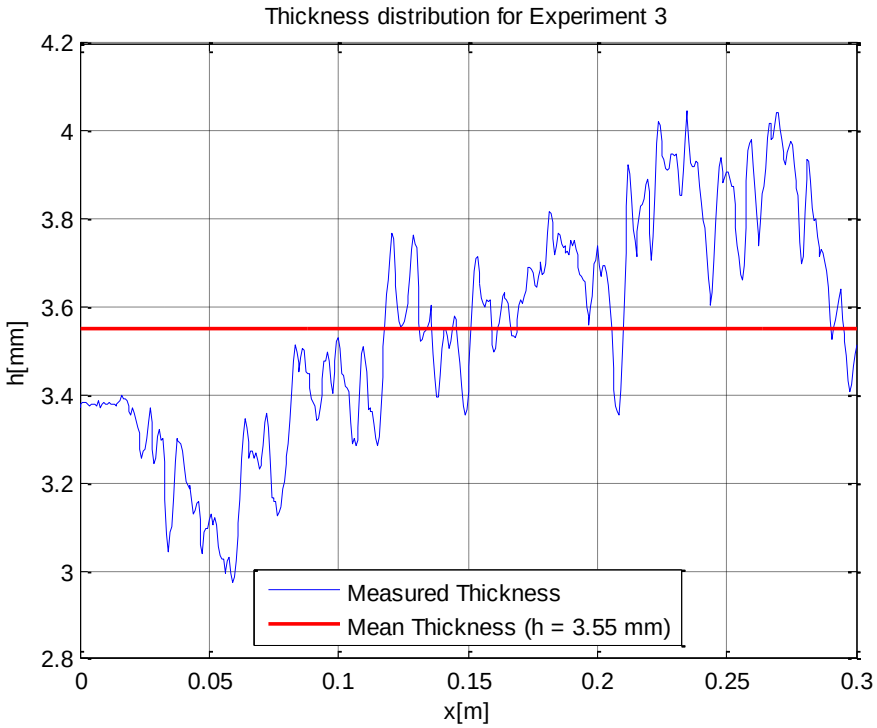
Thickness distribution for Experiment 3
h[mm]
x[m]
Measured Thickness
Mean Thickness (h = 3.55 mm)
4.2
4
3.8
3.6
3.4
3.2
3
2.8
0
0.05
0.1
0.15
0.2
0.25
0.3

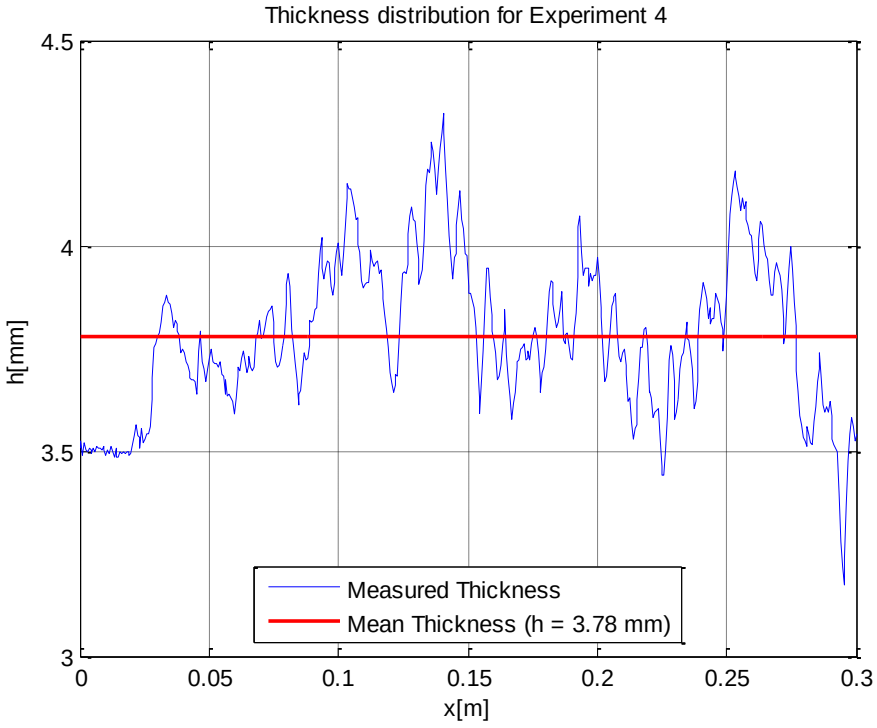
Thickness distribution for Experiment 4
h[mm]
x[m]
Measured Thickness
Mean Thickness (h = 3.78 mm)
4.5
4
3.5
3
0
0.05
0.1
0.15
0.2
0.25
0.3

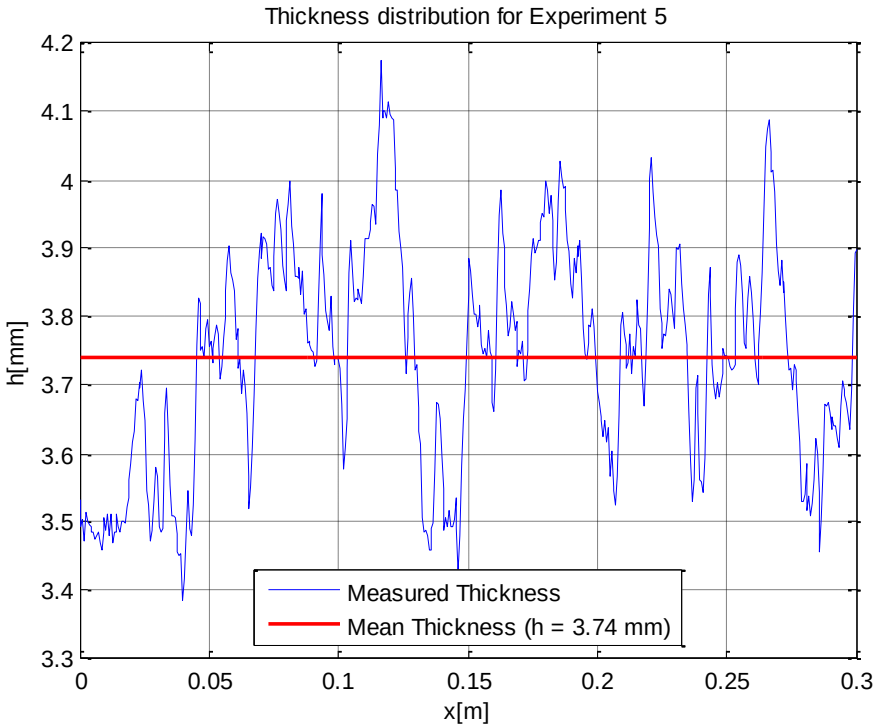
Thickness distribution for Experiment 5
h[mm]
x[m]
Measured Thickness
Mean Thickness (h = 3.74 mm)

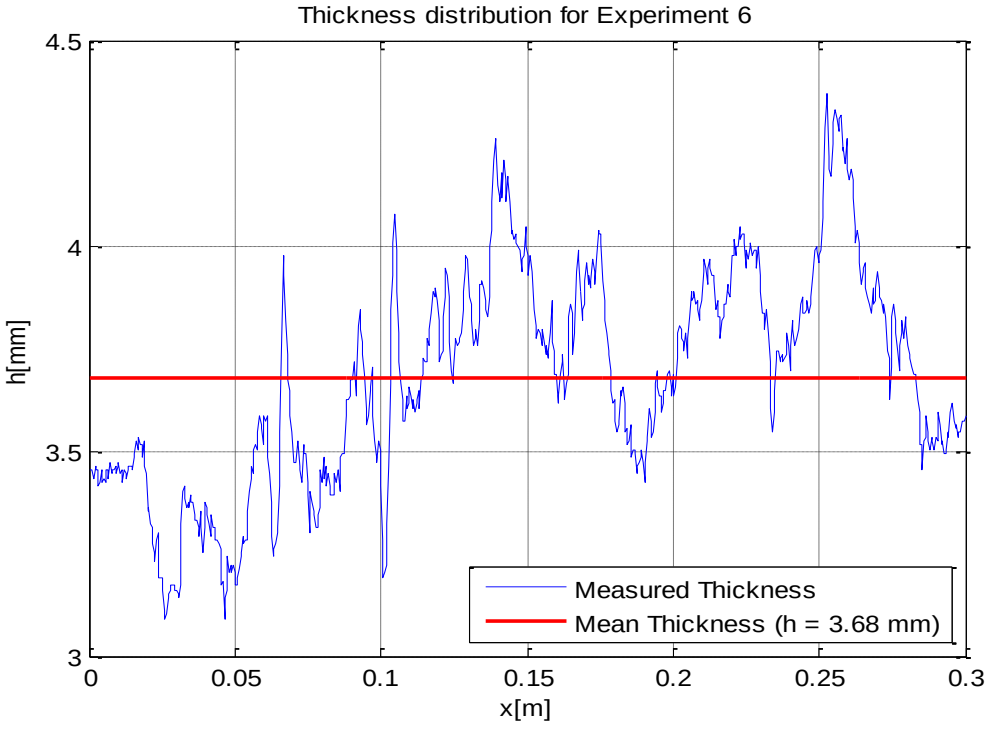
Thickness distribution for Experiment 6
h[mm]
x[m]
Measured Thickness
Mean Thickness (h = 3.68 mm)

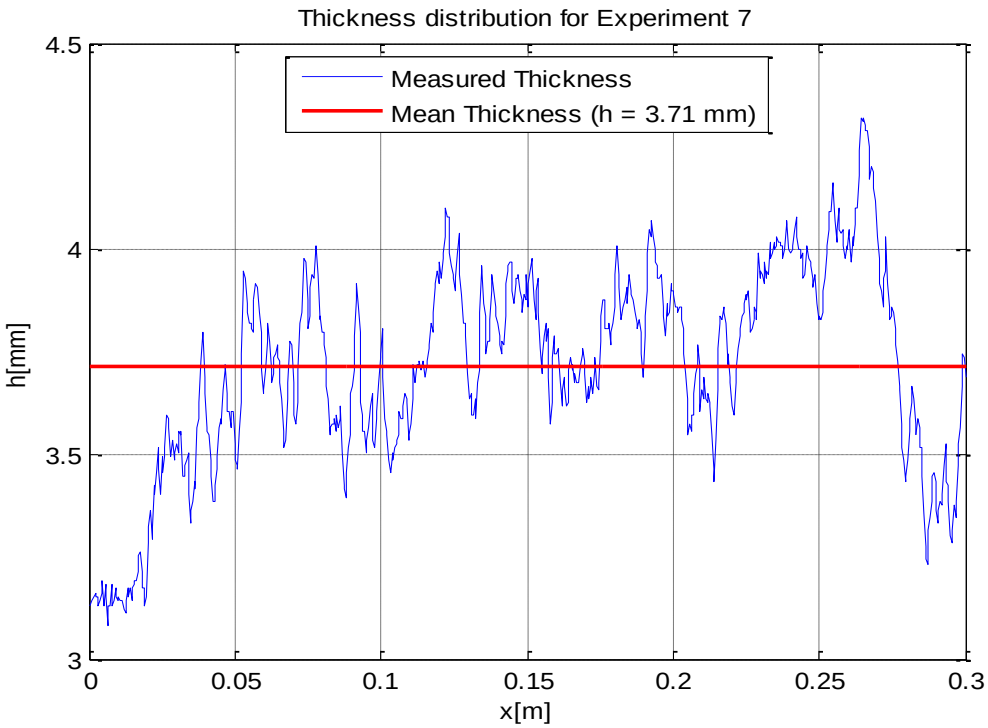
Thickness distribution for Experiment 7
Measured Thickness
Mean Thickness (h = 3.71 mm)
h[mm]
x[m]
4.5
4
3.5
3
0
0.05
0.1
0.15
0.2
0.25
0.3

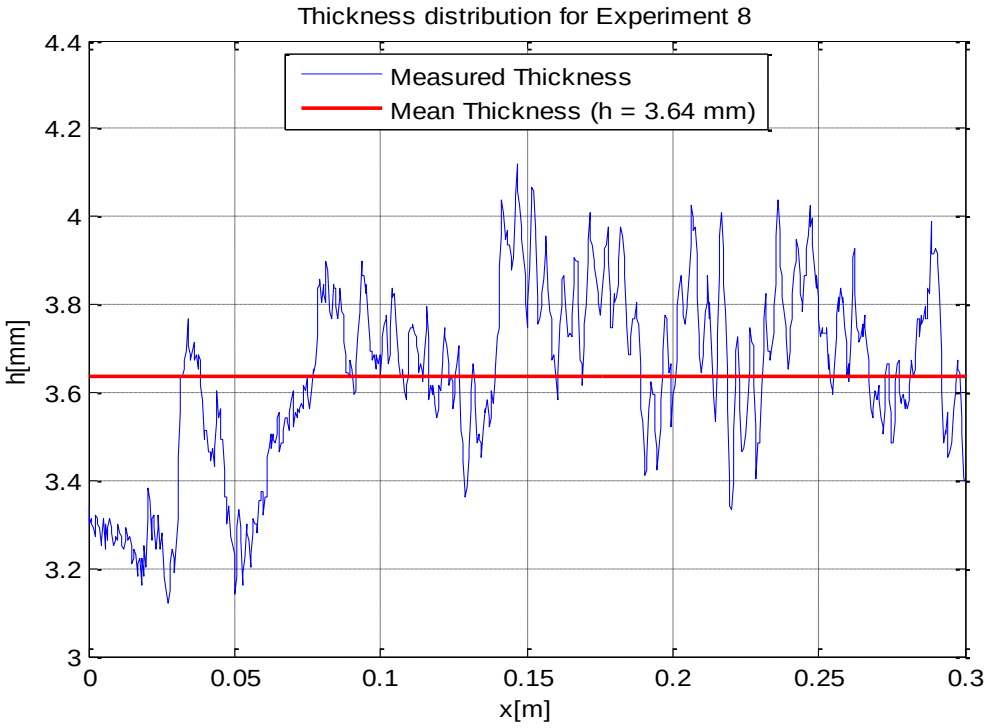
Thickness distribution for Experiment 8
Measured Thickness
Mean Thickness (h = 3.64 mm)
h[mm]
x[m]
4.4
4.2
4
3.8
3.6
3.4
3.2
3
0
0.05
0.1
0.15
0.2
0.25
0.3

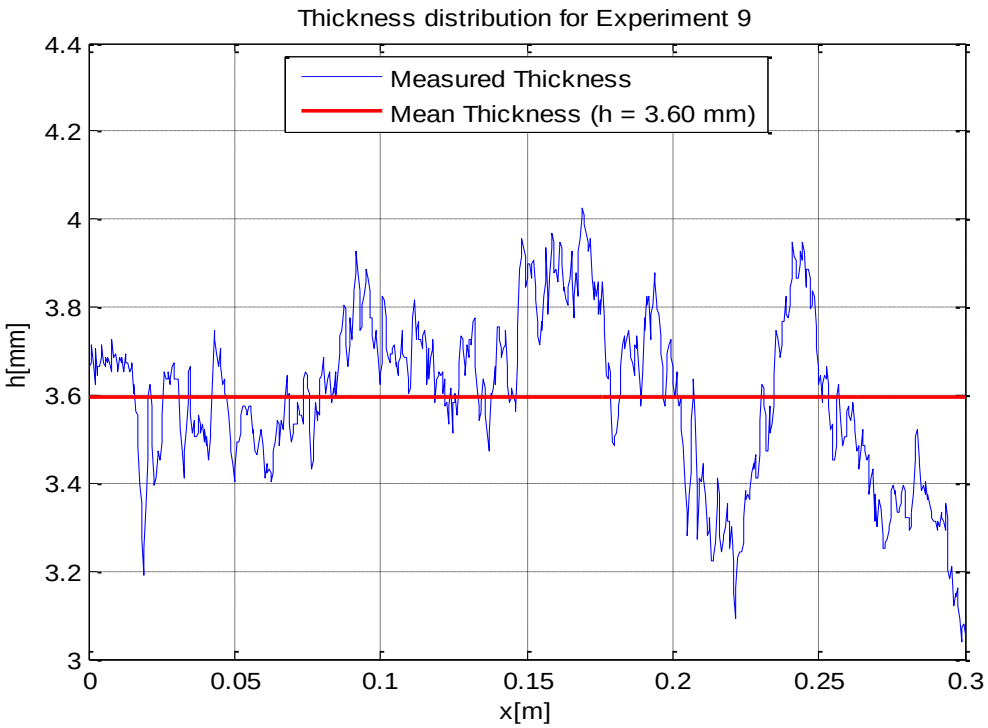
Thickness distribution for Experiment 9
Measured Thickness
Mean Thickness (h = 3.60 mm)
h[mm]
x[m]
4.4
4.2
4
3.8
3.6
3.4
3.2
3
0
0.05
0.1
0.15
0.2
0.25
0.3

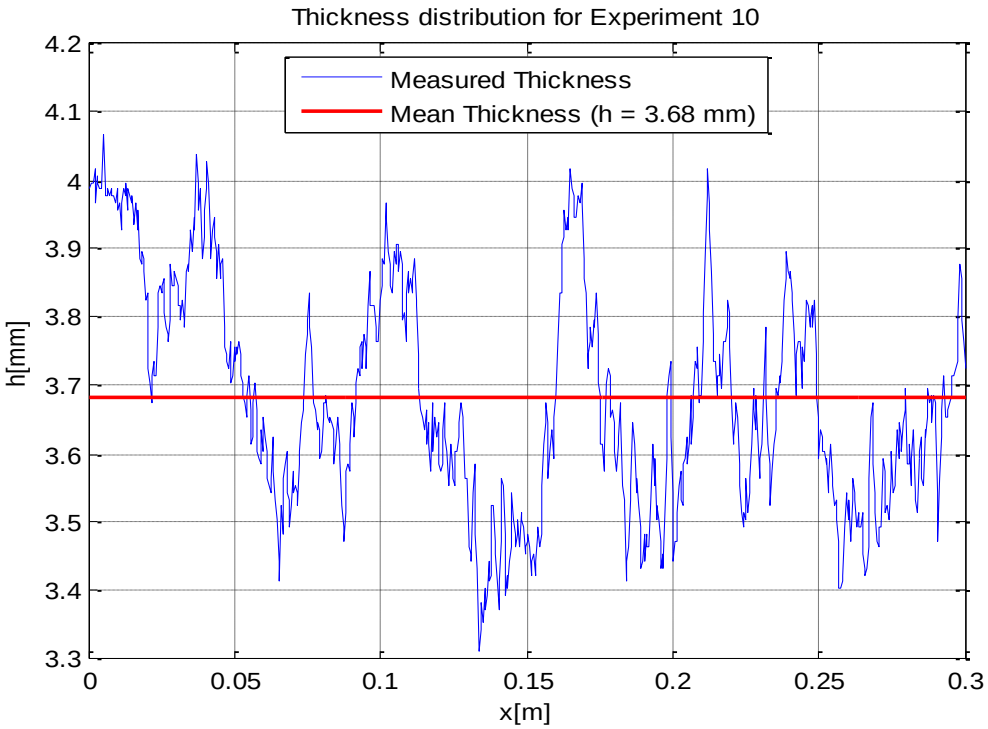
Thickness distribution for Experiment 10
Measured Thickness
Mean Thickness (h = 3.68 mm)
h[mm]
x[m]
4.2
4.1
4
3.9
3.8
3.7
3.6
3.5
3.4
3.3
0
0.05
0.1
0.15
0.2
0.25
0.3

Compaction Experiments

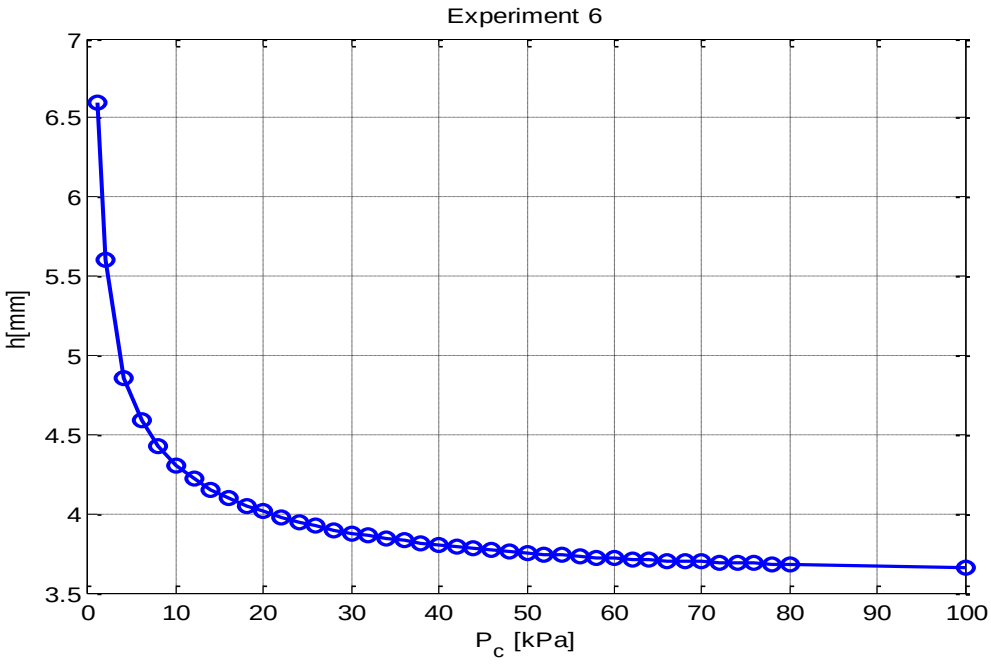

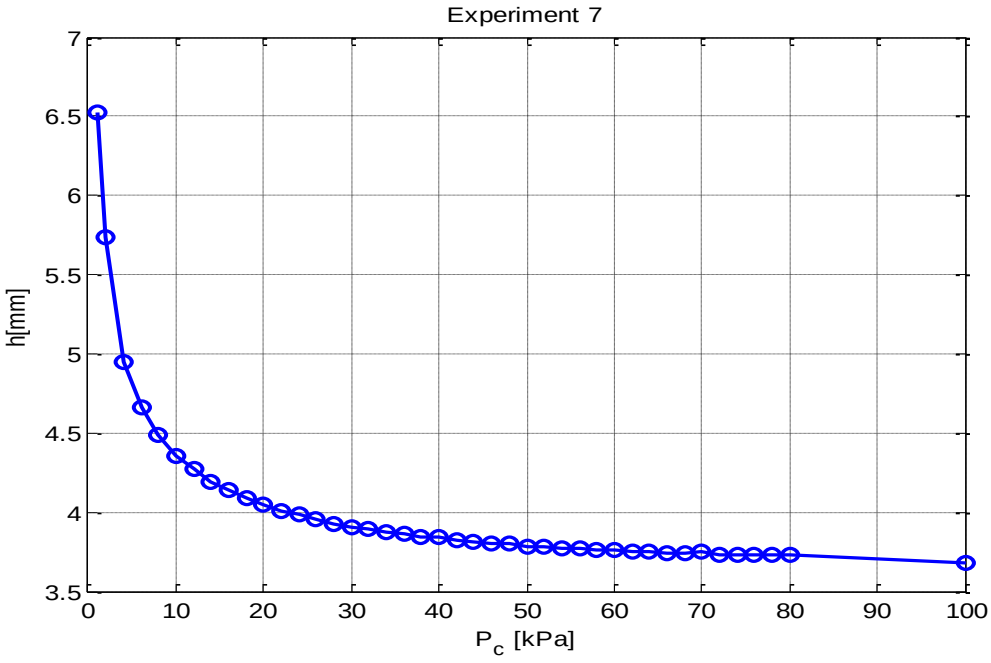

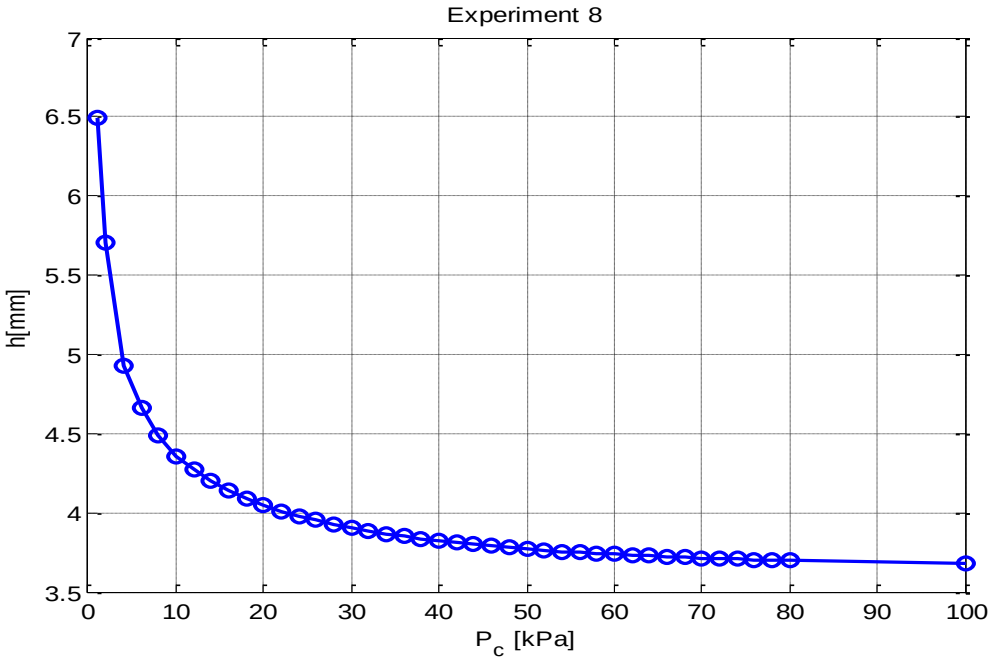
Experiment 8
h[mm]
7
6.5
6
5.5
5
4.5
4
3.5
0
10
20
30
40
50
60
70
80
90
100
P_c [kPa]

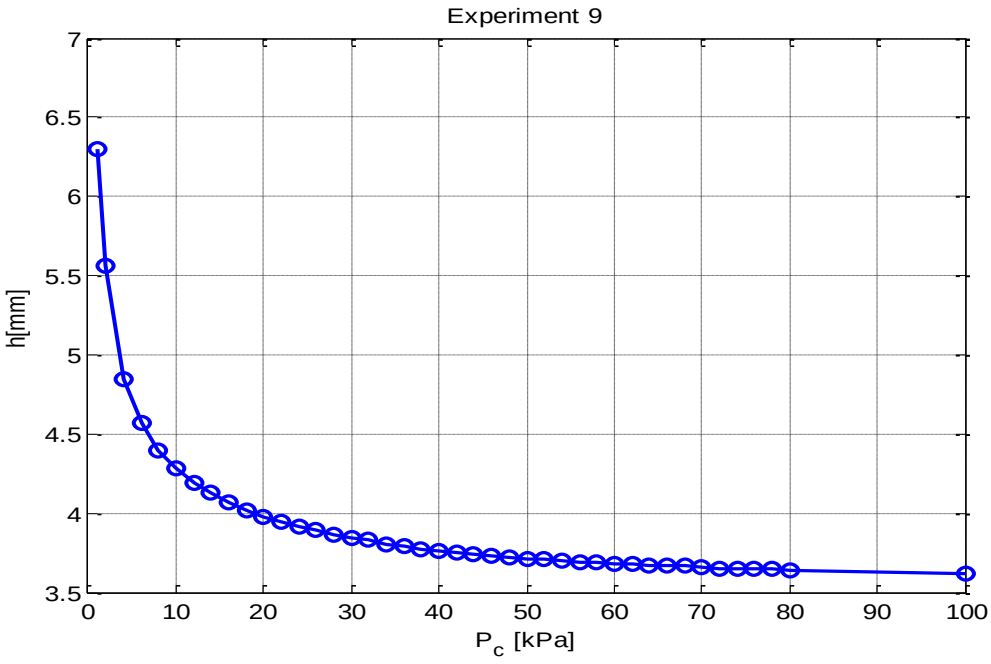
Experiment 9
h[mm]
7
6.5
6
5.5
5
4.5
4
3.5
0
10
20
30
40
50
60
70
80
90
100
P_c [kPa]

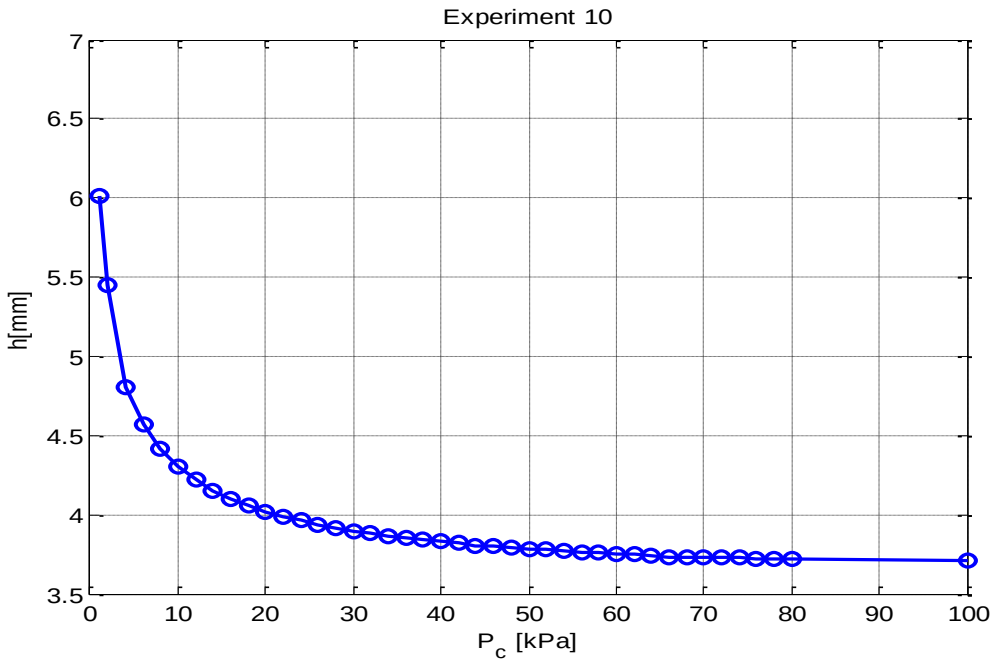
Experiment 10
h[mm]
7
6.5
6
5.5
5
4.5
4
3.5
0
10
20
30
40
50
60
70
80
90
100
P_c [kPa]

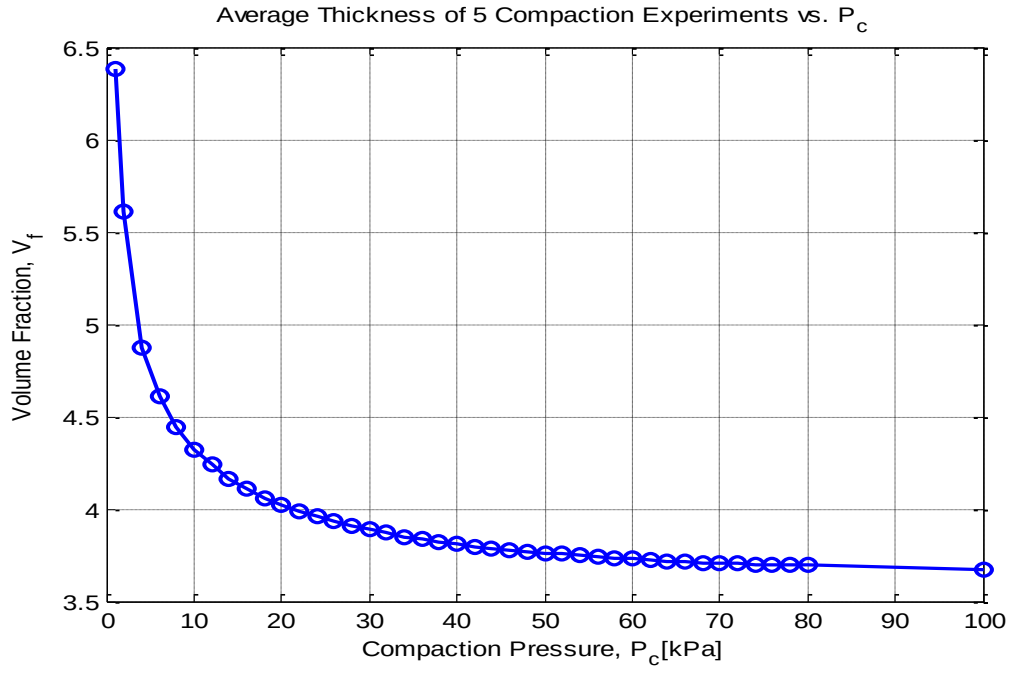
Average Thickness of 5 Compaction Experiments vs. P_c
Volume Fraction, V_f
6.5
6
5.5
5
4.5
4
3.5
0
10
20
30
40
50
60
70
80
90
100
Compaction Pressure, P_c[kPa]

Thickness Profile of the Preform when Flowfront Reaches at x=0, L/4, L/2, 3L/4,L

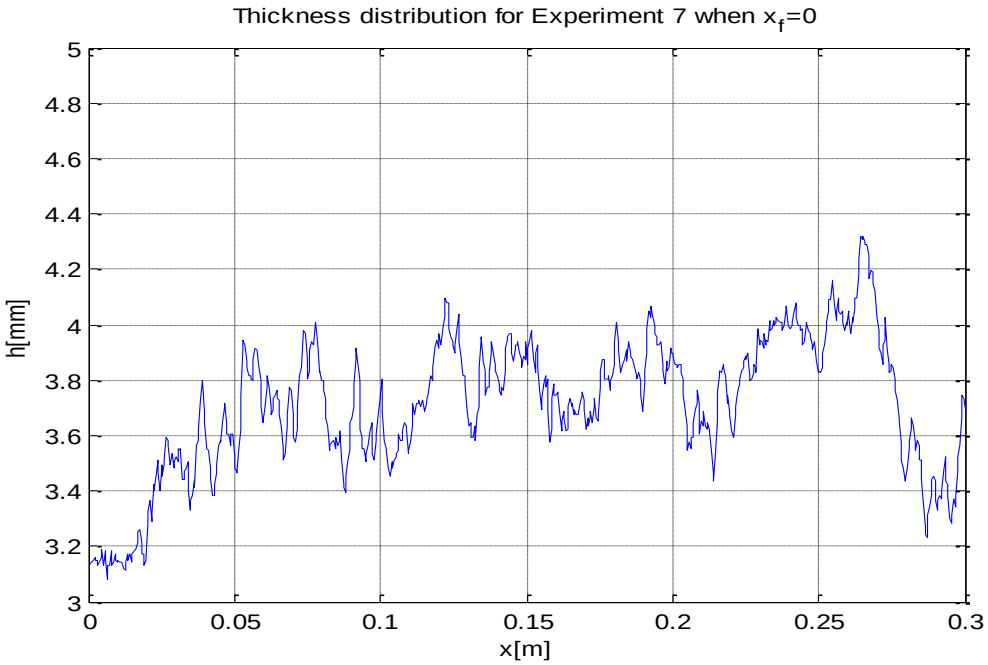

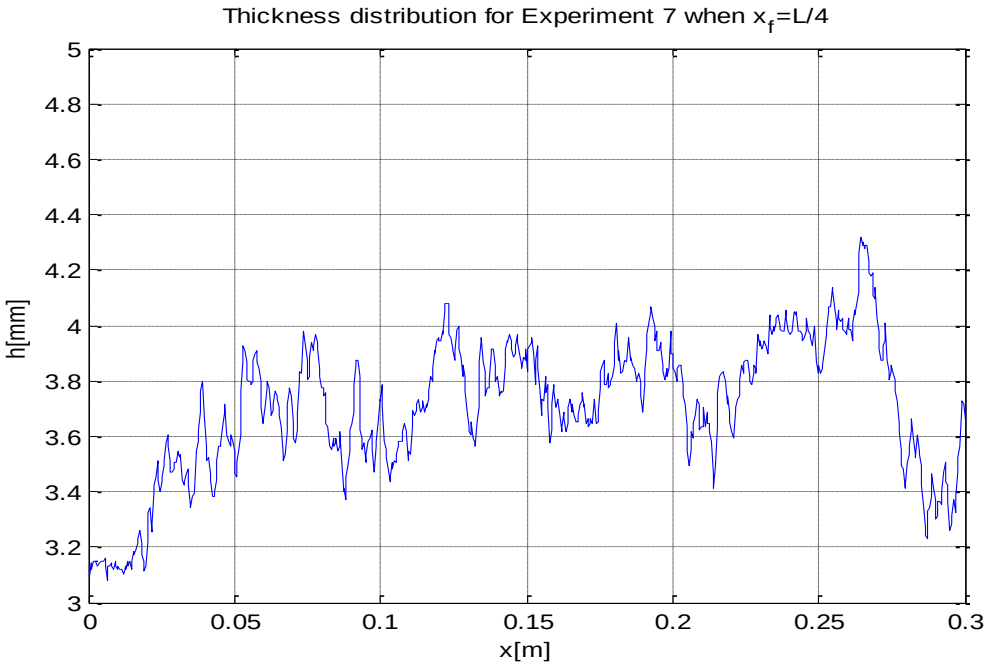

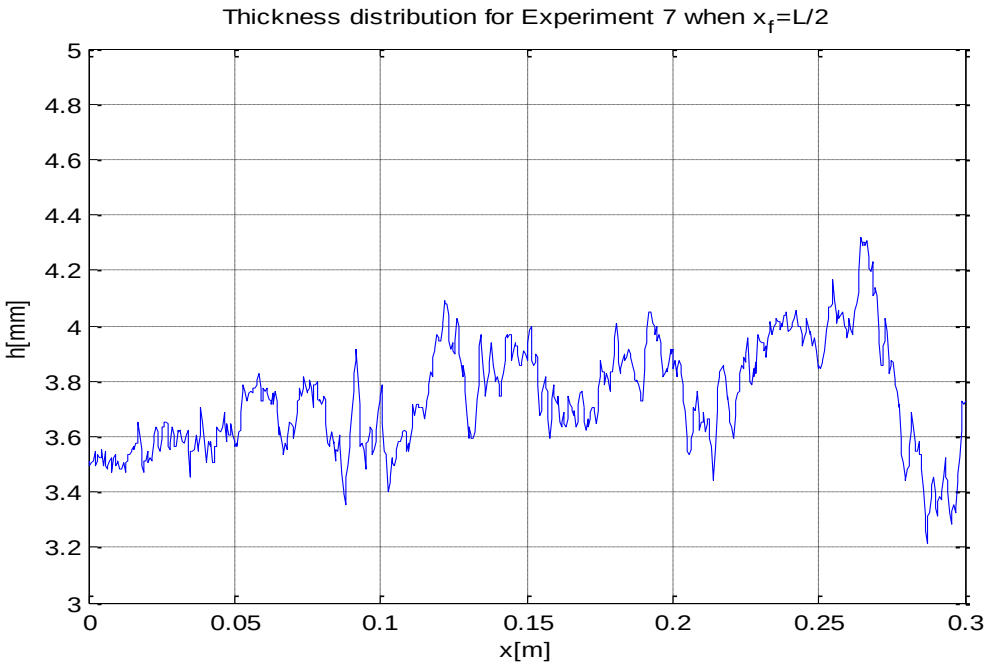
Thickness distribution for Experiment 7 when x_f=L/2
h[mm]
x[m]
5
4.8
4.6
4.4
4.2
4
3.8
3.6
3.4
3.2
3
0
0.05
0.1
0.15
0.2
0.25
0.3

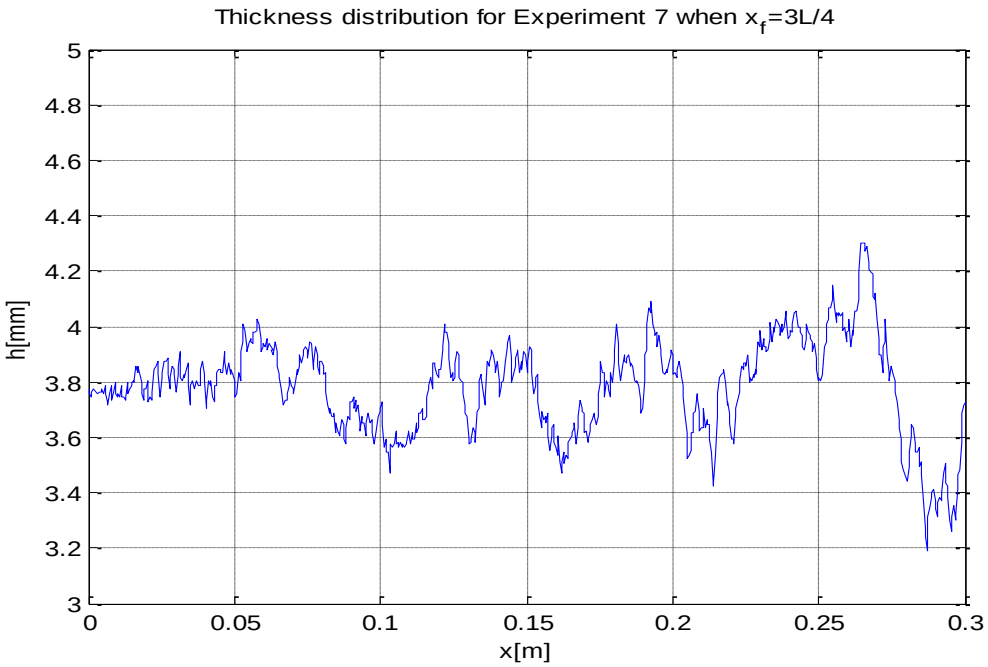
Thickness distribution for Experiment 7 when x_f=3L/4
h[mm]
x[m]
5
4.8
4.6
4.4
4.2
4
3.8
3.6
3.4
3.2
3
0
0.05
0.1
0.15
0.2
0.25
0.3

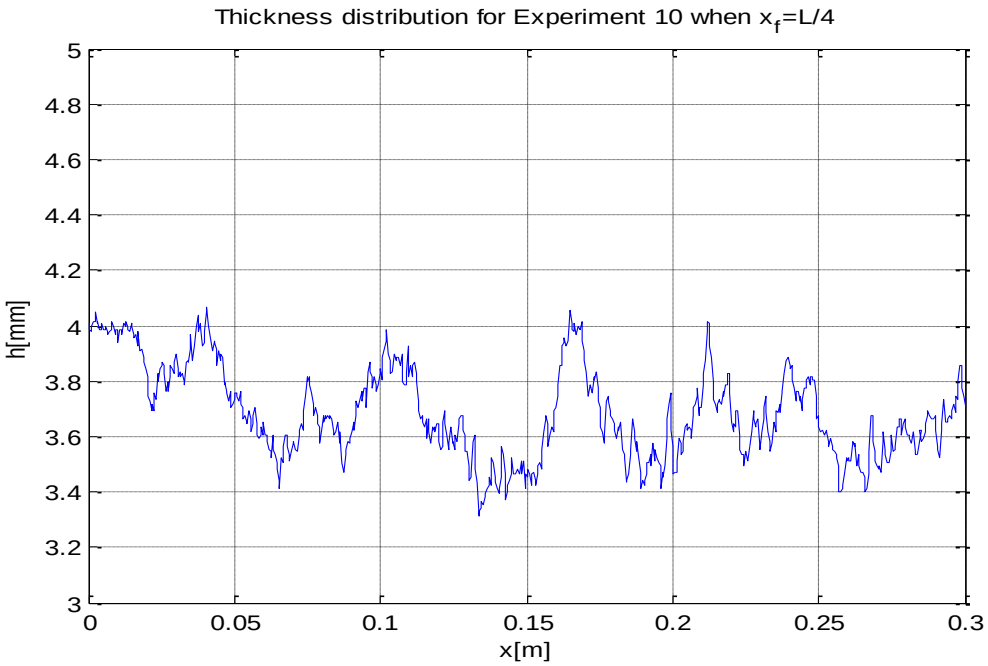
Thickness distribution for Experiment 10 when x_f=L/4
h[mm]
x[m]
5
4.8
4.6
4.4
4.2
4
3.8
3.6
3.4
3.2
3
0
0.05
0.1
0.15
0.2
0.25
0.3

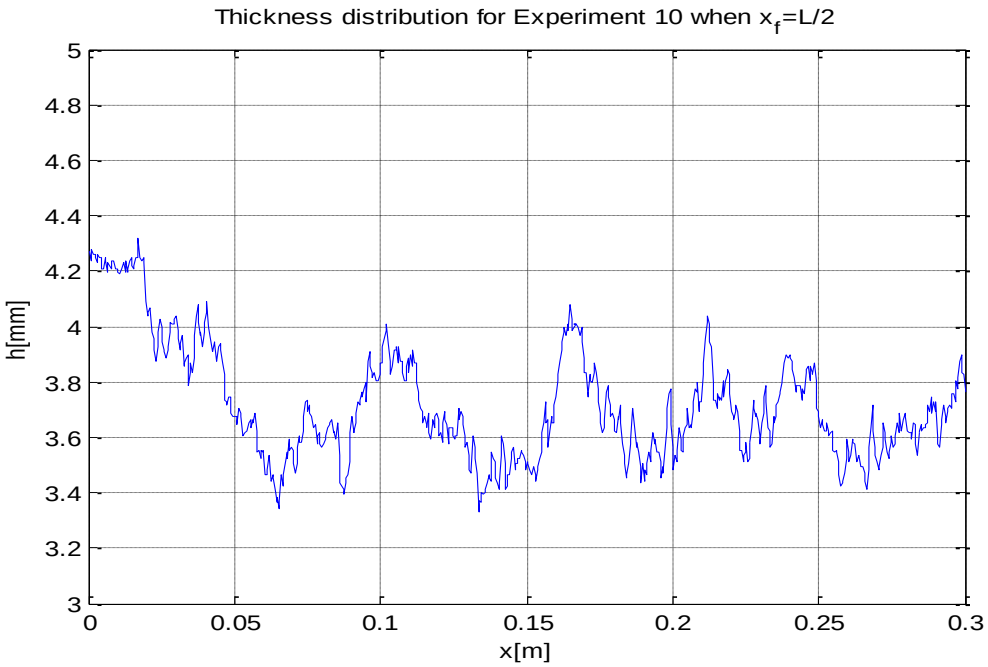
Thickness distribution for Experiment 10 when x_f=L/2
h[mm]
x[m]
5
4.8
4.6
4.4
4.2
4
3.8
3.6
3.4
3.2
3
0
0.05
0.1
0.15
0.2
0.25
0.3

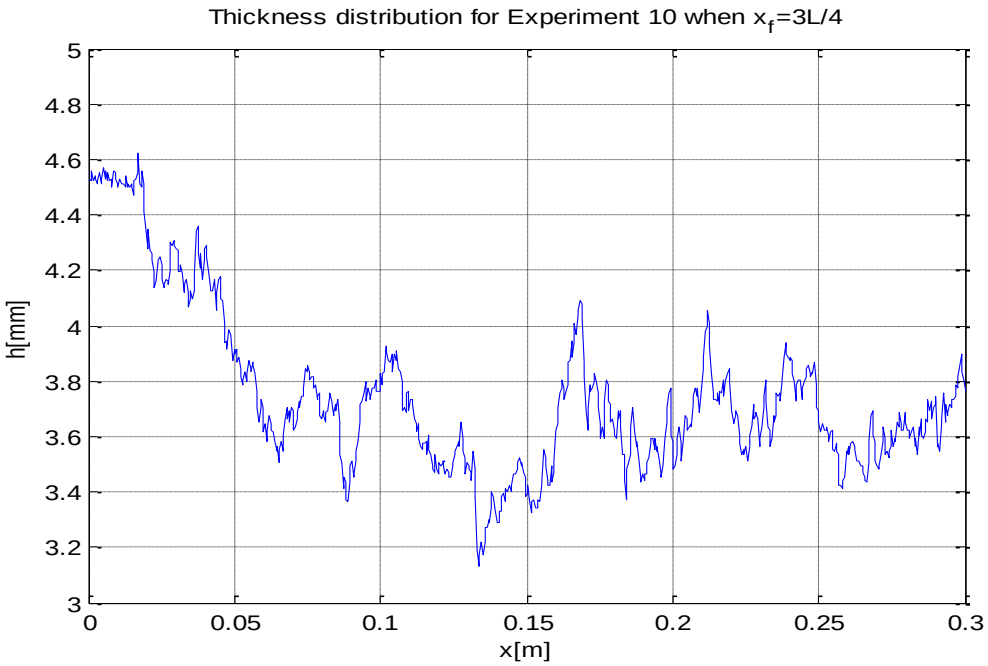
Thickness distribution for Experiment 10 when x_f=3L/4
h[mm]
x[m]
5
4.8
4.6
4.4
4.2
4
3.8
3.6
3.4
3.2
3
0
0.05
0.1
0.15
0.2
0.25
0.3

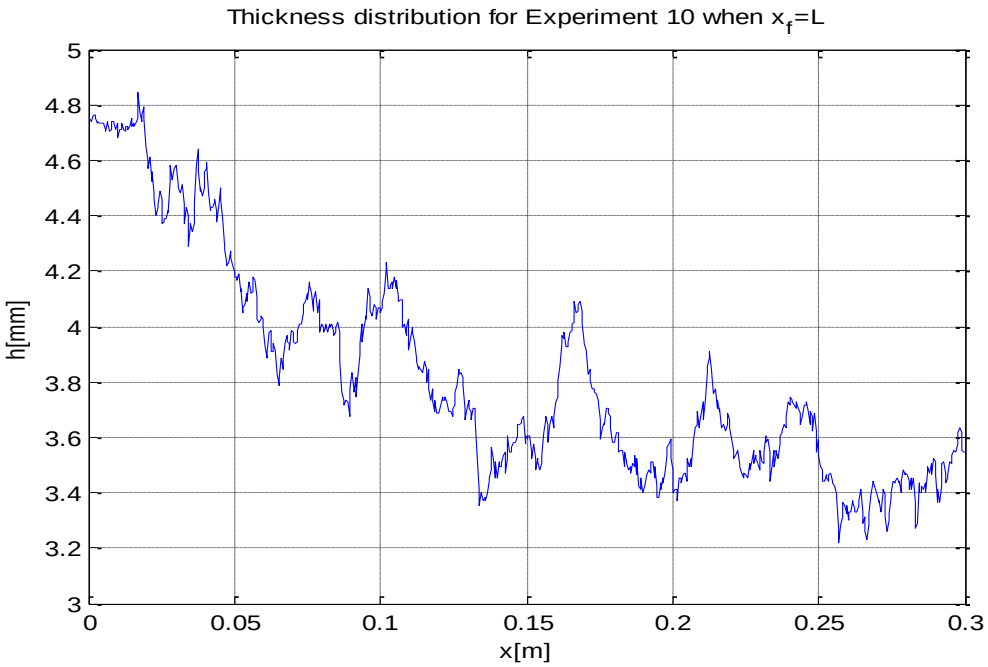
Thickness distribution for Experiment 10 when x_f=L
h[mm]
x[m]
5
4.8
4.6
4.4
4.2
4
3.8
3.6
3.4
3.2
3
0
0.05
0.1
0.15
0.2
0.25
0.3